IDENTIFICATION OF NOVEL INHIBITORS AGAINST *MYCOBACTERIUM TUBERCULOSIS* L-ASPARTATE α- DECARBOXYALSE

REETU SHARMA

THESIS SUBMITTED FOR THE DEGREE OF

DOCTOR OF PHILOSOPHY

DEPARTMENT OF BIOLOGICAL SCIENCES

NATIONAL UNIVERSITY OF SINGAPORE

2012

IDENTIFICATION OF NOVEL INHIBITORS AGAINST *MYCOBACTERIUM TUBERCULOSIS* L-ASPARTATE α- DECARBOXYALSE

REETU SHARMA

(M.Sc. Biotechnology)

A THESIS SUBMITTED FOR THE DEGREE OF

DOCTOR OF PHILOSOPHY

DEPARTMENT OF BIOLOGICAL SCIENCES

NATIONAL UNIVERSITY OF SINGAPORE

2012

Dedicated to

My teachers, family and friends

ACKNOWLEDGMENT

I am thankful to my supervisor Prof. Kunchithapadam Swaminathan for his constant support and guidance at every step of the project. I sincerely appreciate his ready accessibility and availability. I am also thankful to him for providing me an opportunity to prove my acquired skills in research.

I convey my special thanks to Prof. Antonius M.J. VanDongen, DUKE-NUS Graduate Medical School for his collaboration on the chemo-informatics based study.

I am thankful to Prof. Werner Nau, Jacobs University, Germany for allowing me to work in his lab and his guidance. I extend special thanks to Ms. Mara Florea for her help in developing an NMR based enzyme kinetic assay. I cannot forget the help I received from Dr. Maik Jacob, Hamdy El Sheshtawy, Roy D'Souza, Vanya Uzunova, Indrajit Ghosh, Amir Norouzy, Garima Ghale, Khaleel Assaf, Alexandra Irina Lazar and Sweccha Joshi in his lab.

This is a great opportunity to say thanks to the past and present lab members of Lab4 and 5. It was a great experience and pleasure to work with Kanmani, FengXia, Umar, Roopa, Deepthi, Anu, Madhuri, and Pavithra. Also, good friendship with them provided me a constant support throughout my Ph.D. tenture. Thanks to everyone in the structural biology corridor, including Shveta Tivari, Suguna, Thangavelu, Manjeet, Abhilash, Priyanka, Digant and Sharath. I welcome Divya, our new lab member and wish her the best of luck.

I want to thank NUS for my research scholarship, which supported my four years of stay in Singapore and the short term attachment visit in Germany and thus helped me pursue my research.

Last but not the least, I am thankful to my parents and my brother Sachin for his support and encouragement, which was of great help to overcome the work pressure doing my Ph.D.

TABLE OF CONTENTS

SUMMARY

L-Aspartate α-decarboxylase (ADC) belongs to a class of pyruvoyl dependent enzymes and catalyzes the conversion of aspartate to β-alanine in the pantothenate pathway, which is critical for the growth of several micro-organisms, including *Mycobacterium tuberculosis* (Mtb). Its presence only in micro-organisms, fungi and plants and its absence in animals, particularly human, make it a promising drug target. Cleaved *Mycobacterium tuberculosis* L-Aspartate α-decarboxylase (MtbADC) structure was modelled and based on chemoinformatics drug-design approach, potential drug-like inhibitors against MtbADC were identified, following which we employed proton Nuclear Magnetic Resonance (NMR) based assay to systematically screen the inhibitors that we have earlier identified from the Maybridge, National Cancer Institute (NCI) and Food and Drug Administration (FDA) approved drugs databases and those reported earlier in the literature(Sharma et al., 2012a). The concentrations of substrate and product in the reaction were quantified with time and the percentage of conversion and a relative inhibition constant (k_{rel}) were used to compare the inhibitory properties of the previously known molecules: oxaloacetate, DL-threo-β-hydroxy aspartate, L-glutamate and L-cysteic acid with relative inhibition constant k_{rel} values of 0, 0.36, 0.40 and 0.40, respectively and the newly identified molecules: D-tartaric acid, L-tartaric acid and 2,4-dihydroxypyrimidine-5-carboxylic acid with k_{rel} values of 0.36, 0.38 and 0.54, respectively(Sharma et al., 2012b). Novel inhibitors were further tested for their inhibitory activity against Mtb culture. These molecules could serve as potential building blocks for developing better therapeutic agents.

LIST OF ABBREVIATIONS

TB	Tuberculosis
WHO	World Health Organization
HIV	Human immunodeficiency virus
Mtb	*Mycobacterium tuberculosis*
BCG	Bacillus Calmette-Guérin
PZA	Pyrazinamide
DOT	Directly Observed Therapy
MDR	Multiple Drug Resistant
ADC	L-Aspartate α- decarboxylase
CoA	Coenzyme A
E. coli	*Escherichia coli*
NCI	National Cancer Institute
FDA	Food and Drug Administration
NMR	Nuclear Magnetic Resonance
PK	Pharmacokinetic
ADME	Absorption/Distribution/Metabolism/Excretion
MTD	Maximum tolerance dose
RMSD	Root mean square deviation
VDW	Van der Waals
HTVS	High throughput virtual screening
G-scores	Glide scores
SAM	S-adenosylmethionine

LB	Luria Broth
DNA	Deoxyribonucleic acid
DMSO	Dimethyl sulfoxide
MIC	Minimum Inhibitory Concentration
SDS	Sodium dodecyl sulfate
PAGE	Polyacrylamide gel electrophoresis
ESMS	Electrospray ionization mass spectra
HPLC	High performance liquid chromatography

LIST OF FIGURES

LIST OF TABLES

PUBLICATIONS

Singh NS, Shao N, McLean JR, Sevugan M, Ren L, Chew TG, Bimbo A, **Sharma R**, Tang X, Gould KL and Balasubramanian MK (2011). SIN-inhibitory phosphatase complex promotes cdc11p dephosphorylation and propagates SIN asymmetry in fission yeast. ***Current Biology,*** 21, 1968-1978.

Sharma R, Kothapalli R, Dongen AMJV and Swaminathan K. (2012). Chemoinformatic identification of novel inhibitors against *Mycobacterium tuberculosis* (Mtb) L-aspartate α-decarboxylase. ***PLoS ONE*** 7, e33521.

Sharma R, Florea M, Nau WM and Swaminathan K. (2012). Validation of Drug-Like Inhibitors against *Mycobacterium tuberculosis* L-aspartate-α-decarboxylase using Nuclear Magnetic Resonance (1H NMR). ***PLoS ONE,*** 7, e45947.

CHAPTER 1

INTRODUCTION

CHAPTER 1. INTRODUCTION

1.1 TUBERCULOSIS

Tuberculosis (TB) is caused by the respiratory pathogen *Mycobacterium tuberculosis*. The primary organ affected by the bacterium is the lungs. However, TB can also affect the central nervous system, lymphatic system, circulatory system, genitourinary system, bones, joints and the skin (Raviglione and Brien, 2004). The disease continues to be a leading cause of death worldwide (WHO, 2011). Approximately one-third of the world population is infected with Mtb, at an estimated rate of about two million people annually. The WHO 2011 report estimates 8.8 million incidents of TB and 1.1 million HIV-negative deaths and 0.35 million HIV-positive deaths (Dye and Williams, 2010; WHO, 2011).

Not every infected individual will immediately develop the disease and the majority has asymptomatic or latent disease. The disease will develop in approximately one in ten asymptomatic patients. If left untreated, TB could be lethal in more than 50% of patients. According to Kaufmann and McMichael, about two million people succumb to the disease annually (Kaufmann and McMichael, 2005). These data indicate the need to develop effective therapeutics against the bacterium.

1.2 INFECTION WITH TUBERCULOSIS

Inhaled bacteria in the tubercle are engulfed by macrophages and dentritic cells. Some of the dentriticc cells migrate to lymph nodes where they activate T cells and induce containment in small granulomatous lesions of the lung but may not completely eradicate the microbe. Approximately 90% of the infected individual does

not suffer from clinical disease and the bacterium remains in the latent form inside the macrophage. The process of infection is slow and hence disease outbreak gets delayed (Kaufmann, 2001). According to Manabe and Bishai, reactivation of existing foci is responsible for tuberculosis in adults, rather than as a direct outcome of primary infection (Manabe and Bishai, 2000) (Fig. 1.1).

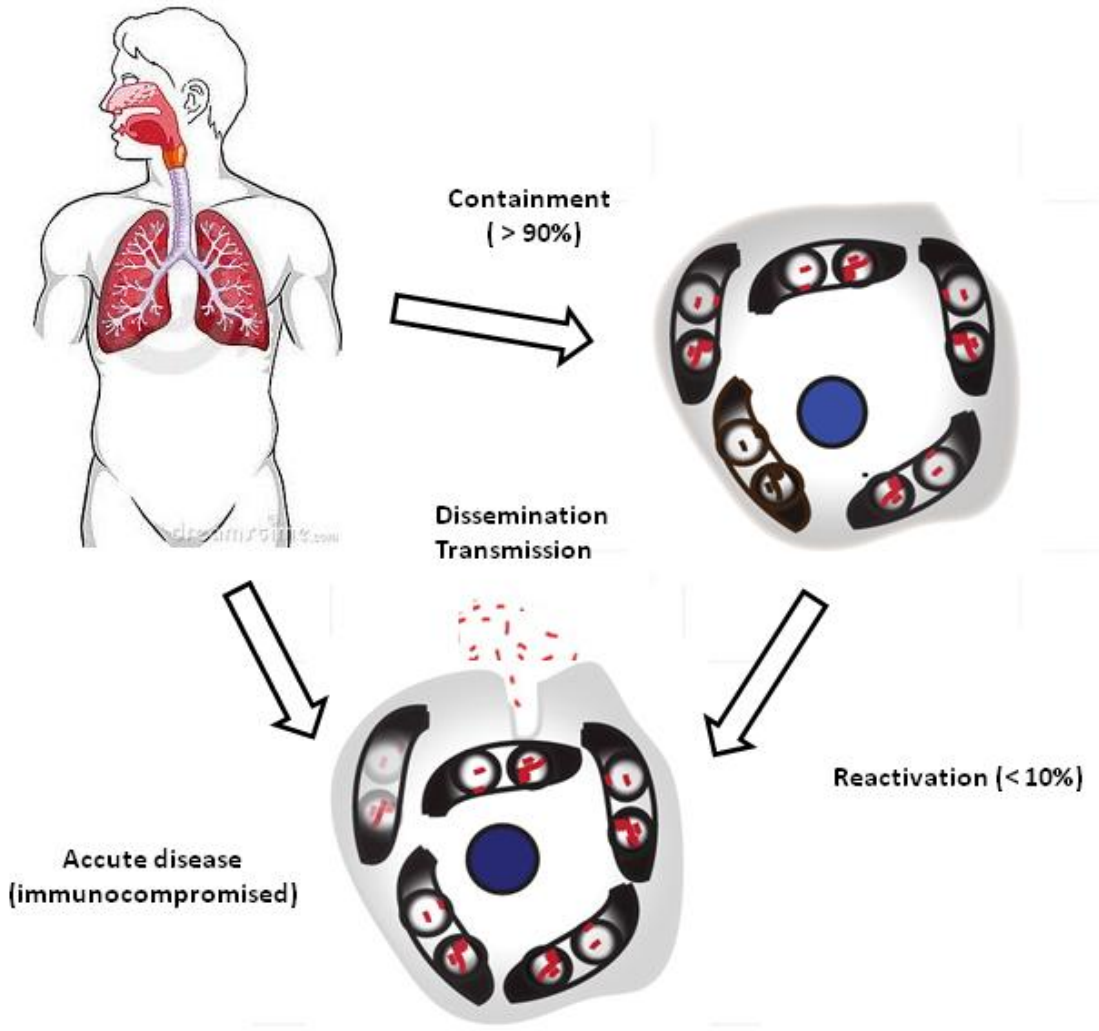

Figure 1.1. **Schematic diagram of *Mycobacterium tuberculosis* infection.** Modified from Kaufmann, 2004.

1.3. MTB INSIDE MACROPHAGE: LATENT PHASE OF THE DISEASE

Mtb is an intracellular pathogen which has developed sophisticated mechanisms of survival within host macrophages, including preventing recognition of

infected macrophages by T cells by inhibiting MHC class II processing and presentation, evading macrophage killing mechanisms, such as those mediated by reactive nitrogen intermediates and phagolysosome fusion (Flynn et al. 2003). Macrophages offer the bacterium a preferred habitat (Schaible et al., 1999). If Mtb interacts with the constant regions of immunoglobulin receptors (FcRs) and toll-like receptors, host defence mechanisms will be stimulated, whereas interactions with complement receptors promote survival of mycobacterium (Armstrong and Hart, 1975; Brightbill, 1999; Schorey, 1997). In the endosome, iron is available to Mtb for its survival (Andrews, 2000; Lounis et al., 2001; Schaible et al., 1999) (Lounis et al., 2001).The bacterium even survives the harsh environment of the phagosome, which is generally detrimental to most microbes . Activation with interferon-γ promotes the maturation of phagosomes, which stimulates anti-mycobacterial mechanisms in macrophages such as reactive oxygen intermediates (ROI) and reactive nitrogen intermediates (RNI)(Schaible et al., 1999) . RNI plays an important role in the control of *M. tuberculosis* (Nathan and Shiloh, 2000). However, *M. tuberculosis* is not fully eradicated even in IFN-γ activated macrophages.

In the dormant stage, the metabolic activity of Mtb gets reduced and facilitates its survival under the conditions of nutrient and oxygen deprivation. Mtb goes into the latent stage where it persists without producing any disease. Nevertheless, the risk of disease outbreak at a later time remains. McKinney et al. have indicated that mycobacteria switch to lipid catabolism and nitrate respiration to ensure their survival (McKinney et al., 2000). Lipids are abundant in the caseous detritus of granulomas, providing a rich source of nutrients during persistence. In less than 10% cases such as immunosuppressive individual, for example HIV infected, newly born or aged person, primary infection transforms into disease. Under the disease condition, cavity lesions

develop and the number of bacteria increases in caeseous detritus. The patient becomes infectious when cavitation is reached (Kaufmann, 2000; Kaufmann, 2004) (Fig. 1.3).

1.4 CONTROL MEASURES FOR TUBERCULOSIS

Acid-fast staining of sputum and skin testing with tuberculin (using purified protein derivative of Mtb, PPD), developed by Robert Koch in 1882 and 1890, respectively, are the two techniques usually employed for the diagnosis of tuberculosis. Treatment measures include the administration of Bacillus Calmette Guerin (BCG) as a vaccine and the use of anti-microbial drugs. The BCG vaccine was developed jointly by Albert Calmette and Camille Guérin in the 1910s. New molecular techniques, which detect T cell reactivity to Mtb specific-antigens not found in BCG, help to identify latently infected healthy TB contacts for targeting prophylactic treatment (Mazurek 2003).

Streptomycin, discovered by Waksman in 1943, was the first drug used to treat TB (Schatz and Waksman, 1944). It interacts with the small 30S subunit of the ribosome and perturbs the biosynthesis of proteins (Carter et al., 2000; Garvin et al., 1974). It was followed later by isoniazid (INH) (Bernstein et al., 1952), rifampicin, pyrazinamide and ethambutol, but all these drugs have significant side-effects (CDC, 2003). Rifampicin, one of the most potent drugs against TB, used even now, has been suggested to act by inhibiting the mycolic acid biosynthesis, an essential component of mycobacterial cell wall (Timmins and Deretic, 2006; Winder and Collins, 1970).

Pyrazinamide (PZA) was discovered as a potential TB drug in 1952 (Malone et al., 1952). Despite similarityin structure, isoniazid and pyrazinamide are different in their mechanism of action. Pyrazinamide activity causes intake of proton and

dysfunction of the pH balance of mycobacteria (Zhang and Mitchison, 2003; Zhang et al., 2003). Shi et al. has shown that Pyrazinamide inhibits translation in *Mycobacterium tuberculosis.* It targets the essential ribosomal protein S1, which is involved in the ribosome-sparing process of translation (Shi et al., 2011). Ethambutol, discovered in 1961 (Thomas et al., 1961), affects the cell wall by inhibiting polymerization of arabinogalactane and lipoarabinomannane (Belanger et al., 1996).

Treatment against the disease has shown to be significantly improved when the drugs are combined in specific quantities and administered to the patient. WHO recommends the directly observed therapy (DOT), a combination of isoniazid, rifampin, ethambutol and pyrazinamide for 6 months and TB patients are observed by medical personnel while taking their daily dose, mainly to monitor and improve patient adherence with the therapy (WHO, 2008).

In recent decades, the bacterium has shown to develop resistance against several available drugs. To treat multiple drug resistant TB, WHO has recommended the use of prothionamide and ethionamide (discovered in 1956, (Libermann et al., 1956), which target the mycolic acids biosynthesis through the inhibition of InhA (Banerjee et al., 1994). D-cycloserine, discovered in 1969, is another cell wall synthesis inhibitor (David et al., 1969) and triggers peptidoglycan synthesis through D-alanine racemase and D-alanine ligase inhibition (Cáceres et al., 1997; Feng and Barletta, 2003).

The emergence of multiple drug resistant tuberculosis (MDR-TB) and extensively resistant tuberculosis (XDR-TB) has increased the failure rate and cost of treatment (Glynn et al., 2002; Reece and Kaufmann, 2008). This has prompted further interest in the development of more effective TB treatment strategies.

1.5 L-ASPARTATE α-DECARBOXYLASE

L-Aspartate α- decarboxylase (ADC, EC 4.1.1.11), encoded by the *panD* gene, is a lyase and catalyzes the decarboxylation of aspartate to β-alanine, which is essential for D-pantothenate formation (Fig. 1.2). Mutants of the *panD* gene are defective in β-alanine biosynthesis (Cronan, 1980). β-alanine and D-pantoate condense to form pantothenate, a precursor of coenzyme A (CoA), which functions as an acyl carrier in fatty acid metabolism and provides the 4′- phosphopantetheine prosthetic group in fatty acid biosynthesis, an essential need for the growth of several micro-organisms, including *Mycobacterium tuberculosis* (Mtb) (Sassetti et al., 2003; Spry et al., 2008), the causative bacterial agent of tuberculosis (Tb).

The distinctive lipid rich cell wall of Mtb is responsible for the unusually low permeability, virulence and resistance to therapeutic agents (Cox et al., 1999; Daffé and Draper, 1997). At the heart of the fight against tuberculosis lies its cell wall, a multilayered structure adorned with a number of lipo-glycans that protect the bacterium in antimicrobial defense against environmental stresses and treatment. Consequently, the metabolism and biosynthesis of lipids and lipo-glycans play a pivotal role in the intracellular survival and persistence of Mtb. Any impediment in the pantothenate pathway will therefore affect the survival of the bacterium. As Mtb is notorious to develop resistance towards drugs, progress in the treatment of tuberculosis will require us to identify new targets in pathways critical for the sustenance of Mtb, and to develop new drugs selectively inhibiting these targets so as to minimize drug resistance and potential side effects (Glickman et al., 2000; Karakousis, 2009). Since pantothenate is synthesized only in microorganisms, fungi

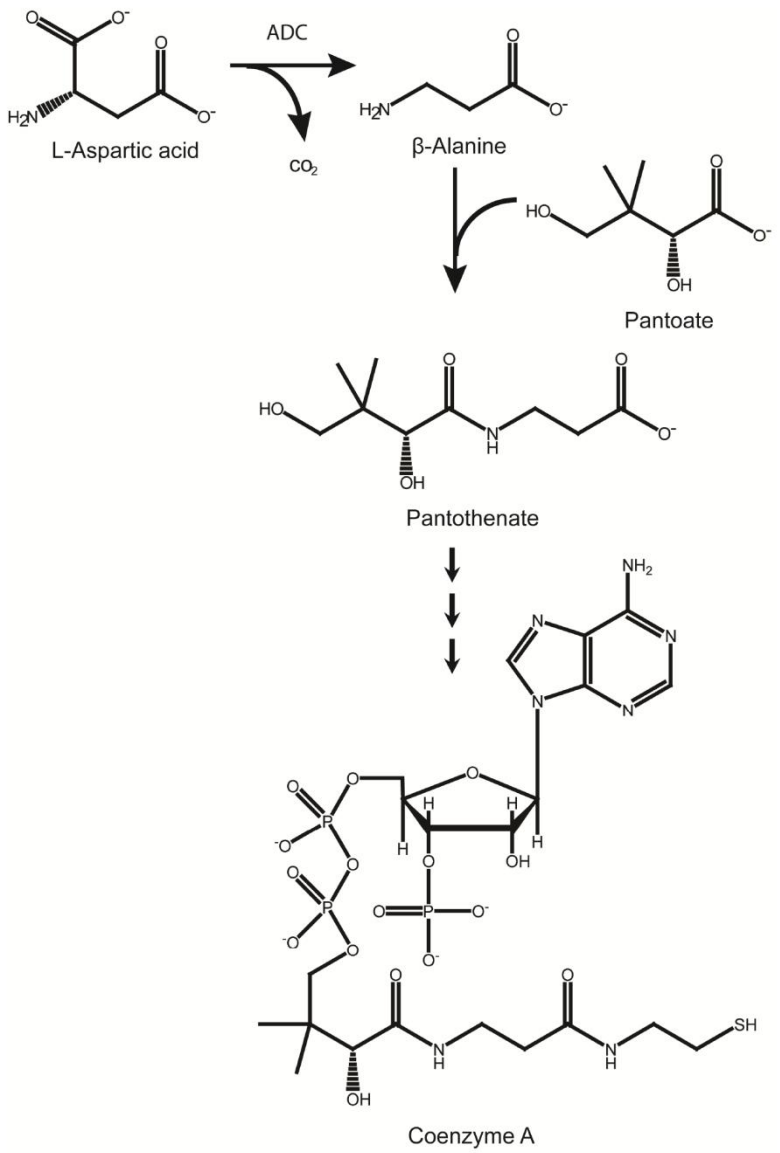

Figure 1.2. Pantothenate and CoA biosynthesis pathway. L-Aspartate α-decarboxylase (ADC) catalyzes the decarboxylation of L-aspartate to β-alanine.

and plants, but not in humans, the enzymes that are involved in this biosynthetic pathway qualify to be potential targets for antibacterial and antifungal agents (Jackowski, 1996). The absence of this pathway in humans ensures that any inhibitor or drug against ADC would have low toxicity in patients. In particular, the chance of

side effects in a long term treatment procedure will be minimal. Moreover, the presence of the ADC gene in only one copy in the Mtb genome further enhances its importance as a suitable drug target.

MtbADC (139 amino acids) undergoes autocatalyzed cleavage between Gly24 and Ser25, where the serine is modified to a pyruvoyl group, resulting in the formation of approximately 13 kDa α-chain containing the N-terminal pyruvoyl group and nearly 2.7 kDa β-chain. The cleavage reaction involves the formation of an ester intermediate by an initial N-O acyl rearrangement (Shao et al., 1996; van Poelje and Snell, 1990). N-terminal dehydroalanine is formed after elimination of the ester, which is hydrolyzed to form the alpha subunit with an N-terminal pyruvoyl group (Albert et al., 1998) (Fig. 1.3). The self cleavage can be thermally promoted (Ramjee et al., 1997). This processed α form is necessary for the conversion of aspartate to β-alanine (Ramjee et al., 1997) and the mutation S25A makes the protein uncleavable and inactive (Kennedy and J., 2004).

So far, crystal structures have been determined for unprocessed (uncleaved) ADC from *E. coli* (PDB id: 1PPY) (Schmitzberger et al., 2003), Mtb (2C45) (Gopalan et al., 2006), and processed ADC from *E. coli* (1AW8) (Albert et al., 1998), *Francisella tularensis* (3OUG), *Campylobacter jejuni* (3PLX), *Thermus thermophilus* ADC (TthADC) (1VC3), TthADC, complexed with substrate analog fumarate (2EEO), *Helicobacter pylori* ADC (HpyADC) (1UHD) (Lee and Suh, 2004) and HpyADC, complexed with substrate analog isoasparagine (1UHE) (Lee and Suh, 2004). The ADC protein folds into a double-ψ β-barrel structure. It forms a homotetramer (Gopalan et al., 2006) (Fig. 1.4 A and Fig. 1.4C) and the active site is shown to be at the interface of a dimer of processed ADC (Lee and Suh, 2004) (Fig.1.4 B).

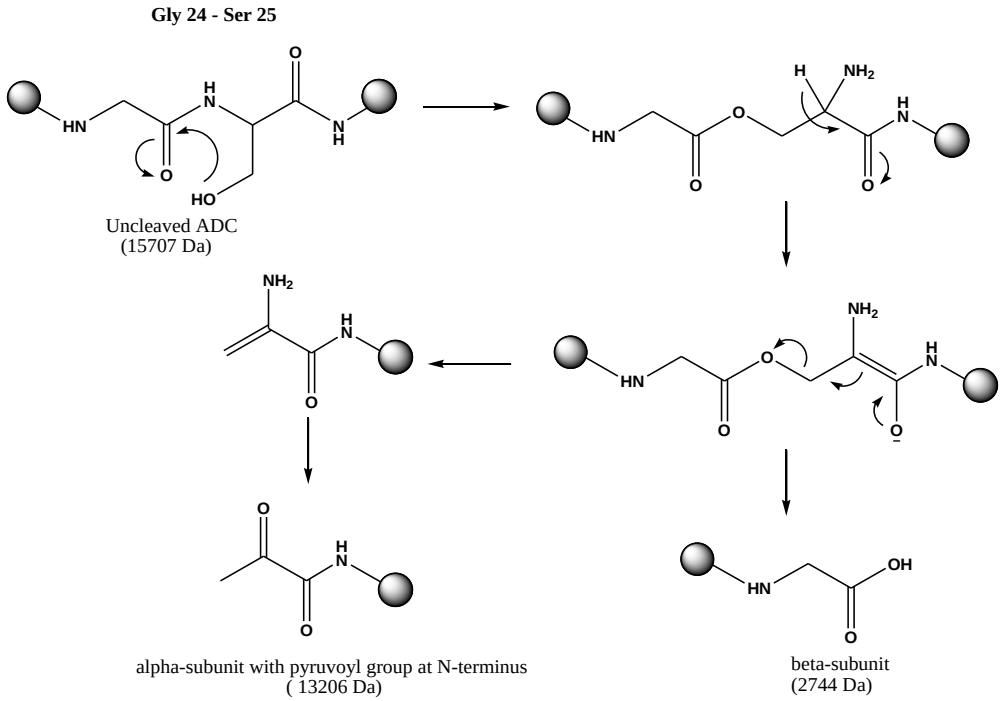

Figure 1.3. Proposed mechanism of self-cleavage of ADC protein
Modified from Albert et al., 1998.

1.6 Mechanism of ADC catalyzing the reaction.

The first step of the catalytic reaction involves a nucleophilic attack of the primary hydroxyl group of Ser25 in the vicinity of the Gly24 - Ser25 peptide bond. Tyr58 protonates the primary amine formed after the formation of the ester. In the second step, the ester intermediate is broken down. Lee and Suh (Lee and Suh, 2004) have proposed the mechanism of action of ADC by analyzing co-crystallization of the substrate analog isoasparagine with the ADC protein where the pyruvoyl group plays an important role as a cofactor. Prior to decarboxylation a Schiff base intermediate is formed at the active site of subunits A and B. The nitrogen atom of ammonium group of Lys9*, N atom of His11*, hydroxyl group oxygen of Tyr58 are in close proximity to the active site at distance of 2.7, 4.5 and 3.3 Å, respectively.

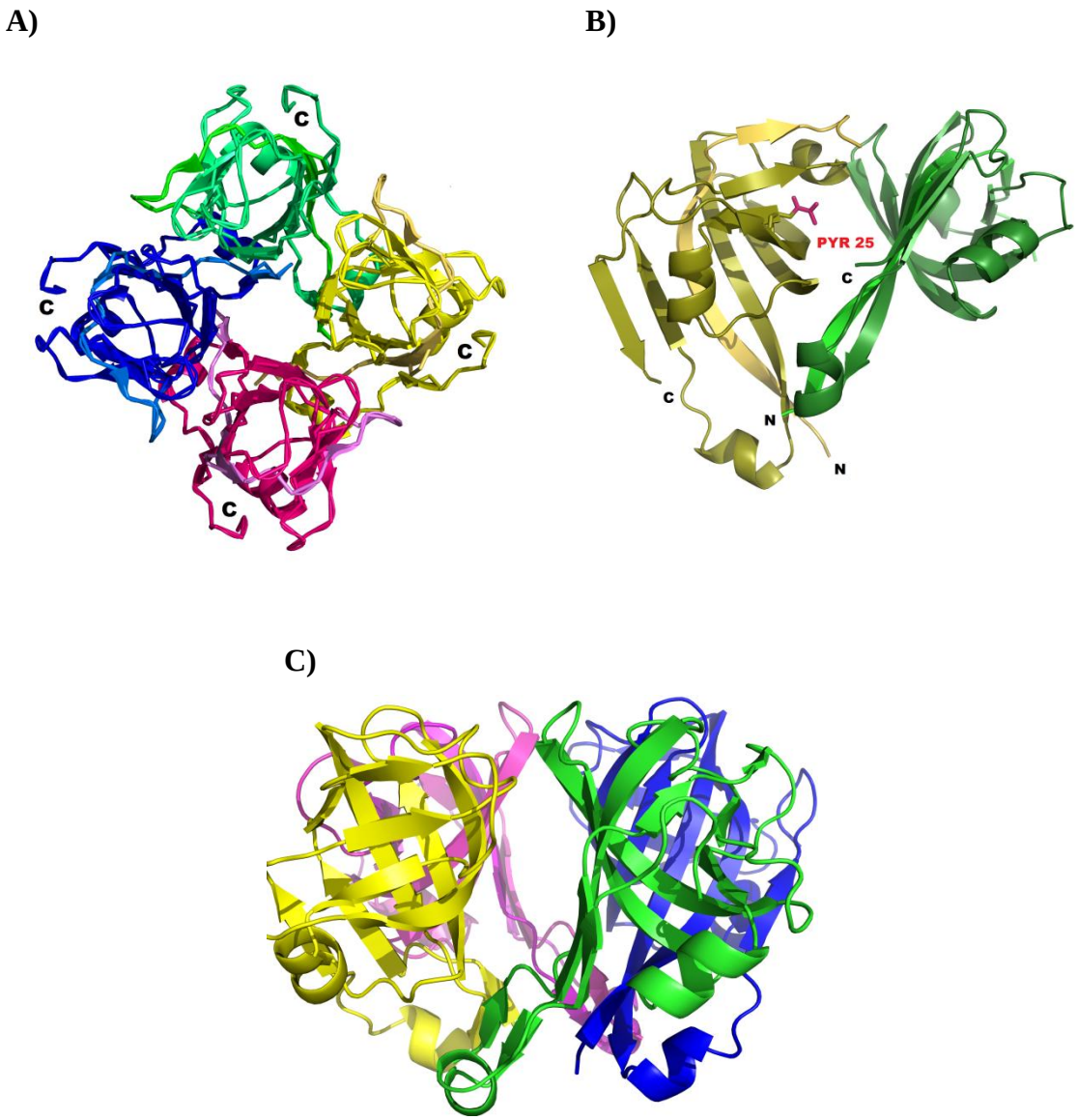

Figure 1.4. Ribbon representation of ADC. (**A)** ADC tetramer with each subunit coded with different color: view along four fold axis (**B)** ADC dimer showing active site with pyruvoyl group **(C)** view perpendicular to non crystallographic four fold axis.

Lee and Suh suggested that Lys9* keeps the α-carboxyl group of the substrate, which is deprotonated by forming an ion pair with the γ-carboxyl group of isoasparagine (Albert et al., 1998; Lee and Suh, 2004). After enzyme-substate Schiff base formation, carbon dioxide is released forming an extended enolate intermediate

where the amine group of the substrate attacks the hydroxyl group of Tyr58, resulting in enzyme-product Schiff base formation, which upon hydrolysis forms β-alanine and releases the pyruvoyl group for catalyzing another reaction (Albert et al., 1998; Lee and Suh, 2004) (Fig. 1.5).

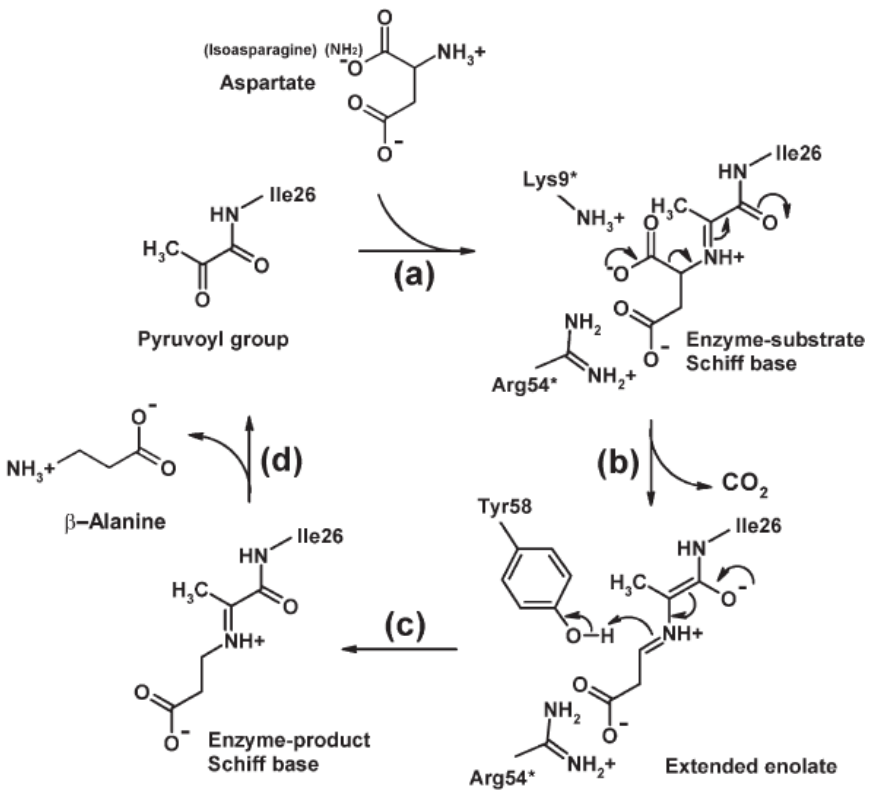

Figure 1.5. Proposed catalytic mechanism of ADC catalyzing the conversion of aspartate to β-alanine (Lee and Suh, 2004).

The unique feature of being absent in human, in addition to its significance in the cellular metabolism of Mtb, endows exclusive significance upon ADC as an important drug and vaccine target. Jacobs and coworkers (Sambandamurthy et al., 2002) constructed a double deletion mutant (Δ*panCD*) with a view to globally impair the ability of Mtb to synthesize lipids. Mice infected with the Δ*panCD* mutant were able to survive 22 weeks longer than those infected with the bacille Calmette-Guerin-

Pasteur (BCG-P) strain. Deletion of the genes significantly attenuates Mtb and protects infected animals against tuberculosis.

In an attempt to discover suitable inhibitors against ADC, *threo*-β-hydroxyaspartic acid , *meso*-diaminosuccinate and L-cysteic were the first compounds identified to directly affect the pentothenate pathway (Ravel and Shive, 1946; Shive and Macow, 1946). Mass and Davis (Maas and Davis, 1950) showed that D-serine is involved in β-alanine synthesis. Cysteic acid is also effective in inhibiting β-alanine synthesis in a variety of bacteria, including *E. coli*, *Lactobacillus casei*, *L. arabinosus* and *Leuconostoc mesenteroides* (Webb et al., 2004). L-glutamate, succinate, oxaloacetate, L-serine, L-cysteic acid, β-hydroxyaspartate and D-serine are also reported as competitive inhibitors of ADC with K_i of 0.76, 0.73, 0.81, 0.73, 0.08, 0.13 and 0.16 mM, respectively (Williamson and Brown, 1979a). In addition, phenylhydrazine binds to the pyruvoyl group to inactivate the protein (Williamson and Brown, 1979a). Webb et al. (Webb et al., 2003) have shown by MALDI-TOF mass spectrometry that D-serine, L-cysteine, β-hydroxyaspartic acid and β-glutamate bind to the enzyme. A recent study (de Villiers et al., 2010) has provided new insights for the development of ADC inhibitors. As these molecules do not have suitable pharmacochemical and pharmacokinetic properties, recent studies have emphasized the need to discover novel selective drug-like inhibitors against MtbADC (Chopra et al., 2002; Gopalan et al., 2006). However, to date no selective drug-like inhibitor against MtbADC has been reported.

1.7 DRUG DEVELOPMENT

In order to identify a drug like inhibitor we applied chemoinformatics based drug design approach. Chemoinformatics, essentially computational chemistry, is a

process of storing and retrieving information about chemical compounds. One of the major applications of chemoinformatics is in drug discovery. In general, drug development is a long process and involves an average of 10-12 years (Heilman, 1995). The estimated cost of developing a new drug is more than $1 billion. The stages of drug development (Fig. 1.6) are simplified as:

- Discovery phase: identification of target
- Lead optimization
- Toxicology
- Clinical development

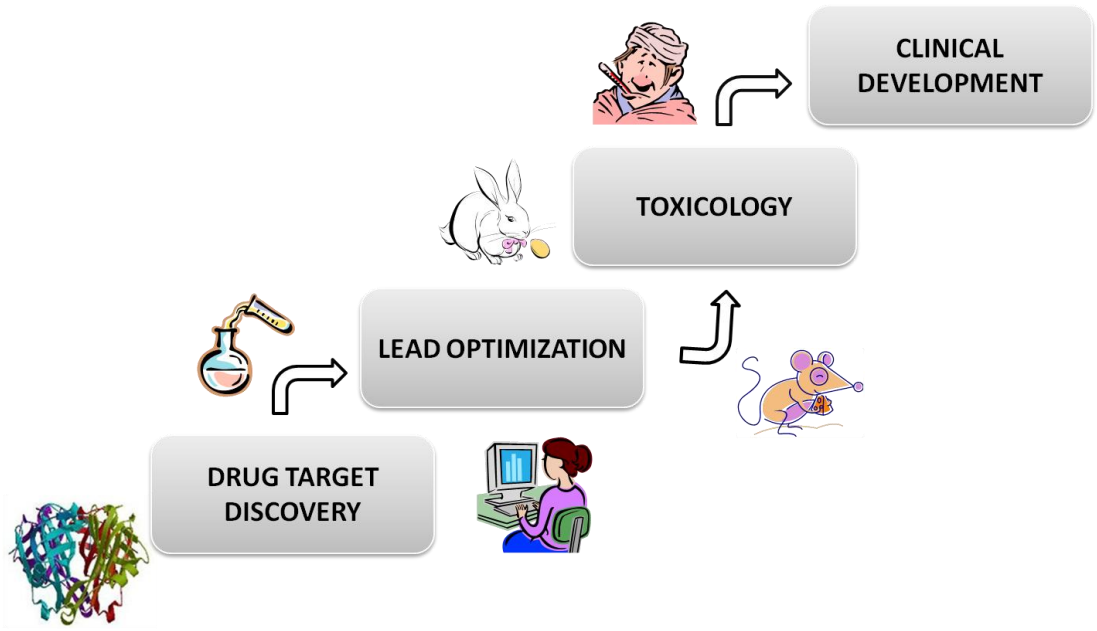

Figure 1.6. Schematic diagram showing the stages in drug development.

Discovery of target. In this phase, a target is first identified against which drugs are developed, designed and synthesized. The target is often a protein that is associated

with the disease and is involved in a biochemical mechanism playing an important role in the cell to accomplish a desired function. At this stage, generally, up to 5,000 to 10,000 candidate molecules are subjected to a rigorous screening process, which can include functional genomics and/or proteomics as well as other screening methods. Once a favored interaction between the drug target and candidate molecules is established, the candidate molecules are validated by additional experiments by checking for the activity of the target protein under the disease condition.

Lead identification and optimization. Lead identification/optimization is one of the important steps in the drug discovery process. Lead molecules can be identified by using structure based drug design where the molecules are stored in a specific format in ligand libraries and are allowed to bind conserved and functionally important residues of the target protein (Fig. 1.7). Binding affinity is measured in terms of docking scores and predicts the *in silico* pose of the candidate molecule with the target protein. Selected molecules are further validated using experimental testing.

Lead molecules can be further optimized by either based on earlier known inhibitors or considering favorable structure-activity relationship of the target protein and candidate drug molecules that possess acceptable pharmacokinetic (PK) or ADME (Absorption/Distribution/Metabolism/Excretion) properties, which provide useful feedback for drug formulation. The PK and ADME studies verify parameters such as AUC (area under the curve), C_{max} (maximum concentration of the drug in blood), and T_{max} (time at which Cmax is reached). These data from animal PK studies are compared with those from early stage clinical trials and correlate the predictive power of animal models. At this, a drug's stability is established. When a candidate molecule shows promises as a therapeutic, it is characterized further by the

molecule's size, shape, strengths and weaknesses, preferred conditions for maintaining function, toxicity, bioactivity, and bioavailability. Early stage pharmacology studies also help to characterize the underlying mechanism of action of the lead compound. Bioanalytical work is the key to proper characterization of the candidate molecule, assay development, developing optimal methods for cell culture or fermentation and determining process yields. It is also critical for supporting preclinical toxicology/pharmacology testing and clinical trials.

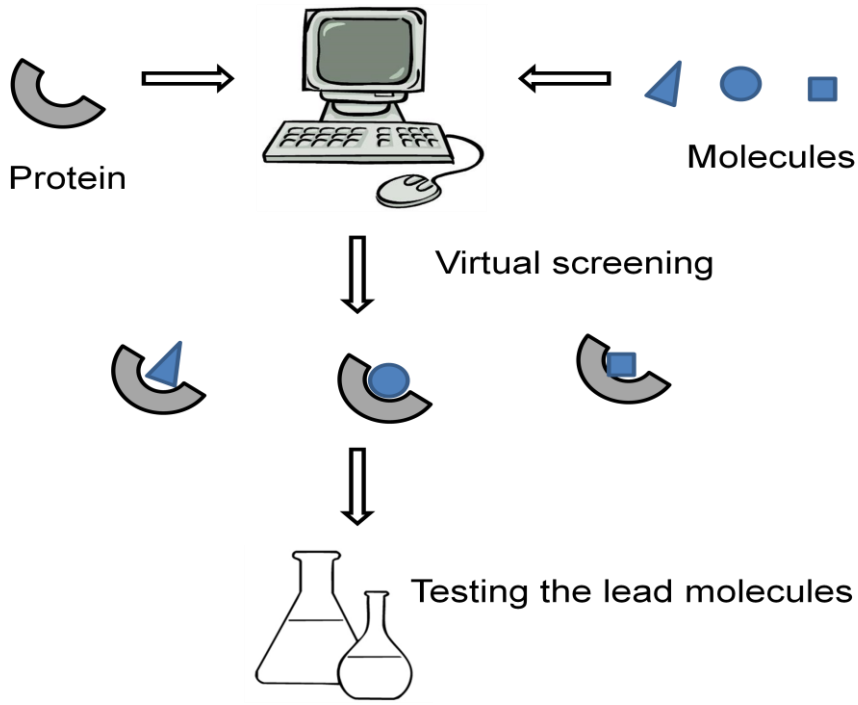

Figure 1.7. Screening for novel inhibitors by molecular docking.

Toxicology. In pre-clinical treatment before administering to human, in vitro and in vivo tests are conducted. Lead molecules need to be tested on animals so as to determine their toxicity. Acute and short term toxicity of the lead molecules are evaluated on animals. The physiological and biological effects of escalating levels of

the lead molecules are observed and how the molecule is absorbed, distributed, metabolized and excreted in animals need to be addressed. Lethal doses of the lead molecules are determined in this phase. Only one out of approximately 5000-10000 molecules facing pre-clinical tests is usually approved for marketing (Klees and Joines, 1997).

1.7.1 Clinical trials

Clinical studies are grouped according to their objectives into three types or phases, Table 1.1.

Phase I clinical development (Human Pharmacology)*:* The Phase I studies are used to evaluate pharmacokinetic parameters and tolerance, generally in healthy volunteers, normally about 20-80 individuals. It is the first stage to test a drug on human subjects. The test usually starts with very small doses and subsequently increased. Escalating doses of a drug are administered to determine the maximum tolerance dose (MTD), which can induce the first symptom of toxicity (Freedman, 1990).

Phase II clinical development (Therapeutic Exploratory) After the Phase I trials, when the initial safety levels of a drug have been confirmed, Phase II clinical studies are conducted on about 100 to 300 patients to assess its efficacy and to determine how well the drug works. Additional safety, clinical and pharmacological studies are also included in this study. During this phase, effective dose, method of delivery, safety and dose intervals of a lead molecule are established (Heilman, 1995; Klees and Joines, 1997; Leonard, 1994).

Phase III clinical development (Therapeutic Confirmatory): This is the final step before FDA approval. Phase III studies are large-scale clinical trials for safety and efficacy in a large patient population, usually 1000 to 3000.

Table 1.1. Phases of clinical trials

	Phase I	**Phase II**	**Phase III**
Purpose	Safety dose Side effects	Safety Efficacy Side effects	Effectiveness Side effects
Sample size	20-80	100-300	1000-3000
Sample criteria	Healthy volunteers	Patients	Patients
Placebo controlled	No	Yes	Yes
Estimated duration	1 year	2 years	3-3.5 years
Estimated cost	$100,000- 1 million	$10-100 million	$10-500 million

1.7.2 Flow chart of the drug development process

Successful virtual screening further confirmed by experimental methods led to identification of several lead inhibitors against proteins involved in important processes of cell(Kolb et al., 2009). AHAS (Acetohydroxy Acid Synthase) (Wang et al., 2007), Aldose reductase (Steuber et al., 2007), CDC25 phosphatase (Montes et al.,

2007) , DNA gyrase (Ostrov et al., 2007), FFAR1 (Free Fatty Acid Receptor 1) (Tikhonova et al., 2008), Histamine H4 (Kiss et al., 2008), Pim-1 kinase (Pierce et al., 2008), PNP (Purine Nucleoside Phosphorylase) (Pereira et al., 2007), EphB4 (Kolb et al., 2008) with inhibitors having IC_{50} 15.2, 0.53, 13, 50, 95.8, 0,091, 18.9, 1.5 µM, respectively were identified by bioinformatics followed by experiments.

To determine potential inhibitors against Mtb ADC, the structure based drug design approach was used. To the best of our knowledge, this is the first chemoinformatics-based drug design approach to identify novel and selective inhibitors of MtbADC.

After determining potential lead molecules, we validated if they could inhibit ADC activity using proton NMR. We compared the inhibition properties of the newly identified and previously known ADC inhibitors. This approach allows rapid pharmacophore development for novel protein targets. Furthermore, we tested the efficiency of the lead molecules if they are able to kill Mtb. Below is the flow chart showing the steps in drug development (Fig. 1.8).

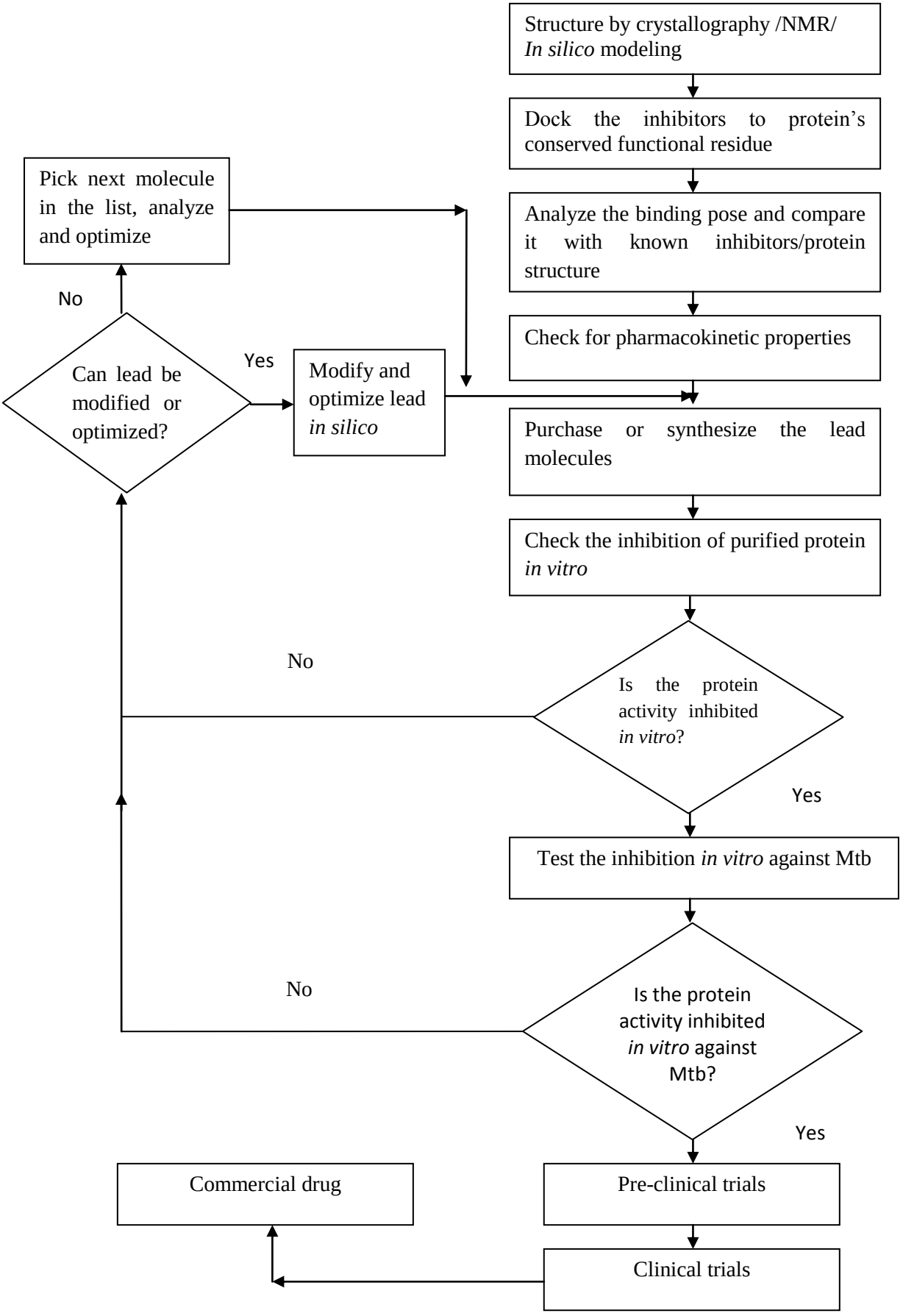

Figure 1.8. The flow chart of the process used to identify inhibitors against MtbADC.

CHAPTER 2

MATERIALS AND METHODS

CHAPTER 2. MATERIALS AND METHODS

2.1 MODELING OF PROCESSED MTBADC STRUCTURE

Structural alignment of unprocessed and processed *E. coli* ADC structures (Schmitzberger et al., 2003) by the use of Multiprot (Shatsky et al., 2002) shows a root mean square deviation (RMSD) of 0.19 Å for 89 Cα atom pairs. This suggests that the unprocessed and processed ADC structures are highly similar. Thus, in preparation for virtual screening, unprocessed *Mycobacterium tuberculosis* L-aspartate α-decarboxylase (MtbADC, PDB ID: 2C45) was modified to the processed form, in which Ser25 was substituted with a pyruvoyl group by the use of Modeller (Eswar et al., 2001). The active site and conserved and functionally important residues were selected by structural alignment of the processed MtbADC with processed *Thermus thermophilus* ADC (TthADC)TthADC:fumarate and *Helicobacter pylori* ADC (HpyADC) HpyADC:isoasparagine complex structures using Multiprot (Shatsky et al., 2002) and visualized using PYMOL (DeLano, 2002). As the active site is at a dimer interface, an appropriate dimer was prepared. The model was further refined by adding missing hydrogen and was submitted to a series of restrained and partial minimization using the optimized potentials for liquid simulations all-atom (OPLS_AA) force field (Jorgensen et al., 1996) in the Protein Preparation Wizard of Schrödinger (2009)(Fig. 2.1).

2.2 STRUCTURE BASED VIRTUAL SCREENING

To identify inhibitors against the above processed MtbADC, flexible ligand based high-throughput virtual screening (HTVS) mode of Glide 5.5 (Halgren et al., 2004) was carried out using 333,761 molecules of commercially available ligands from the

Maybridge (14,400 molecules; www.maybridge.com) and Zinc (Irwin and Shoichet, 2005)zinc.docking.org, including National Cancer Institute (hereafter NCI; 316,181 molecules) and the United States of America Foods and Drug Administration approved drugs (hereafter FDA; 3,180 molecules)] databases.

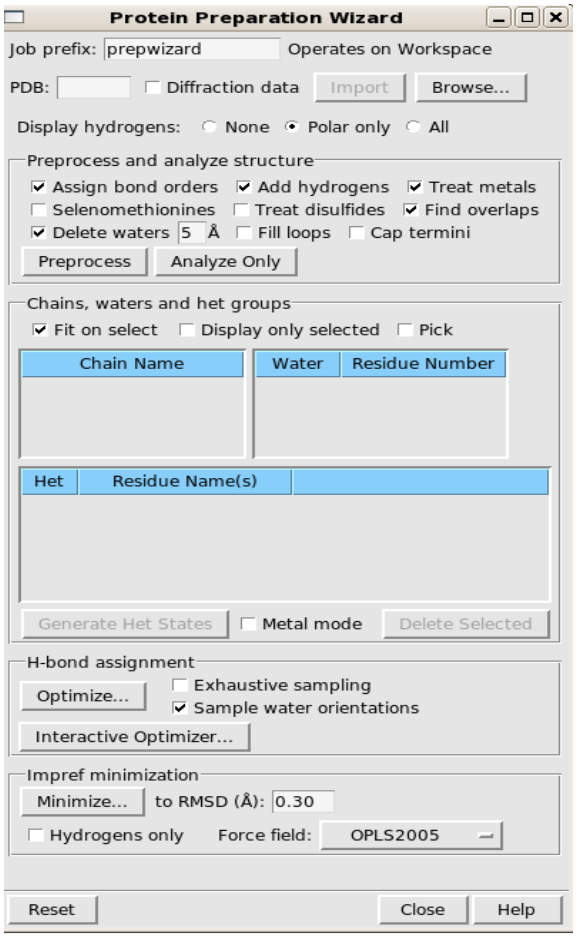

Figure 2.1. Preparation of protein by the use of Protein Preparation wizard in Schrödinger suite.

Using the TthADC:fumarate crystal structure as a guide, fumarate was docked with processed MtbADC and the docking score was used as a reference to identify drug-like inhibitors. The Maybridge, NCI and FDA molecules, as well as fumarate, were prepared by accounting for missing hydrogens, possible ionized states,

tautomers and low energy ring conformations using the Glide LigPrep application (2009) (Fig. 2.2).

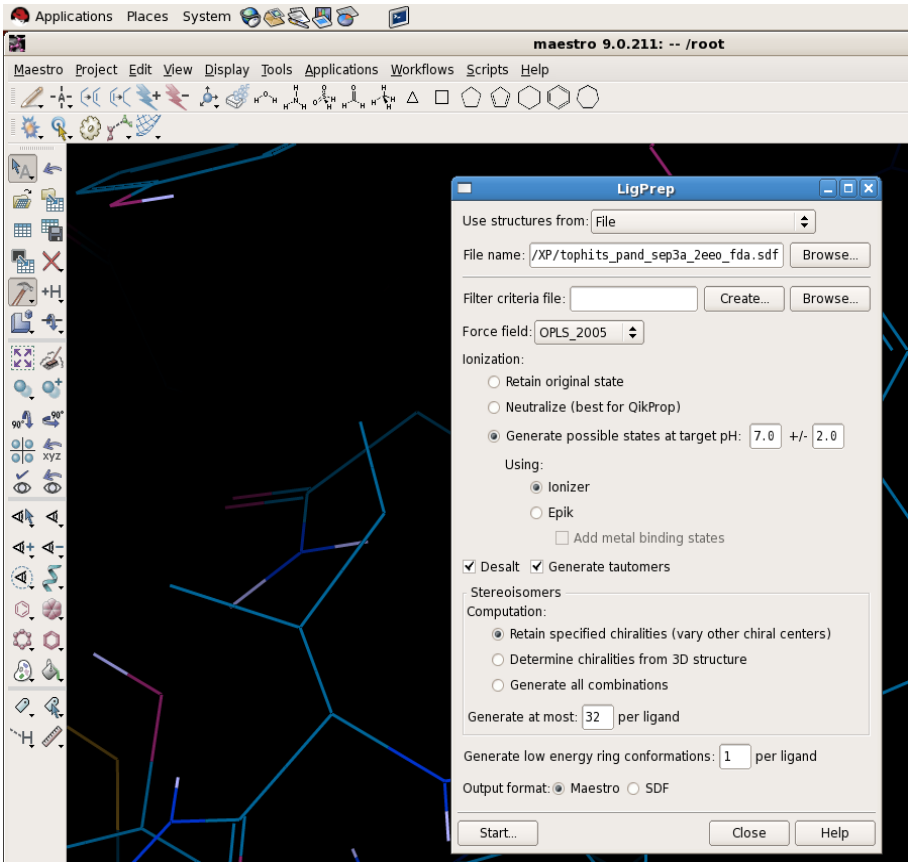

Figure 2.2. Ligand preparation by the use of Ligprep panel in Schrödinger suite.

Receptor tab has three sections: defining receptor, Van der Waals radii scaling, and charge scaling (Fig.2.3). Fumarate was selected so that receptor grid can be generated excluding it in define receptor section. In Van der Waals radii scaling section, a scaling factor of 1.0 was set to van der Waals (VDW) radii for the atoms of the residues that presumably interact with ligands and the partial atomic charge was set to less than 0.25. By scaling of van der Waals radii, Glide provides an account of protein flexibility. Vander Waals radius of the non polar receptor atoms can be

controlled by Vander Waals radius scaling section. Default value is 1.0. Partial charge threshold define nonpolar atoms. Those non polar atoms whose partial charge is less than or equal to the text box, scaling of Vander Waals radii is performed, Default value is 0.25 (Fig 2.3).

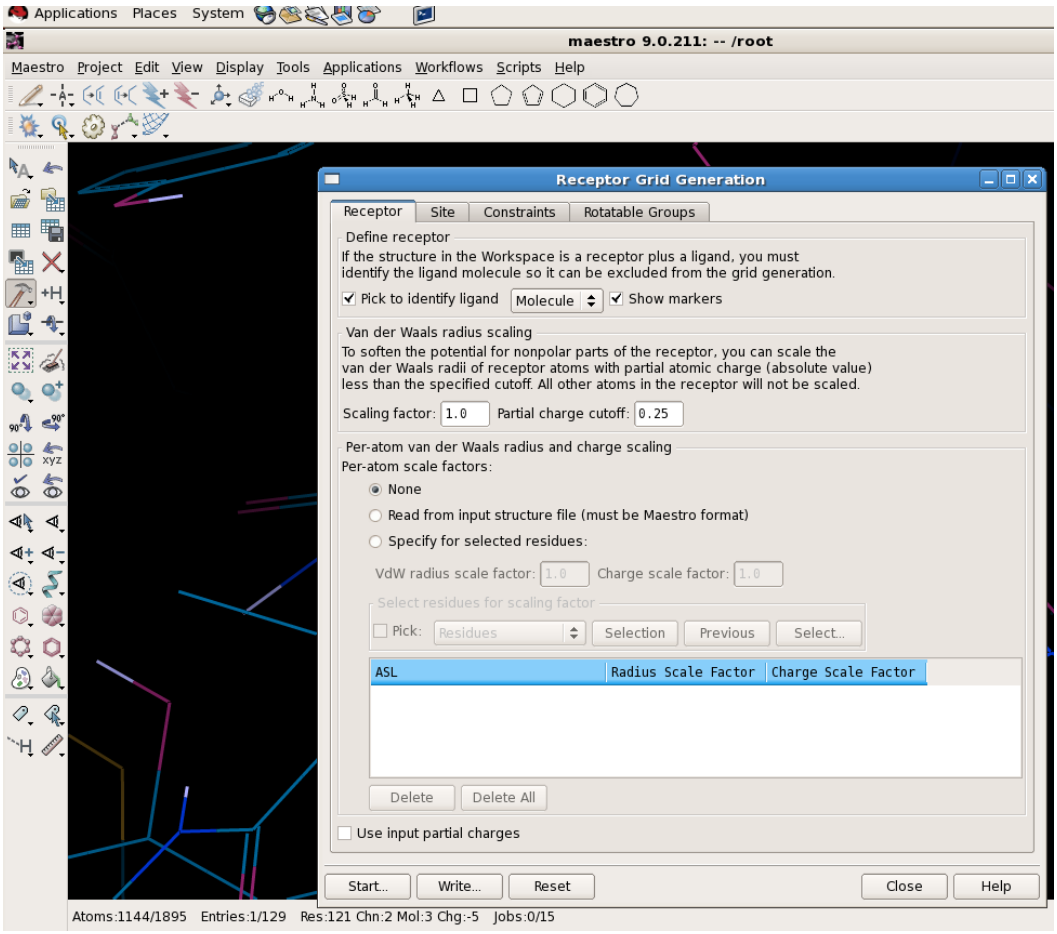

Figure 2.3. Receptor tab of Receptor Grid generation panel in Schrödinger suite.

A grid file was generated using the Receptor Grid Generation protocol with centroid at the active site of the enzyme (Fig.2.4). Ligands were then allowed to dock with the high throughput screening (HTVS) mode and all the obtained molecules were subjected to the Glide extra precision (XP) mode of docking, which performs

extensive sampling and provides reasonable binding poses (Halgren et al., 2004) (Fig.2.5).

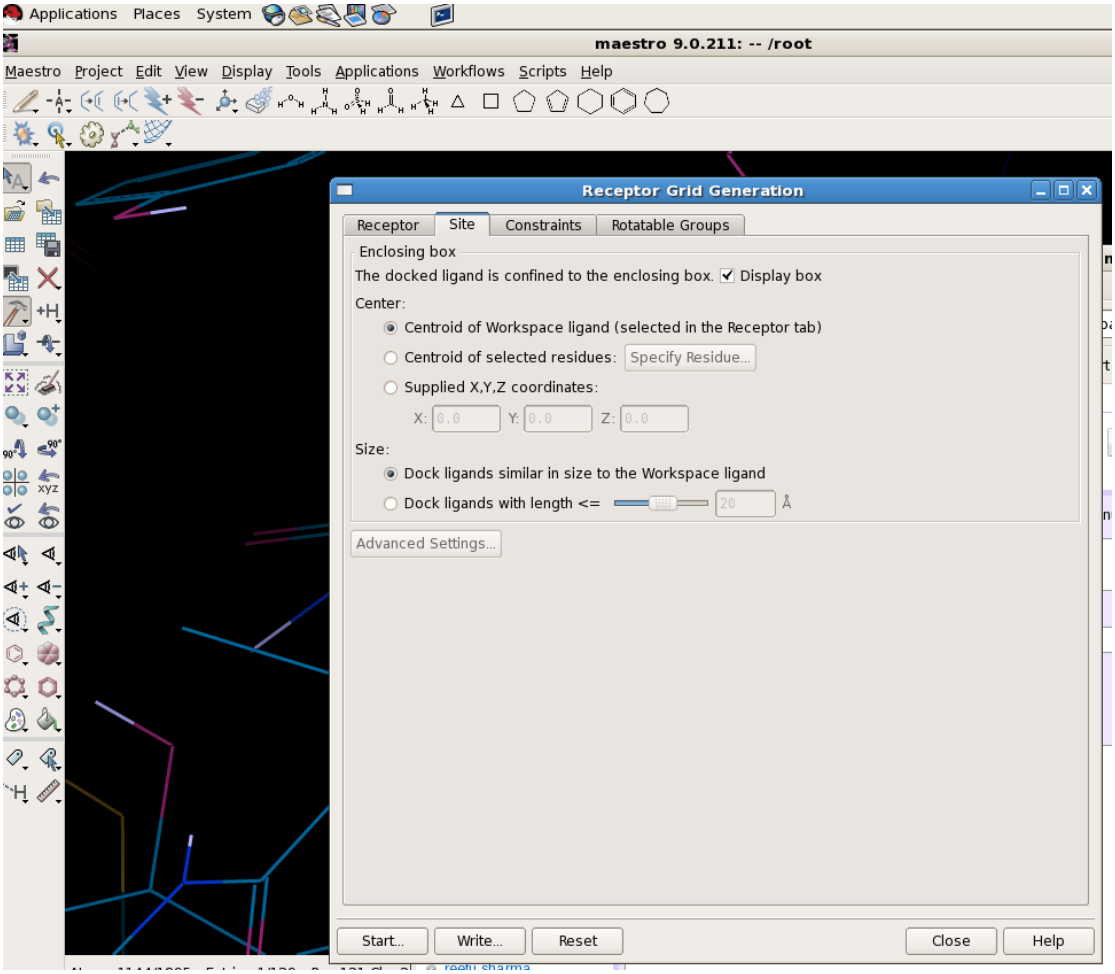

Figure 2.4. Site tab in Receptor Grid generation panel of Schrödinger suite.

At this stage, ligands were accepted only if: (i) they interacted with the residues that bind substrate analogs in the TthADC:fumarate and HpyADC:isoasparagine complex structures, and (ii) the binding affinity glide scores (G-scores) were better than the reference MtbADC:fumarate score. These ligands were further assessed for their drug-like properties based on Lipinski's rule of five (Lipinski et al., 1997) and also the absorption, distribution, metabolism, excretion and

toxicity (ADMET) properties, calculated with QikProp version 3.2 (Schrödinger) (Jorgensen, 2006). In addition, the docking poses and structural properties of some of the known ADC inhibitors, phenylhydrazine (PubChem chemical database ID CID7516), L-cysteic acid (CID72886), Oxaloacetate (CID164550) and D-serine (CID71077), were compared with those of the selected drug-like molecules. As the active site of MtbADC is located at the interface of a dimer, the selected molecules were cross-verified by performing virtual screening against processed monomeric ADC.

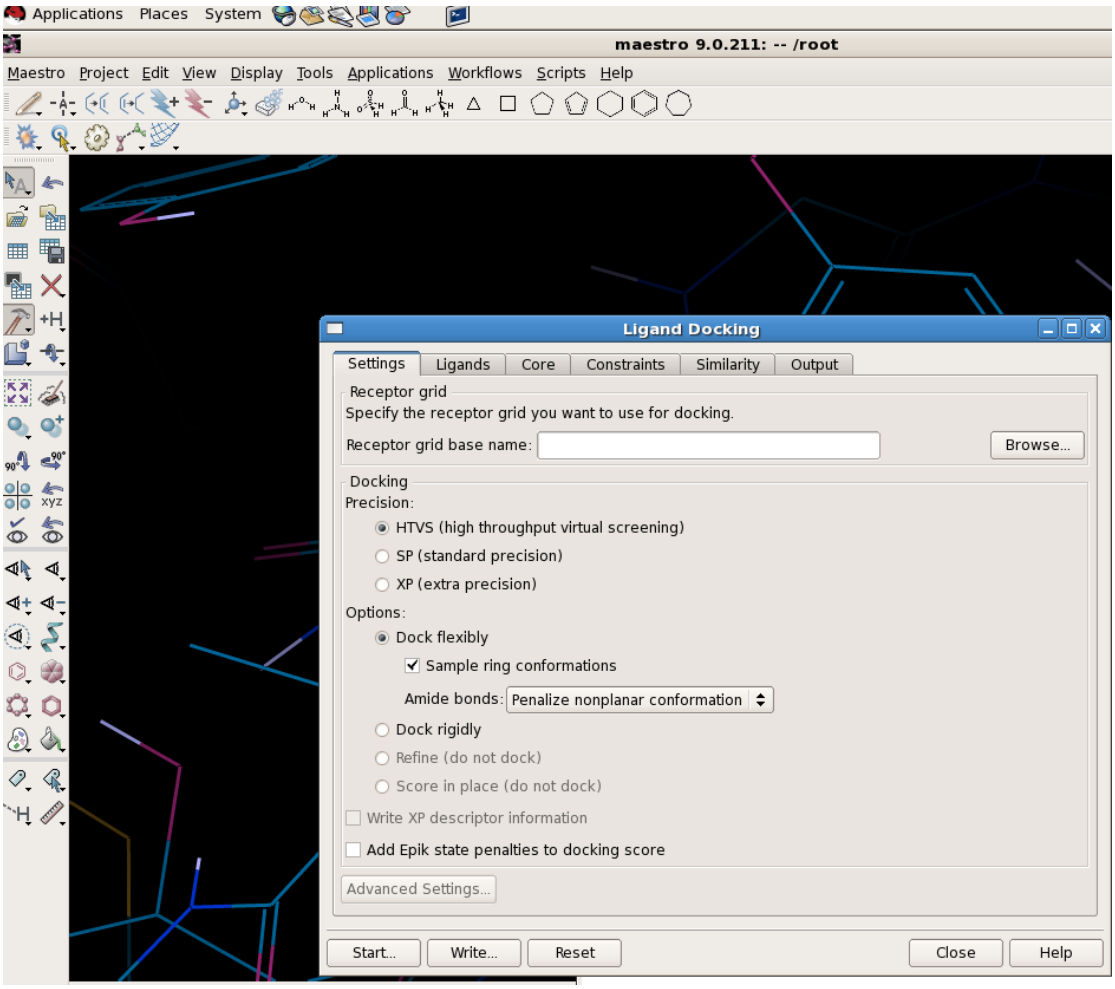

Figure 2.5. Ligand docking to receptor by ligand docking panel of Schrödinger suite.

2.3. NON CROSS-REACTIVITY WITH HUMAN PYRUVOYL-DEPENDENT ENZYMES

The mechanism of action of the ADC protein is similar to other pyruvoyl dependent enzymes, such as histidine decarboxylase, S-adenosylmethionine (SAM) decarboxylase and phosphatidyl serine decarboxylase, which catalyze reactions utilizing the pyruvoyl residue as a prosthetic group (Recsei and Snell, 1984; Williamson and Brown, 1979a). As of now, only the crystal structure of human SAM decarboxylase (PDB id: 3H0W) (Bale et al., 2009) is available. In order to avoid any potential side-effect and cross reactivity of lead molecules with SAM decarboxylase, the inhibitors from the previous step that interacted with the pyruvoyl group or conserved substrate binding residues Glu247, Phe223, Phe7 or Glu67 (SAM decarboxylase numbering) were rejected (Fig. 3.2). Furthermore, the inhibitors were checked for suitable ADMET properties and accepted.

2.4 PREPARATION OF *E. COLI* BL21 (DE3) COMPETENT CELLS

Original *E. coli* BL21 (DE3) cell stock was streaked on an LB plate without any antibiotics and colonies were allowed to grow overnight at 37 °C. A single colony from the plate was inoculated in 5 ml LB overnight, with shaking at 37 °C. The next day, the culture was transferred to 100 ml LB and incubated until OD_{600} reached 0.4-0.5. The culture was chilled on ice for 10 min and was centrifuged at 4000 g for 15 min at 4 °C. The supernatant was discarded and the pellet was gently re-suspended in 50 ml 0.1M $CaCl_2$. It was kept on ice for 40 min, again centrifuged at 4000 g for 15 minutes at 4 °C and the supernatant was discarded. The pellet was re-suspended in chilled solution containing 0.1M $CaCl_2$ and 15% glycerol and was stored in 50 µl aliquots at -80 °C.

2.5 PROTEIN EXPRESSION AND PURIFICATION

The gene encoding full length MtbADC was inserted into the pET21c(+) expression vector between the NdeI and XhoI restriction sites (Chopra et al., 2002). 1 µl of 105 ng DNA was added to 50 µl of thawed competent cells and kept on ice for 30 min. Heat shock was given in 42 °C water bath for 45 sec and the competent cells were was kept on ice for 2 min before adding 1 ml of LB and incubated at 37 °C for 60 min. 50-100 µl of the transformed cell culture was spread on an LB agar plate containing 100 µg/ml ampicillin and incubated overnight at 37 °C.

Cleaved MtbADC protein was overexpressed, purified and processed as previously described (Chopra et al., 2002; Gopalan et al., 2006). A single colony was inoculated in 50 ml culture in 250 ml flask with 100 µg/ml ampicillin and was allowed to grow overnight at 37 °C. 10 ml of the overnight culture was used to inoculate 1 litre of LB with ampicillin and after approximately 2 hours, at OD_{600nm} 0.6, protein overexpression was induced with 0.5 mM IPTG at 37 °C for 4-5 hours. Cells were harvested at 5000 g for 15 min. Bacterial pellet from 1 litre culture was resuspended in 30 ml of lysis buffer A (10 mM Tris–HCl, pH 8.0, 0.8% NaCl, 1 mM PMSF, 1 mM β-mercaptoethanol) and sonicated at 25% amplitude for 2 rounds of 3min each (1 sec on and 2 sec off pulse) using the Sonics Vibra system. The lysate was then pelleted at 39,000 g for 30 minutes. The supernatant was then applied to 2.5 ml of pre-equilibrated Ni^{2+}-NTA resin (Clontech) and rotated on a rocker for 1 hour at 4 °C for binding. The resin containing bound protein was then subjected to three washes with buffer A. The protein was eluted with elution buffer (10 mM Tris-HCl pH 7.5, 0.8% NaCl and 250 mM imidazole).

The Ni-NTA affinity purification was followed by gel filtration where pre-equilibrated Superdex-200 column (GE Healthcare) with buffer (10 mM Tris-HCl pH

7.5, 50 mM NaCl, 1 mM PMSF) and the fractions corresponding to molecular weight approximately 60 kDa were pooled together, concentrated using Centricon concentrator (Millipore) and protein concentration was determined by the Bradford assay method and stored at -80 °C. Purity of the protein was analyzed by 15% SDS PAGE and mass spectroscopy. The protein was kept at 37 °C for 48 hours for self cleavage to form the active α-form with N-terminal pyruvoyl group (Chopra et al., 2002).

2.6. INHIBITOR PREPARATION

After determining potential inhibitors using chemoinformatics based drug design approach the following known ADC inhibitors: Oxaloacetate (***K1***), DL-*threo*-β-hydroxyaspartate (***K2***), L-glutamate (***K3***), L-cysteic acid (***K4***), succinate (***K5***), L-serine (***K6***), and D-serine (***K7***), while D-tartrate (***I1***, ZINC00895296), L-tartrate (***I2***, ZINC00895301), 2,4-dihydroxypyrimidine-5-carboxylate (***I3***, ZINC00901606), D-tagatose (***I4***, ZINC03830878), (4S)-1,3-thiazolidin-3-ium-4-carboxylate (***I5***, ZINC00967474), α-D-arabinopyranose (***I6***, ZINC03606295), and 1,2-dihydropyrazolo[3,4-d]pyrimidin-4-one (***I7***, ZINC05177572) were tested for the first time, stimulated by the hits recently identified in the chemoinformatics study . The compounds were purchased from Sigma-Aldrich, Germany (***K1***-***K7*** and ***I1***-***I4***), or from Labotest KG, Germany (***I5***-***I7***), in the highest commercially available purity (> 97%)(Sharma et al., 2012a). Williamson and Brown (Williamson and Brown, 1979a) reported the inhibition constant (K_i) of most of the known compounds. The inhibitors and substrate (aspartic acid) were prepared in D_2O as 2-30 mM stock solutions and 1 mM working solution. Determination of IC_{50}, the concentration of an inhibitor for

50% inhibition *in vitro*, was quantified on 1 mM substrate, based on the Cheng-Prusoff equation ——— (Yung-Chi and Prusoff, 1973).

2.7 NUCLEAR MAGNETIC RESONANCE SPECTROSCOPY

To examine the inhibitory property of the potential inhibitors we employed a proton NMR based assay**.** Proton NMR spectra were collected on a 400 MHz Nuclear Magnetic Resonance, (JEOL ECX 400) instrument using 5 mm 400 series NMR tubes (Sigma Aldrich, Germany). For NMR experiments, the protein was prepared in deuterium oxide (D_2O, Sigma-Aldrich) at final protein concentration of 2.8 µM, as determined by spectroscopy, using a calculated extinction coefficient of using an extinction coefficient ε_{280} = 6400 $M^{-1}cm^{-1}$ (Chopra et al., 2002) and measured on a Varian Cary 4000 UV-Vis spectrophotometer).. The Michaelis Menten constant K_m of the enzyme has been reported as 219 µM (Chopra et al., 2002). The enzymatic activity was followed by ^1H NMR using a Jeol JNM-ECX 400 spectrometer.

Experiment was initiated with 1 mM aspartic acid and 2.8 µM enzyme. Time course reactions were carried out at room temperature. NMR spectra with peaks corresponding to the protons of aspartic acid and β-alanine were recorded with time. Well separated peaks that correspond to the hydrogens at C1 (around 3.85 ppm) and C2 (around 2.75 ppm) of the substrate aspartate and the counterparts (around 3.05 and 2.5 ppm) in the product β-alanine were integrated to compute the concentrations $[A_{asp}]_t$ and $[A_{ala}]_t$, at any given time 't'. The percentage of product formed (or conversion of substrate) at any time is given by ———— . The experiments were repeated in triplicate.

2.8. *IN VITRO* ACTIVITY AGAINST *M. TUBERCULOSIS*

Compounds were dissolved in either distilled water or DMSO at a concentration of 5 or 10 mg/ml. *M. tuberculosis* H37Rv was grown in the MB 7H9 - tween media (ADC was added as media enrichment) until the early-logarithmic phase (A_{600nm} of 0.8) and the cells were subsequently diluted to an A_{600nm} of 0.02 (~2×10^6 cfu/ml) in the same media. 1 ml aliquots of this culture were incubated with varying concentrations of the compounds along with controls (containing appropriate concentrations of DMSO) for 7 days at 37 °C with constant shaking at 200 g. The cultures were serially diluted with the MB 7H9 media and CFU was determined by plating on MB 7H11 agar plates after incubation at 37 °C for 3–4 weeks. MIC_{99} value is the concentration of the compound which resulted in 99% inhibition of the growth.

CHAPTER 3

RESULTS

CHAPTER 3. RESULTS

3.1. STRUCTURAL OVERVIEW OF L-ASPARATE α-DECARBOXYLASE

Gopalan et al. (Gopalan et al., 2006) have solved the crystal structure of uncleaved MtbADC (PDB ID: 2C45) at 2.99 Å resolution. MtbADC has a double-Ψ β-barrel structure, consisting of two α-helices, seven β-strands and two 3_{10} helices.

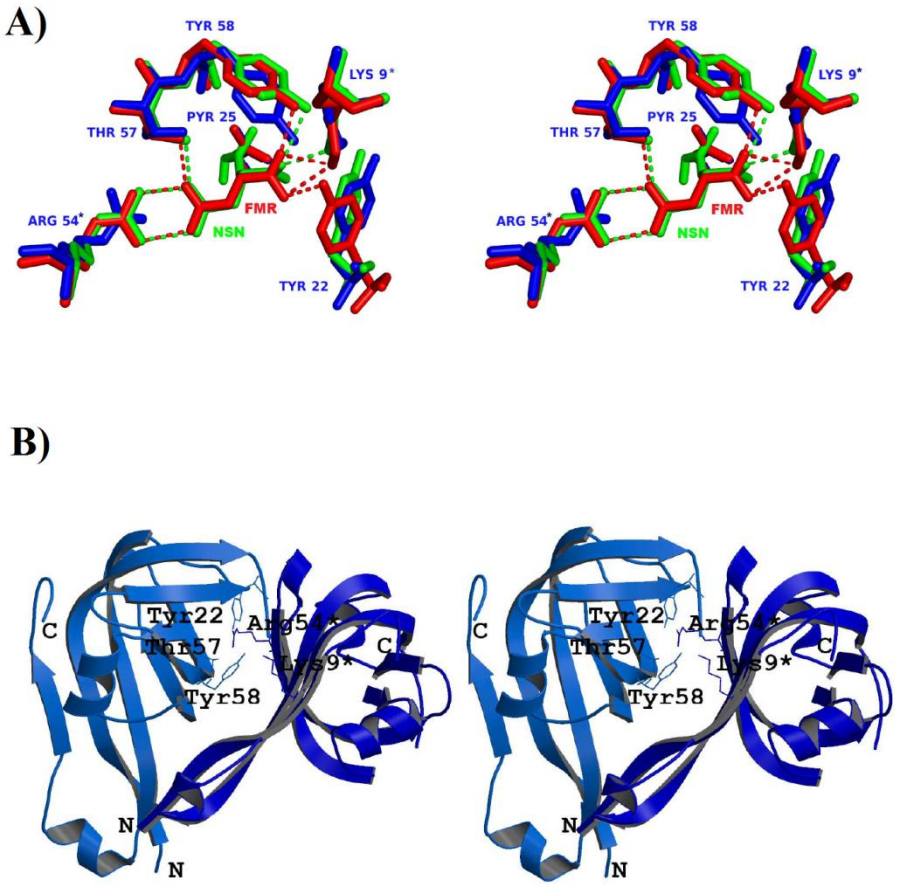

Figure 3.1. Conserved functional residues of ADCs that bind to substrate. (A) Stereo view of structural superimposition of processed MtbADC (blue), processed *Thermus thermophilus* ADC complexed with substrate analog fumarate (red and PDB id: 2EEO) and *Helicobacter pylori* ADC complexed with substrate analog isoasparagine (green, PDB id: 1UHE). The conserved and interacting

residues are labeled according to MtbADC and the interactions are shown as dashed lines. (**B**) Stereo view of the active site in the dimer interface. The figure was prepared using Molscript (Kraulis, 1991) and Raster3D (Merritt and Bacon, 1997).

The structural superimposition of modeled processed MtbADC, TthADC:fumarate complex and HpyADC:isoasparagine complex shows that both substrate analogs bind to the active site (Fig. 3.1A), which is formed at the interface of a dimer in a similar orientation and are surrounded by conserved residues (Fig. 3.1B). The three proteins align with pair-wise RMSDs of less than 1 Å. Also, the binding of the substrate analogs to TthADC and HpyADC does not significantly change the structure of the enzyme which is evident from the RMSD values of 0.19 and 0.13 Å for 95 C_α atom pairs, respectively. Sequence and structural analyses reveal that the strictly conserved residues among ADCs are Lys9, His11, Tyr22, Gly24, Pyr25, Arg54, Thr57, Tyr58, Gly73, Ala74, Ala75, Ile86 and Asn112 (MtbADC numbering). The substrate analogs interact with Lys9*, Pyr25, Arg54*, Thr57, Tyr58 (* represents a residue from another subunit of the dimer), where Lys 9* keeps the α-carboxyl group of the substrate deprotonated by forming an ion pair (Lee and Suh, 2004), and Pyr25 is a cofactor responsible for the activity of the enzyme (Schmitzberger et al., 2003). Furthermore, Arg54* contributes to substrate specificity (Lee and Suh, 2004), Thr57 interacts with substrate and plays an important role in catalysis (Lee and Suh, 2004) and Tyr58 acts as a proton donor in the decarboxylation reaction (Saldanha et al., 2001).

3.2. SELECTION OF INHIBITORS

Binding of a ligand to at least one conserved functional residue is likely to interfere with the binding or catalysis of substrate and would result in inhibition of the function of the protein. Out of 333,761 molecules from the three public ligand databases, 190 hits from the Maybridge, 473 hits from NCI and 140 hits from FDA databases were initially obtained with the high throughput virtual screening (HTVS) mode. The ligands were allowed to bind with processed MtbADC in the more precise Glide extra-precision mode (Glide XP) and subsequently 28 ligands (3 Maybridge, 7 NCI and 18 FDA) with binding energy (-4.9 kcal/mol or higher) better than that for fumarate (-4.2 kcal/mol) were selected. These ligands interact with at least one of the experimentally determined conserved functional residues (Table 3.1).

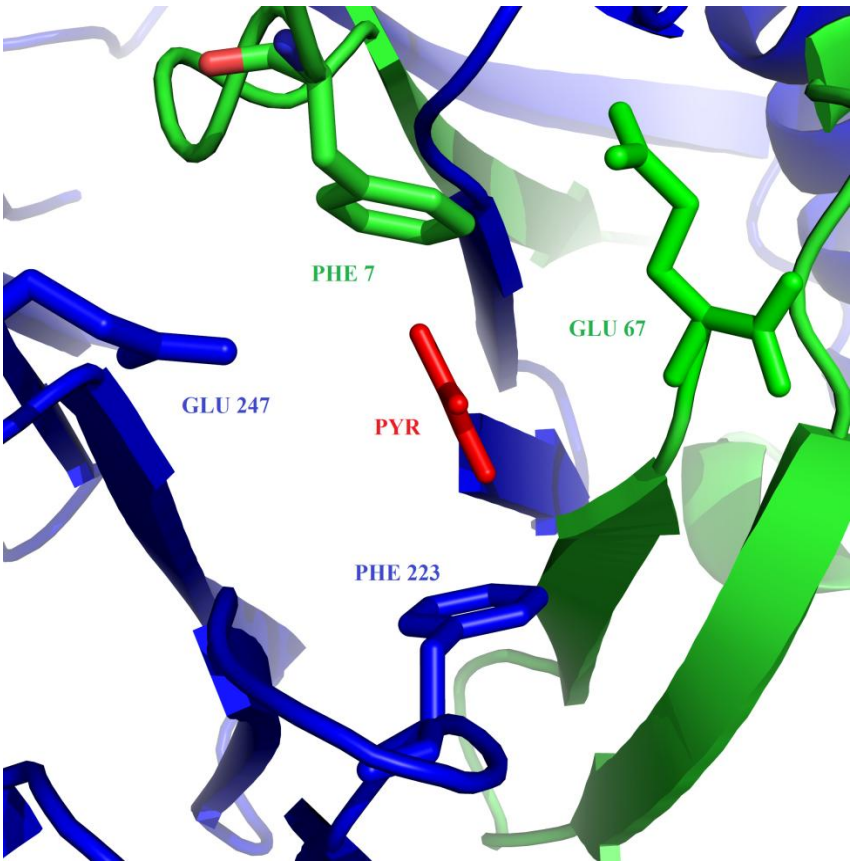

Figure 3.2. Active site residues of SAM decarboxylase (SAM decarboxylase numbering.).

Of 28, seven ligands (5 FDA and 2 NCI) interact with the MtbADC pyruvoyl group, suggesting that they could cross-react with other pyruvoyl dependent enzymes. An assessment of cross-reactivity of the putative inhibitors with the human SAM decarboxylase structure, a representative of pyruvoyl dependent enzymes, identified that only one (ZINC03871163) of the seven molecules does not interact with any of the conserved substrate binding residues Glu247, Phe223, Phe7 or Glu67 (SAM decarboxylase numbering) or the pyruvoyl group of SAM decarboxylase (Fig. 3.2).

Eight lead molecules significantly satisfy the pharmacokinetic factors that are defined for human use and qualify as potential drug-like molecules. They are: (2S,3R,4S,5S)-2,3,4,6-tetrahydroxy-5-mercaptohexanal (ZINC03871163), (2S,3S,4S,5R)-2(hydroxymethyl)tetrahydro-2H-pyran-2,3,4,5-tetraol (ZINC03830878), 3-amino-4-(propylamino) cyclobutane-1,2-dione (LIGAND10436), (S)-thiazolidin-3-ium-4-carboxylate (ZINC00967474), (S)-5-acetoxy-4-methylpentanoate (ZINC02036492), (2S,3S,4R,5R)-tetrahydro-2H-pyran-2,3,4,5-tetraol (ZINC03606295), (2S,3S,4R,5S)-2,5-bis(hydroxymethyl)tetrahydrofuran-2,3,4-triol (ZINC03830875) and 1H-pyrazolo[3,4-d]pyrimidin-4(7H)-one (ZINC05177572). The interacting residues for these lead molecules are shown in Table 3.1 and their structures are shown in Fig. 3.3. The pharmacokinetic properties of the 28 ligands were assessed by the use of Qikprop (Table 3.2).

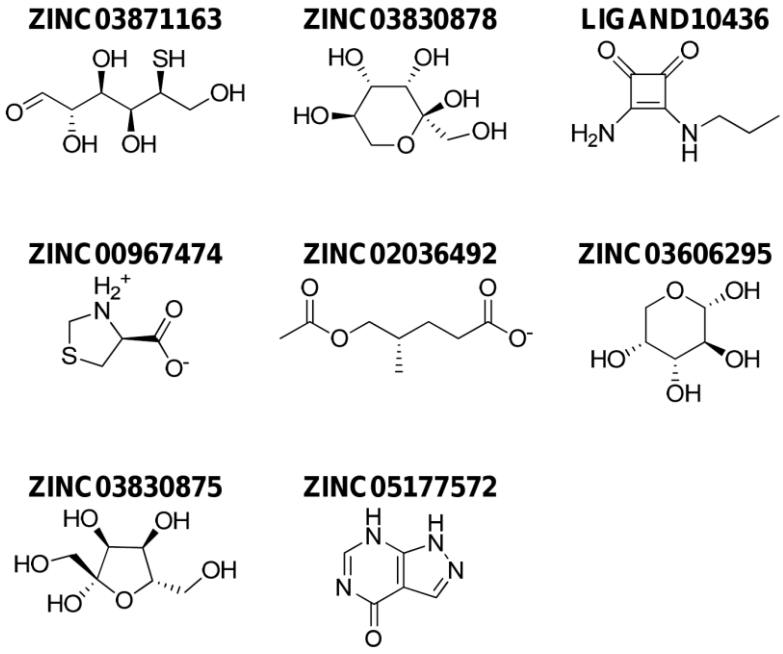

Figure 3.3. Chemical structures of the eight lead molecules. ZINC03871163: (2S,3R,4S,5S)-2,3,4,6-tetrahydroxy-5-mercapto-hexanal, ZINC03830878: (2S,3S,4S,5R)-2(hydroxymethyl) tetrahydro-2H-pyran-2,3,4,5-tetraol, LIGAND10436: 3-amino-4-(propylamino)cyclobutane-1,2-dione, ZINC00967474: (S)-thiazolidin-3-ium-4-carboxylate, ZINC02036492: (S)-5-acetoxy-4-methylpentanoate,ZINC03606295:(2S,3S,4R,5R)tetrahydro2Hpyran2, 3,4,5tetraol,ZINC03830875:(2S,3S,4R,5S)2,5bis(hydroxymethyl)tetra hydrofuran-2,3,4-triol,ZINC05177572: 1H-pyrazolo[3,4-d]pyrimidin-4(7H)-one. tetraol (ZINC03606295), (2S,3S,4R,5S)-2,5-bis(hydroxymethyl)tetrahydrofuran-

Table 3.1. The 28 ligand hits from the Maybridge, NCI and FDA databases which interact with at least one of the conserved functional residues of MtbADC residues involved in substrate binding and their glide score (kcal/mol). The ligands are ranked according to their glide scores in their respective databases. The ligands that interact with Pyr25 are in bold. The entries of Table 3.3 are underlined. Two Inhibitors validated after NMR based assay (Sharma et al., 2012b) are in italics.

Molecule ID	**Glide score**	**Interacting residues**				
<u>FDA database</u>						
	-6.783547	Thr57	Gly73	Asn72	Arg54	
ZINC00895296						
ZINC03831017	-6.524427	Pyr25	Asn72	Thr57		
ZINC02556854	-6.378547	Asn72	Gly73	Thr57		
ZINC02041302	-6.352301	Arg54	Gly73	Asn72	Pyr25	Tyr58
ZINC02507451	-6.256358	Asn72	Gly73	Arg54	Pyr25	Tyr58
ZINC00895297	-6.062757	Asn72	Thr57	Tyr58	Lys9	
ZINC01532640	-6.057464	Thr57	Asn72			

ZINC03830878	-6.028674	Arg54	Asn72			
ZINC12358606	-5.884999	Asn72	Thr57	Tyr58	Lys9	
ZINC03831018	-5.879572	Arg54	Asn72	Thr57	Tyr58	
ZINC12362045	-5.620917	Gly73	Asn72	Pyr25		
ZINC00967474	-5.424642	Tyr58	Asn72			
ZINC03830688	-5.11056	Gly73	Thr57	Pyr25		
ZINC03606295	-5.106771	Arg54	Thr57	Asn72	Tyr58	Gly73
ZINC01532526	-5.001161	Arg54	Thr57	Asn72	Gly73	
ZINC03830875	-4.965374	Asn72	Arg54	Thr57		
ZINC05177572	-4.9588	Asn72	Arg54	Tyr58		
ZINC01529732	-4.940066	Arg54	Thr57	Tyr58	Lys9	

Maybridge database

LIGAND10436	-6.001754	Tyr58	Gly73	Asn72		

LIGAND7497	-5.43	Asn72	Thr57	Arg54		
LIGAND6555	-5.415633	Asn72	Arg54	Tyr58		
NCI Database						
ZINC18141652	-6.667792	Asn72	Tyr58			
ZINC03871163	-6.049714	Gly73	Asn72	Tyr22	Arg12	Pyr25
	-5.77977	Tyr58	Gly73	Thr57	Arg54	
ZINC00901606						
ZINC01583698	-5.709624	Arg54	Thr57	Pyr25	Tyr22	Asn72
ZINC08733367	-5.669926	Asn72	Gly73	Tyr58		
ZINC02597098	-5.51695	Arg54	Thr57	Tyr58		
ZINC02036492	-5.286988	Thr57	Tyr58	Lys9		

Table 3.2. Pharmacokinetic properties of the 28 ligands

Molecule ID	MW	HD	HB	QPlogPo/w	QPlogS	QPlogHERG	QPPCaco	Percent human oral absorption
FDA database								
ZINC00895296	150.088	2	5.4	-0.399	-0.479	1.033	1.573	28.133
ZINC03831017	182.173	6	10.2	-3.06	-0.091	-2.987	82.485	30.372
ZINC02556854	182.173	6	10.2	-3.08	-0.081	-2.954	62.848	28.137
ZINC02041302	182.173	6	10.2	-3.099	-0.07	-3	49.602	26.19
ZINC02507451	307.966	4	6.8	0.252	-1.433	-3.38	513.35	76.934
ZINC00895297	150.088	2	5.4	-0.415	-0.47	1.069	1.472	27.518
ZINC01532640	182.173	6	10.2	-3.093	-0.074	-2.989	55.067	27.033
ZINC03830878	180.157	5	8.3	-1.697	-0.812	-2.529	106.912	53.326

ZINC12358606	150.088	2	5.4	-0.415	-0.47	1.069	1.472	27.518
ZINC03831018	182.173	6	10.2	-3.084	-0.08	-3.046	64.442	28.312
ZINC12362045	182.173	6	10.2	-3.074	-0.084	-2.964	68.789	28.879
ZINC00967474	133.165	2	4	-2.033	-0.416	-1.401	41.887	44.073
ZINC03830688	307.966	4	6.8	0.253	-1.378	-3.278	538.306	77.308
ZINC03606295	150.131	4	8.5	-1.722	-0.861	-2.105	192.429	57.744
ZINC01532526	146.146	5	5.5	-4.215	1.237	-0.419	1.03	2.491
ZINC03830875	180.157	5	8.3	-1.689	-0.677	-2.678	106.382	53.333
ZINC05177572	136.113	2	4.5	-0.551	-2.262	-2.942	166.698	63.49
ZINC01529732	179.19	4	5.5	-2.512	-0.261	-0.059	0.66	9.007
Maybridge database								
LIGAND10436	154.168	3	6	-0.859	-1.13	-3.286	125.584	59.484

LIGAND7497	166.197	1	4	0.825	-2.516	-3.899	634.788	81.939
LIGAND6555	152.152	2	3.5	0.464	-1.13	-3.427	687.454	80.444
ZINC database								
ZINC18141652	194.141	4	9.8	-2.03	-0.376	-1.262	3.574	24.959
ZINC03871163	196.218	3.8	8.3	-1.308	-0.389	-2.866	89.098	54.183
ZINC00901606	156.098	0	2.5	-0.055	-0.662	-0.907	6.464	41.131
ZINC01583698	181.188	7	9.5	-2.769	0.698	-3.805	11.541	16.783
ZINC08733367	125.13	1	2.5	0.538	-1.075	-3.179	572.481	79.456
ZINC02597098	156.098	2	4	-0.144	-0.835	0.677	1.404	28.743
ZINC02036492	174.196	1	4	1.228	-1.746	-1.534	74.793	67.672

The eight underlined lead molecules above fulfill drug-like properties based on Lipinski's rule of five (Table 3.3)

Table 3.3. Assessment of drug-like properties of the lead molecules and fumarate as verified by Qikprop (Schrodinger 9.0).

Ligand IDs[a]	MW[b]	HD[c]	HA[d]	QPlogPo/w[e]	QPlogS[f]	QPlogHERG[g]	QPPCaco[h]	Percent human oral absorption[i]	QPlogKhsa[j]
3871163	196.2	3.8	8.3	-1.3	-0.4	-2.9	89.1	54.2	-1.1
3830878	180.2	5.0	8.3	-1.7	-0.8	-2.5	106.9	53.3	-0.9
10436	154.2	3.0	6.0	-0.9	-1.1	-3.3	125.6	59.5	-0.8
967474	133.2	2.0	4.0	-2.0	-0.4	-1.4	41.9	44.1	-0.9
2036492	174.2	1.0	4.0	1.2	-1.7	-1.5	74.8	67.7	-0.7
3606295	150.1	4.0	8.5	-1.7	-0.9	-2.1	192.4	57.7	-0.8
3830875	180.2	5.0	8.3	-1.7	-0.7	-2.7	106.4	53.3	-0.9
5177572	136.1	2.0	4.5	-0.6	-2.3	-2.9	166.7	63.5	-0.7
Fumarate	114.1	2.0	4.0	-0.3	-0.2	0.8	4.1	36.5	-1.2

[a]Ligand IDs are of the Maybridge, NCI, FDA ligand databases.

[b]Molecular weight (< 500 Da).

[c]Hydrogen bond donors (< 5).

[d]Hydrogen bond acceptors (< 10).

[e]Predicted octanol/water partition co-efficient log p (recommended range: -2.0 to 6.5).

[f]Predicted aqueous solubility; S in mol/L (acceptable range: -6.5 to 0.5).

[g]Predicted IC_{50} value for blockage of HERG K+ channels (acceptable range: above -5.0).

[h]Predicted Caco-2 cell permeability in nm/s (acceptable range: 25 is poor and 500 is great).

[i]Percentage of human oral absorption (< 25% is poor and > 80% is high).

[j]Prediction of binding to human serum albumin (acceptable range: –1.5 to 1.5).

The molecular weight of the lead molecules are less than 500 Da, number of hydrogen bond donors is less than 5 and hydrogen bond acceptors are less than 10. The predicted octanol/water partition coefficient (QPlogPo/w) and aqueous solubility (QPlogS) are in the acceptable range i.e. -2.0 to 6.5 and -6.5 to 0.5, respectively. The predicted IC_{50} value for the blockage of HERG K^+ channels (QPlogHERG) is in the acceptable range of above -5.0. The cell permeability (QPPCaco), a factor that is responsible for drug metabolism and its access to the biological membrane, is within the acceptable range 25 to 500. As the cell wall of *Mycobacterium tuberculosis* is thicker than that of other bacteria, the selected inhibitors must have a reasonable cell permeability value to cross the membrane. The predicted value of binding to human serum albumin (QPkhsa) is within the acceptable limit -1.5 to 1.5. Absorption is one of the important pharmacokinetic factors, especially when the most convenient way of drug administration is oral consumption. Percentage of human oral absorption is also within the acceptable range (< 25% is poor and > 80% is high). The selected inhibitors form 2 to 5 hydrogen bond contacts with the conserved residues of MtbADC, with glide XP scores of -5 to -6 kcal/mol, which are superior to the -4.0 kcal/mol score of fumarate. The hydrogen bond distances range from 1.6 to 2.3 Å, suggesting strong ligand-MtbADC interaction. The binding pose of the selected eight lead molecules are illustrated in Fig. 3.4.

3.3. *IN SILICO* VALIDATION

The reliability of the docking protocol was evaluated by comparing the crystallographic pose of the TthADC:fumarate complex structure with the processed MtbADC:fumarate docking model, obtained from the Glide XP mode. The docking procedure precisely predicted the experimental result. This indicates that the Glide

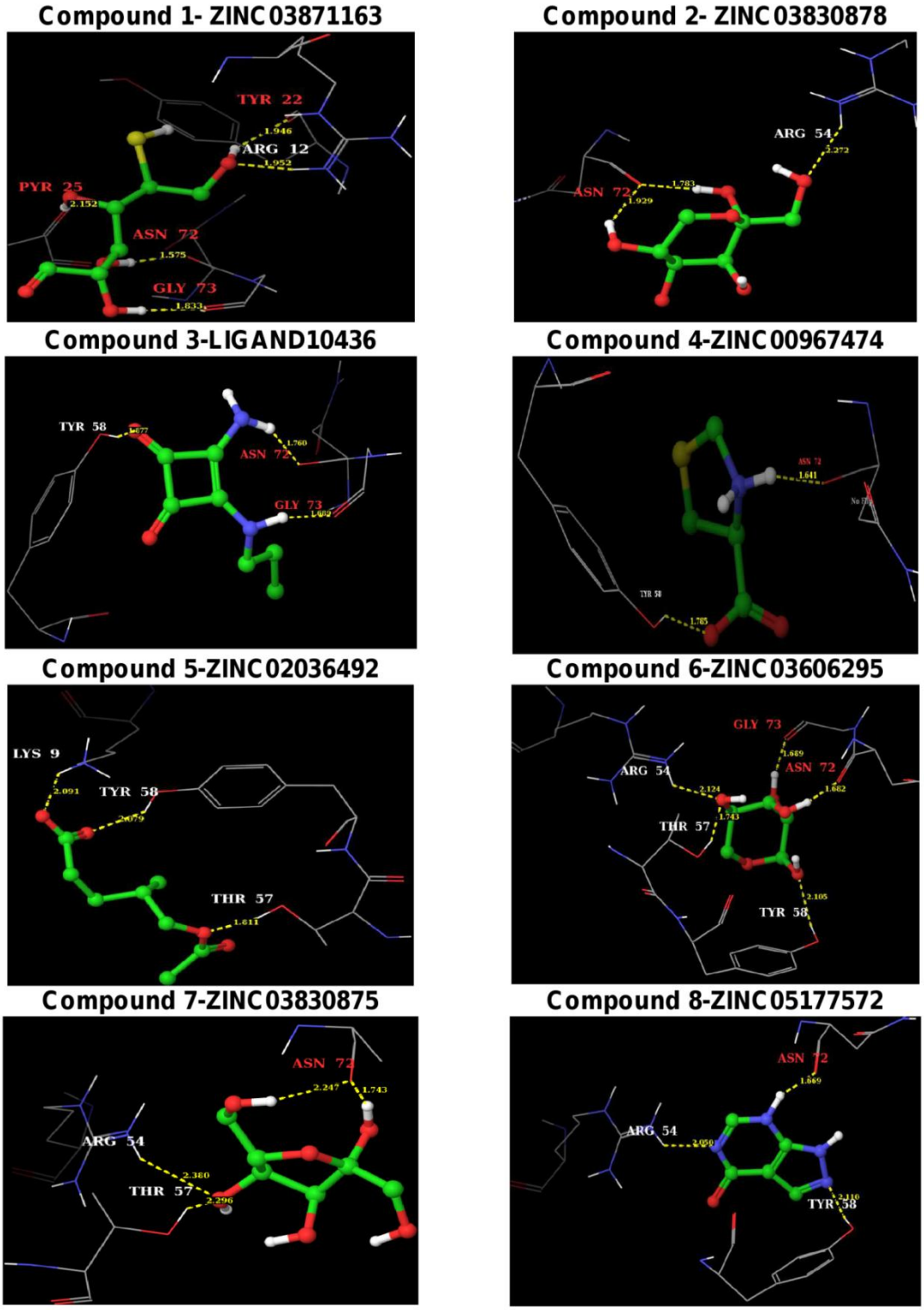

Figure 3.4. Binding poses of the identified eight lead molecules with MtbADC. The binding modes of the proposed lead molecules are

shown as ball and stick. Atoms colors are: H: white, C: green, N: blue, O: red and S: yellow.

The interacting docking protocol represents nearly the same binding conformation that is present in native crystal structure. In both cases, fumarate binds to the same binding site and interacts with residues, Lys9*, Arg54*, Thr57 and Tyr58 (Figure 3.5).

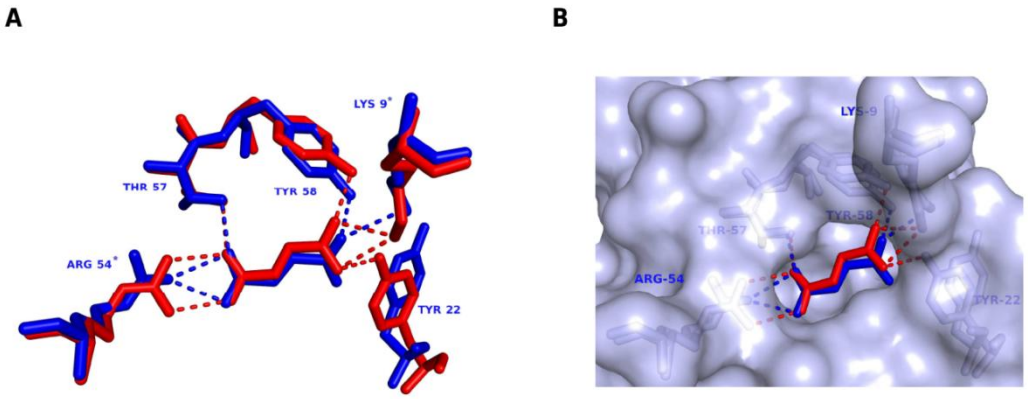

Figure 3.5. Fumarate binding in ADC. (**A**) The superimposed view of the TthADC:fumarate crystal structure (red) and MtbADC:fumarate docking model (blue) is shown. The processed model for MtbADC was generated from the crystal structure of unprocessed protein and docking of fumarate was achieved using the Glide Extra Precision mode. The interacting conserved residues are labelled for MtbADC and the interactions between the protein and fumarate are shown as dashed lines in the corresponding colors. (**B**) Surface diagram around the substrate binding cavity in the same orientation of panel A. The interacting protein residues are also shown in faint trace.

MtbADC residues are drawn as thin wireframe in the same color scheme and are labeled. Hydrogen bond interactions are shown as dotted yellow lines, along with the distance between donor and acceptor atoms. The binding pose of protein:lead molecule interactions were generated with the Maestro program in the Schrodinger software suite.

The ADC active site is formed by the interface of a dimer, with relatively small volume. This cleft can support only molecules of relatively small size (Webb et al., 2003). The reliability of the identified drug-like lead molecules is justified by the fact that they are small in size, when compared to some known ADC inhibitors (Fig. 3.6 and 3.8).

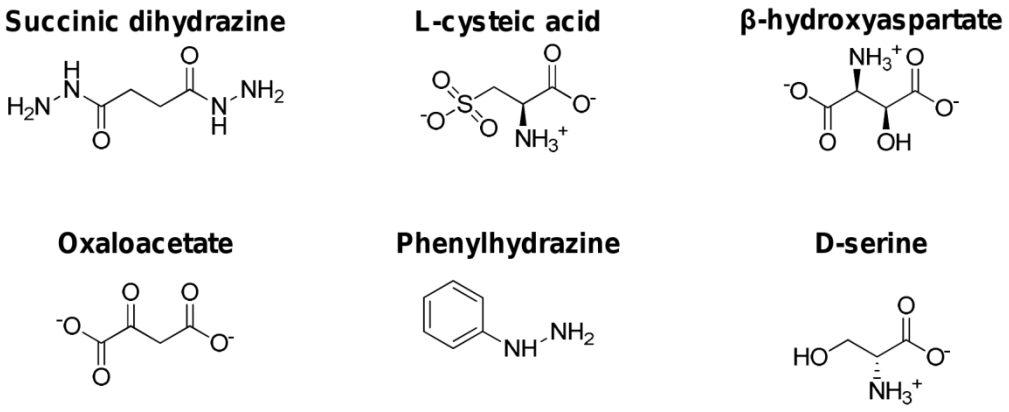

Figure 3.6. Structures of known inhibitors against ADC.

To further support our results, fumarate was docked with the MtbADC monomer and dimer. It binds to the ADC monomer with -1.5 kcal/mol glide score, whereas docking to the ADC dimer gives a Gscore of -4.2 kcal/ mol in the Glide XP mode. This clearly underlines the fact that the active site, formed by the dimer interface, favors the binding of only small ligands. Furthermore, the conserved

functional residue Arg54, which is responsible for substrate specificity (Lee and Suh, 2004), is brought to the proximity of the substrate binding site only in the dimeric conformation.

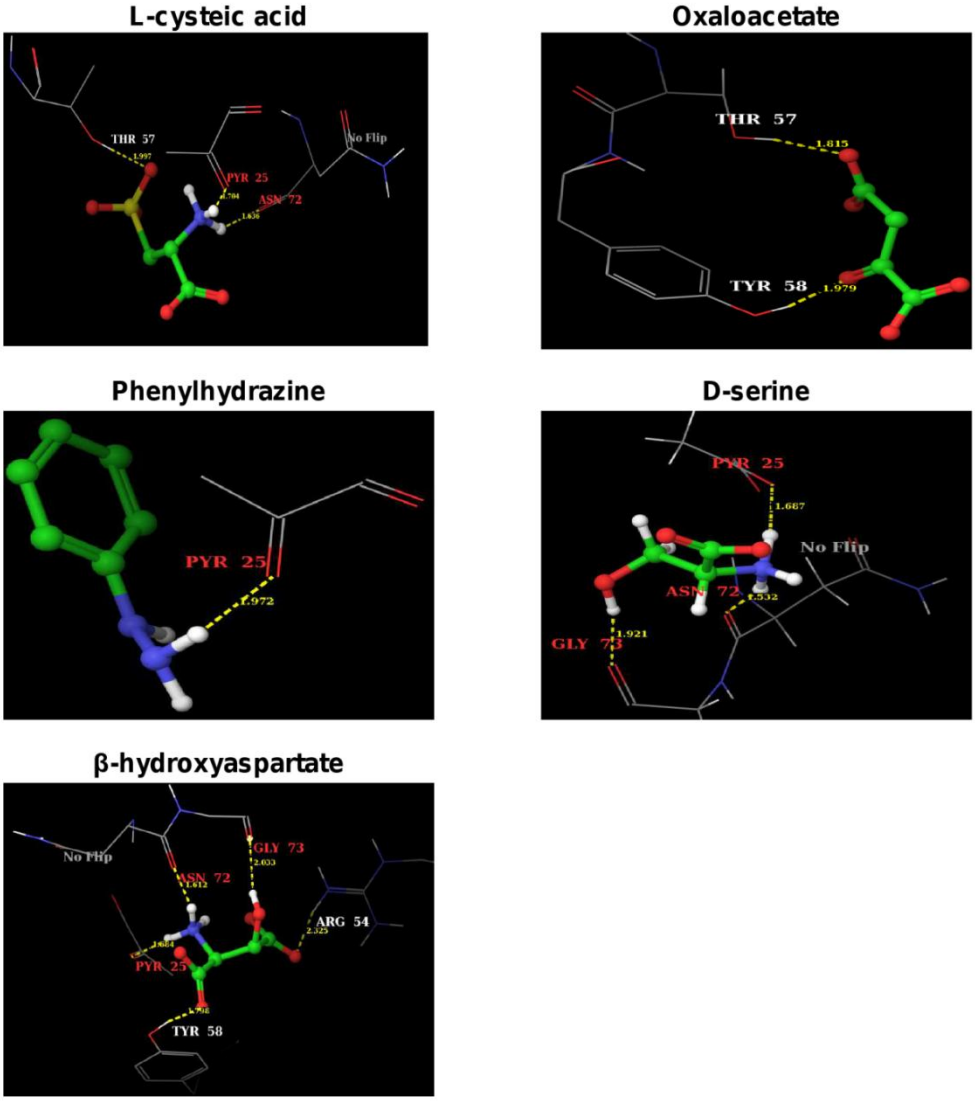

Figure 3.7. Binding poses of known inhibitors/ligands. The known inhibitors or ligands are shown as thick ball and stick. Atoms are colored as: H: white, C: green, N: blue, O: red and S: yellow. The interacting MtbADC residues are drawn as thin wireframe with the same color scheme and are labeled. Hydrogen bond interactions are

shown as dotted yellow lines, along with the distance between donor and acceptor atoms.

Our results were cross checked with the binding modes of the known ADC inhibitors, which were modeled using docking studies. These inhibitors bind to the same site as fumarate and isoasparagine, and interact with at least one of the conserved experimentally determined functional residues (Table 3.4 and Fig. 3.7). In addition, as suggested by *in silico* study, Mtb dimer can only accommodate small inhibitors unlike Mtb monomer (Fig. 3.8). Summary of chemoinformatics based drug design approach is in Fig. 3.9.

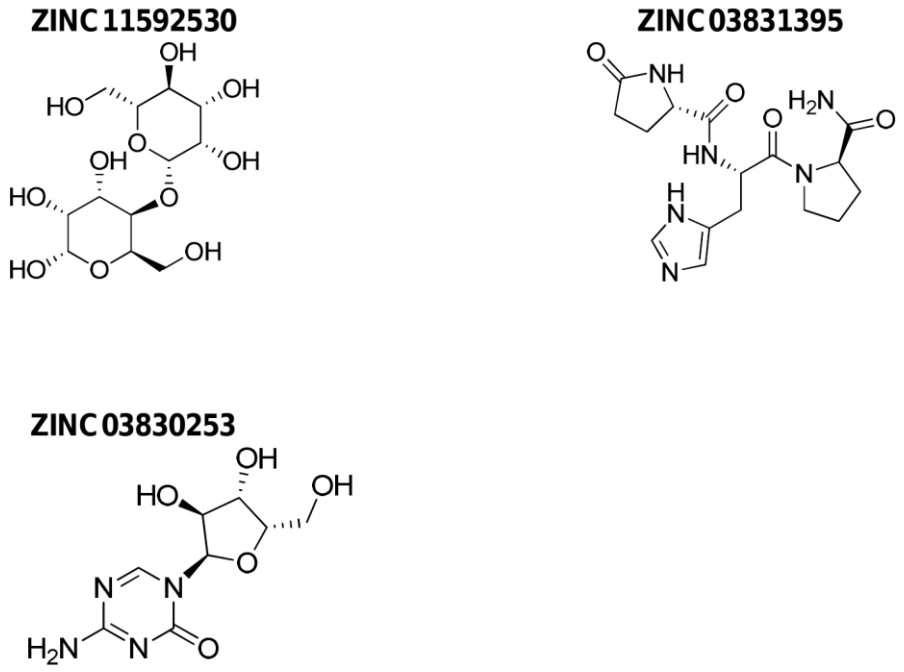

Figure 3.8. Ligands docked to monomeric MtbADC. The structures of the top three hits, obtained by docking the Maybridge, NCI and FDA databases with the processed monomeric MtbADC structure. These molecules are big and cannot be genuine inhibitors as the actual

active site is formed in the cleft of a dimer with relatively smaller volume and only molecules of small size can bind in the pocket.

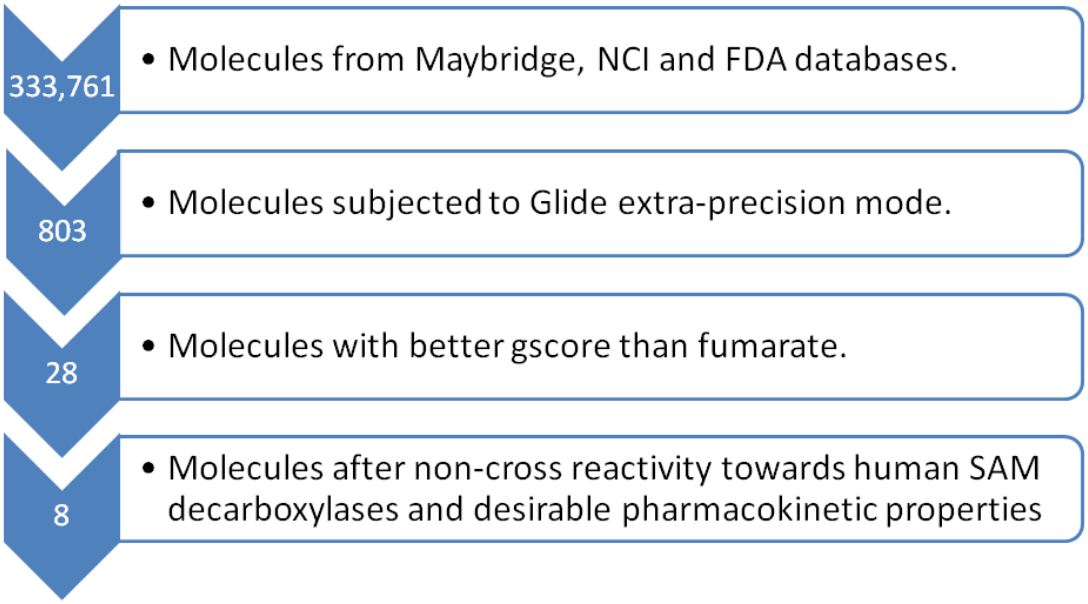

Figure 3.9. Summary of the drug design approach.

3.4. EXPRESSION AND PURIFICATION OF ADC

His-tagged ADC was purified by Ni-NTA affinity followed by gel filtration chromatography (Figs. 3.10 and 3.11).

A)

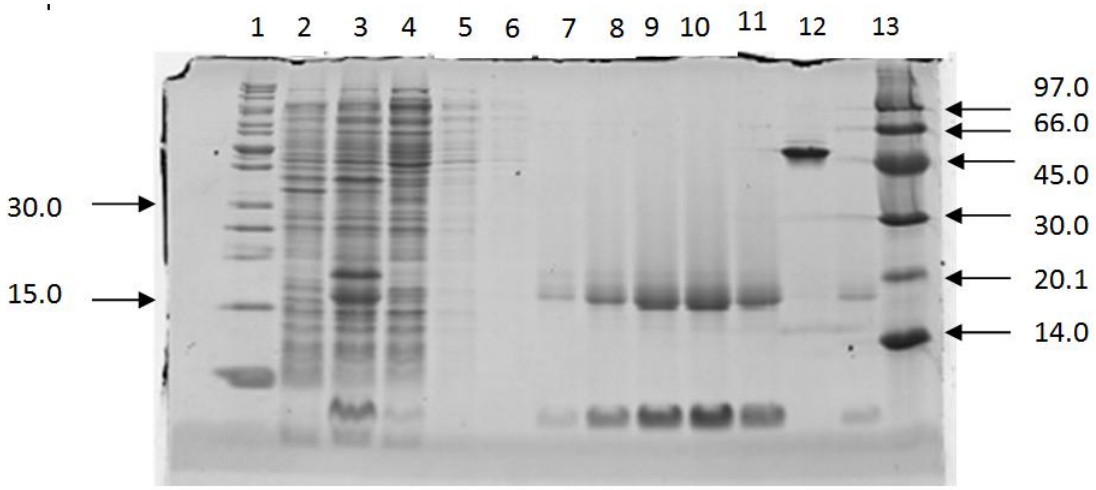

B)

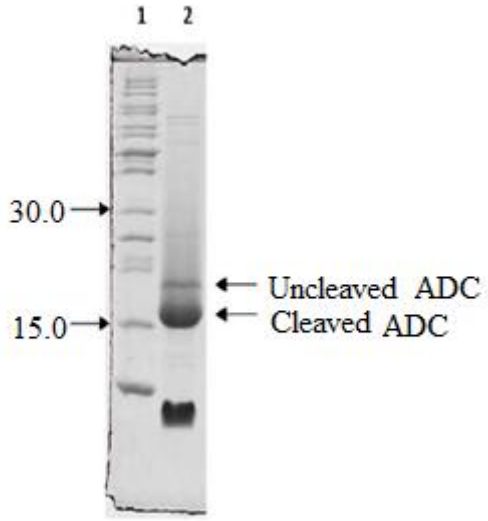

Figure 3.10. **Expression and purification of MtbADC in *E. coli*. (A)** Whole cell lysate was incubated with loading buffer containing 1% SDS and boiled for 5 min before loading onto a 15% SDS–PAGE. Lanes: 1, Page ruler unstained protein marker (in kDa); 2, uninduced cells; 3, induced cells; 4, flow-through in Ni-NTA affinity purification; 5, wash 1; 6, wash 2. The protein eluted with 250 mM imidazole is shown in panel **(B).** Lane 1, Pageruler unstained protein marker; 2, eluted protein. Lanes 7-11 in Panel A show alternate gel filtration samples; 12, protein loaded without boiling; 13, GE low molecular weight protein marker (in kDa).

After gel filtration, the protein purity was more than 95%. Mass spectrometry results confirmed that more than 90% of the protein was in the cleaved form with an N-terminal pyruvoyl group in the longer α-fragment (Fig. 3.12). The protein was concentrated to 5-10 mg/ml and stored frozen at -80 °C.

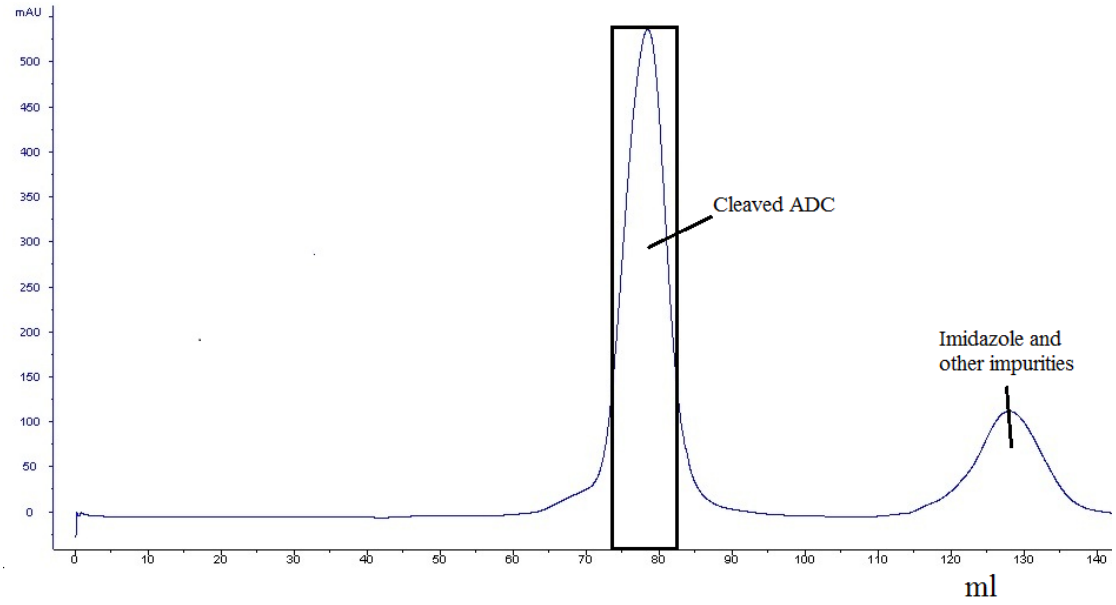

Figure 3.11. Gel filtration profile of ADC-his tagged in superdex-200 column. ADC was purified to homogeneity by gel filtration and is eluted as a tetramer.

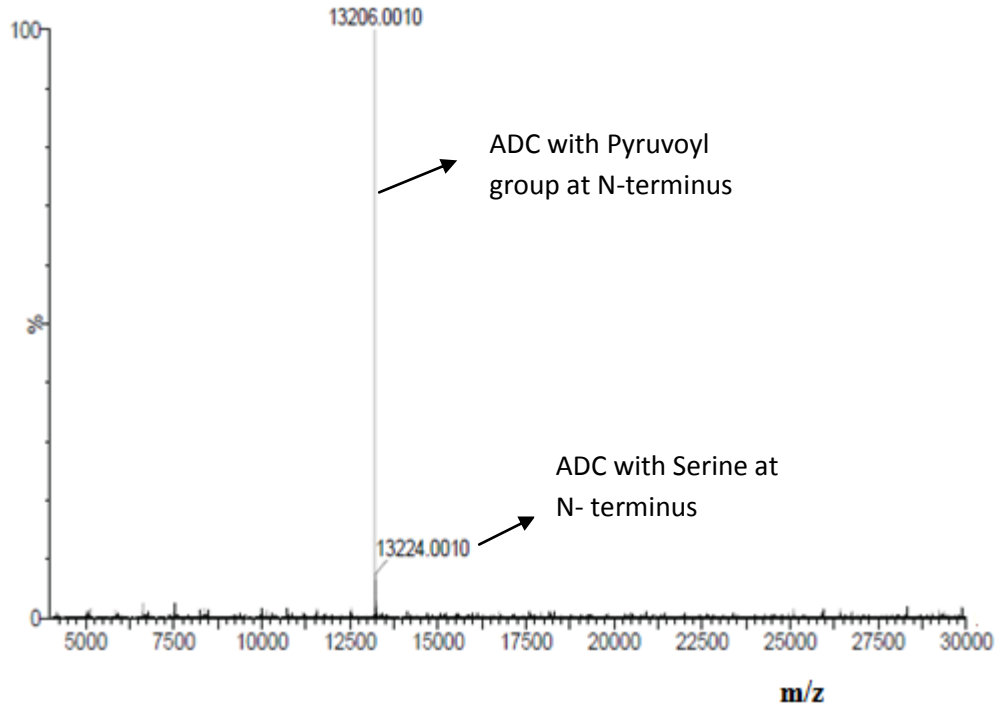

Figure 3.12. Electrospray ionization mass spectra of Mtb cleaved aspartate decarboxylase. Purified aspartate decarboxylase was completely processed by incubation at 37°C for 48 hours, and then

analysed by ESMS. The peak at 13206 corresponds to the a-subunit with an N-terminal pyruvoyl group. The peak at 13224 is due to α-subunit retaining a serine at the N-terminus.

3.5 EXPERIMENTAL VALIDATION OF THE INHIBITORS BY NMR

Before proceeding to the inhibitor screening, a convenient assay for monitoring the ADC activity was established. Since during an enzymatic transformation, structural changes, which may be detected by differences in spectra of the substrate and product of the reaction, occur almost inevitably (Belliveau and Romero-Zerón, 2009; Vandenberg et al., 1986), we opted for NMR spectroscopy as the technique of choice. Therefore, we validated a simple protocol using ^{1}H NMR for monitoring the enzymatic depletion of L-aspartate and concomitant formation of β-alanine. The advantage of ^{1}H NMR is that the technique is label-free and allows direct monitoring. As ADC catalyses the conversion of aspartate to β-alanine, integration of corresponding peaks determines the proportion of the molecules in the reaction. As 1 mM aspartate was used as substrate, the total concentration of all molecules should remain as 1 mM throughout the reaction. It is obvious that with respect to time, the concentration of β-alanine increases with the equivalent depletion of α-aspartate (Fig. 3.13).The ratio of integration of the peaks that correspond to the one and two hydrogen atoms at C1 and C2, respectively, is 1:2. The NMR spectra confirm the increase of product (β-alanine) formation with the disappearance of substrate (aspartate) with time at room temperature. The percentages of substrate left and product formed were calculated after integrating the corresponding peaks and were plotted with respect to time (Fig. 3.14). Experiment was optimized such that after 30 minutes nearly half of the aspartate was converted to β-alanine and hence after 30 minutes of the reaction, peaks corresponding to aspartate and β-alanine were

integrated to determine their concentration. After standardizing the condition, similar study was conducted in presence of the mentioned inhibitors.

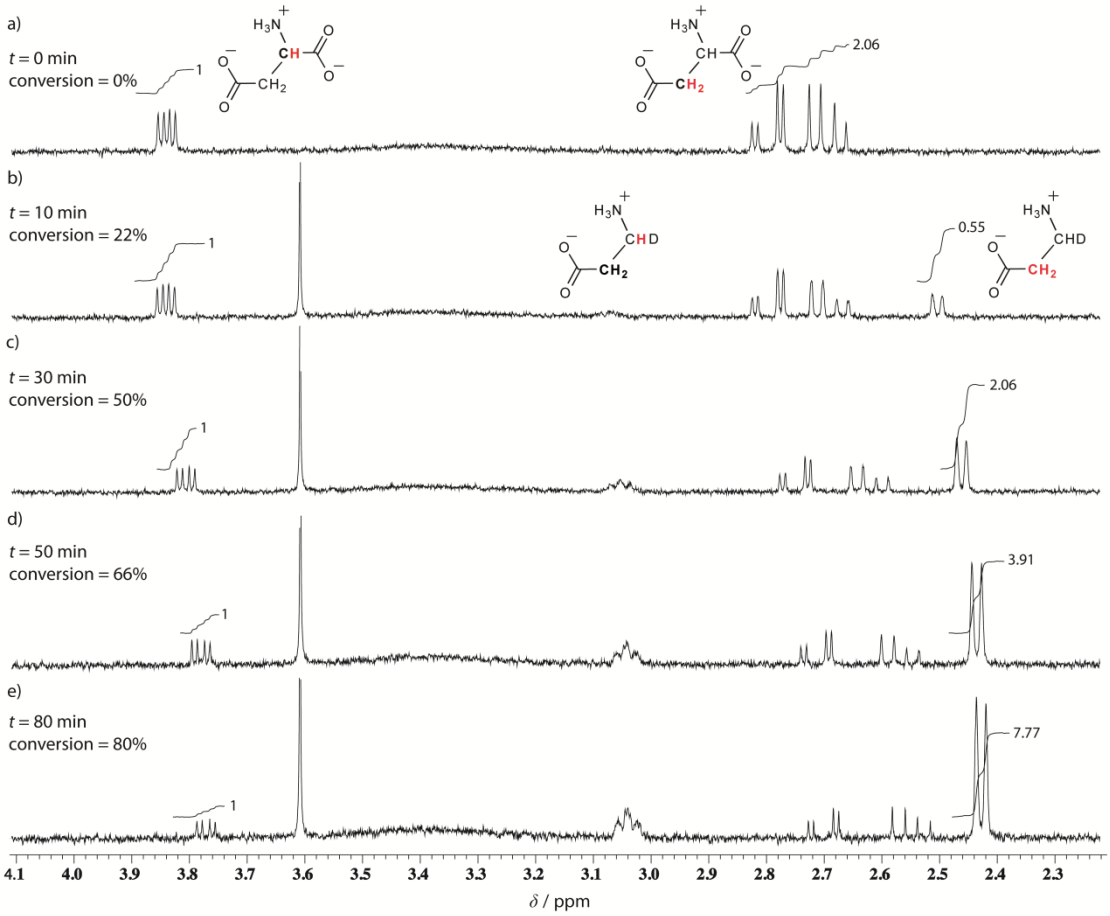

Figure 3.13. NMR spectra of the time study of aspartate decarboxylation. a) before and b) to e) (10-80 min) after addition of 2.8 µM ADC in D_2O at 25 °C. The diminishing signals of L-aspartate and the emerging of those corresponding to alanine have permitted a direct monitoring of the enzymatic transformation and integration of the proton signals have allowed for a kinetic profiling of the reaction

The half time of reaction, $t_{1/2}$, where the amounts of substrate left and product formed are equal, is 30 minutes. The reaction was monitored in the presence of different inhibitors. The relative inhibition constant of an inhibitor, k_{rel}, a unitless

quantity, refers to the ratio of the percentage of substrate conversion to product at $t_{1/2}$ in the presence and absence of that inhibitor (Table 3.4).

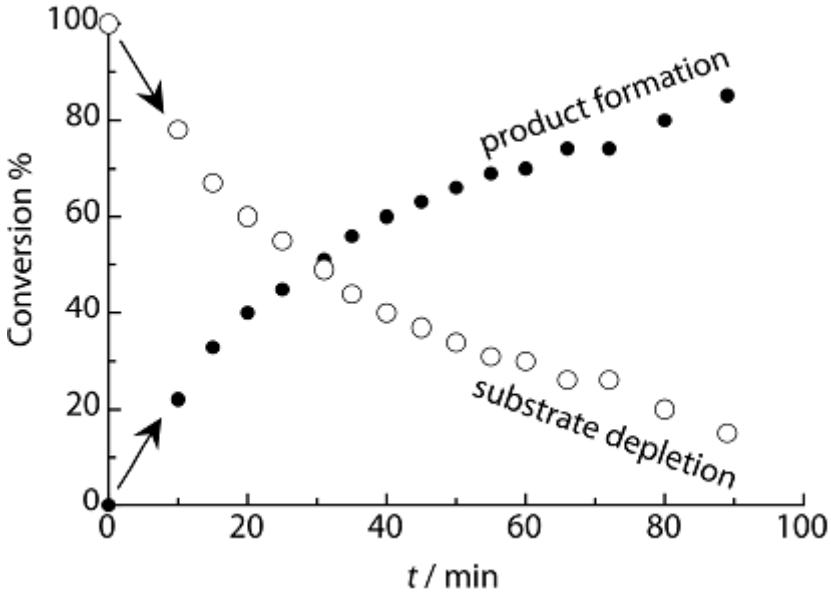

Figure 3.14. Enzyme kinetics of the decarboxylation reaction. The percentage conversion (or percentage of product) (filled circles) and the percentage of remaining substrate (empty circles) were derived from Fig. 3.13.

After standardizing the assay conditions, at first reactions were performed in presence of reported inhibitors (Fig. 3.15).

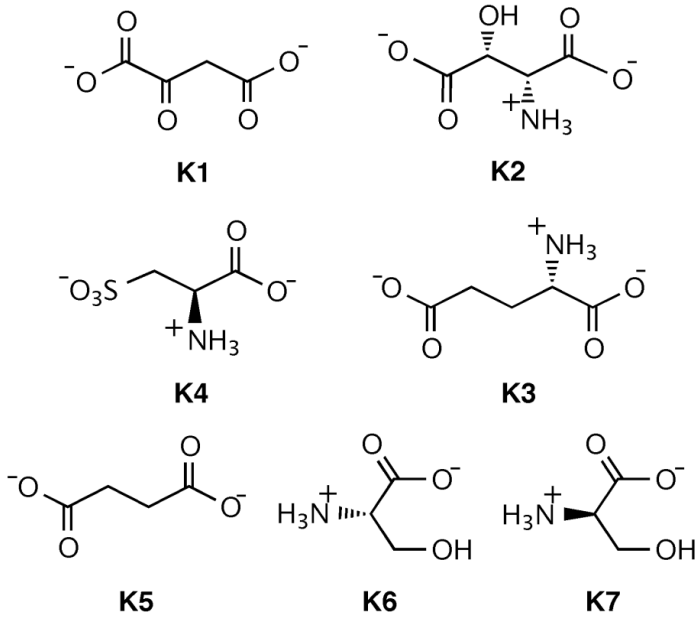

Figure 3.15. Structure of reported molecules tested for inhibitory activity. Oxaloacetate (***K1***), DL-*threo*-β-hydroxyaspartate (***K2***), L-glutamate (***K3***), L-cysteic acid (***K4***), succinate (***K5***), L-serine (***K6***), and D-serine (***K7***).

Known inhibitors (Fig. 3.15) were used as controls and reactions were carried out in presence of them. In presence of oxaloacetate, after 30 min of reaction, no product (β-alanine) was formed. Hence, percentage of conversion was 0% with k_{rel} 0 (Fig. 3.16).

A)

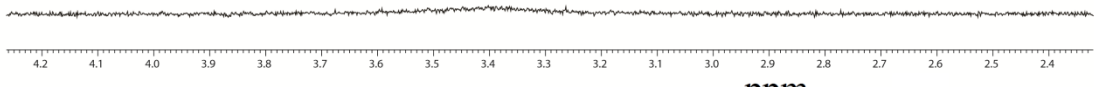

B)

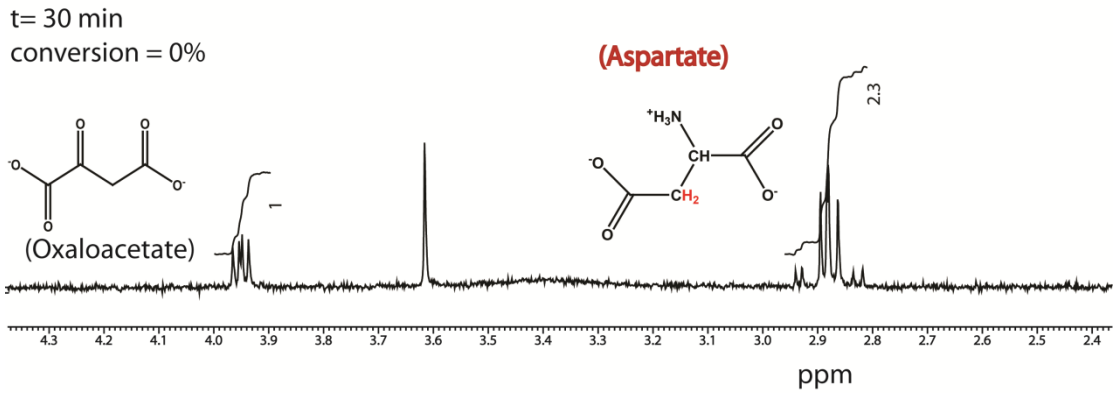

Figure 3.16. NMR spectra in presence of oxaloacetate (*K1*). (A) NMR spectra in presence of only oxaloacetate in D_2O. **(B)** NMR spectra of the reaction, with oxaloacetate, with 1mM initial concentration of substrate (aspartate) and 2.8 μM ADC after 30 min of the reaction. The peak corresponding to aspartate was integrated. No product (β-alanine) was formed after 30 min of reaction.

In the presence of **β-hydroxyaspartate (*K2*)**, percentage of conversion was 18% with k_{rel} 0.36 after 30 min of reaction, classified it as a strong inhibitor (Fig.

3.17A). β-hydroxyaspartate alone in D_2O showed corresponding peaks at ~ 3.5 and ~ 4.25 ppm (Fig. 3.17B).

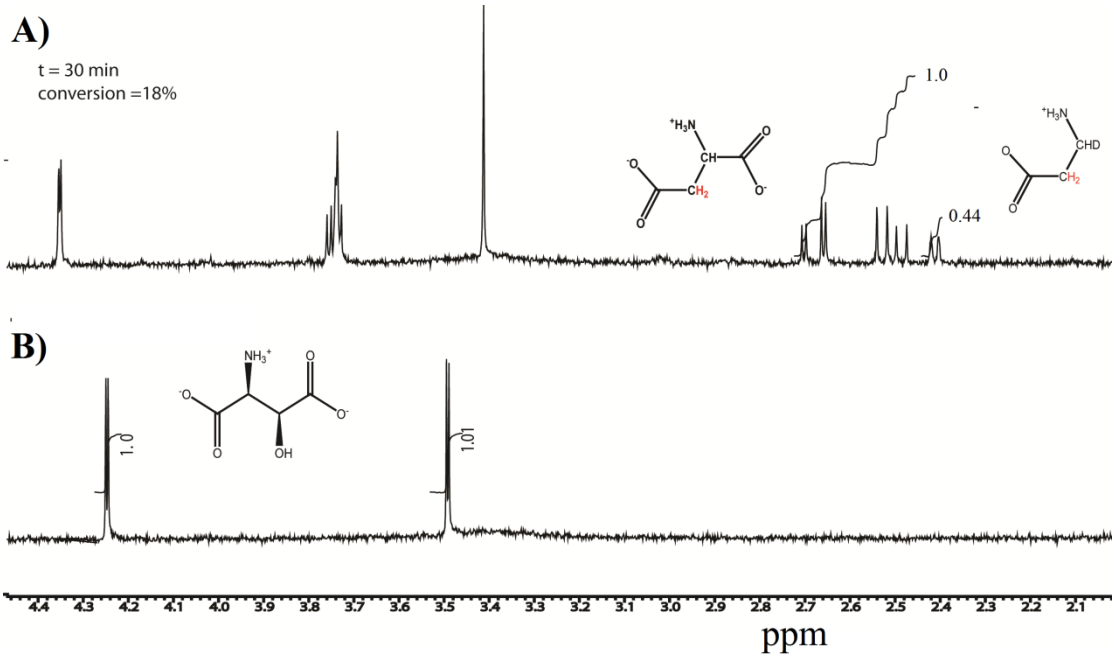

Figure 3.17. NMR spectra in presence of β-hydroxyaspartate (*K2*). **(A))** NMR spectra of the reaction, with β-hydroxyaspartate, with 1mM initial concentration of substrate (aspartate) and 2.8 µM ADC after 30 min of the reaction. The peaks corresponding to aspartate and the product (β-alanine) are integrated. **(B)** NMR spectra in presence of only β-hydroxyaspartate in D_2O.

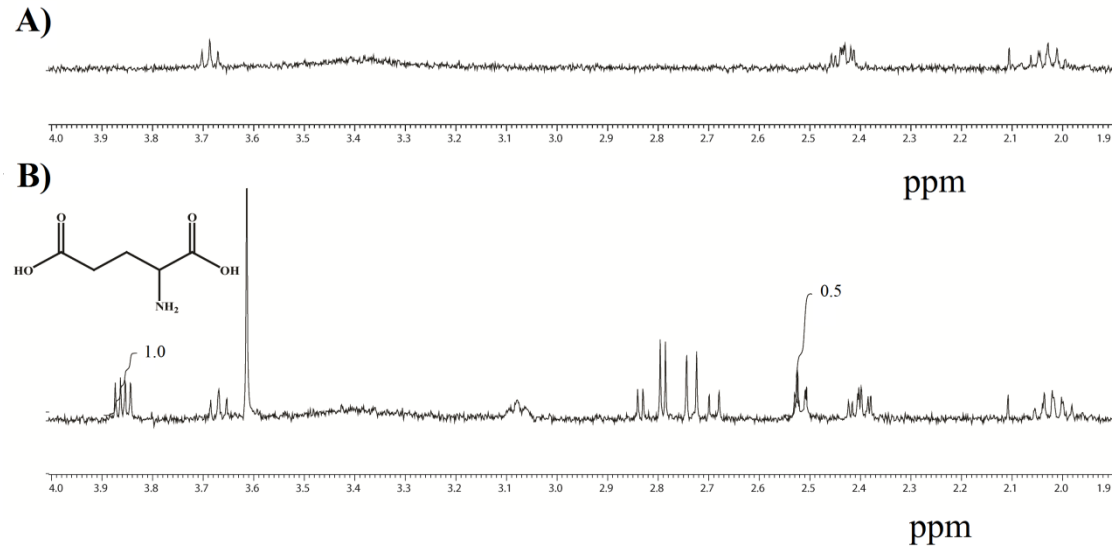

Figure 3.18. NMR spectra in presence of L-glutamate (*K3*). (A) NMR spectra in presence of only L-glutamate in D_2O. **(B)** NMR spectra of the reaction, with L-glutamate, with 1mM initial concentration of substrate (aspartate) and 2.8 μM ADC after 30 min of the reaction. The peaks corresponding to aspartate and the product (β-alanine) were integrated.

In the presence of **L-glutamate (*K3*)**, percentage of conversion was 20% with k_{rel} 0.40 after 30 min of reaction. L-glutamate alone in D_2O showed corresponding peaks at ~2.02, ~2.43 and ~3.68 ppm (Fig. 3.18). In the presence of **L-cysteic acid (*K4*)**, percentage of conversion was 20% with k_{rel} 0.40 after 30 min of reaction as was observed in presence of L-glutamate (Fig. 3.19).

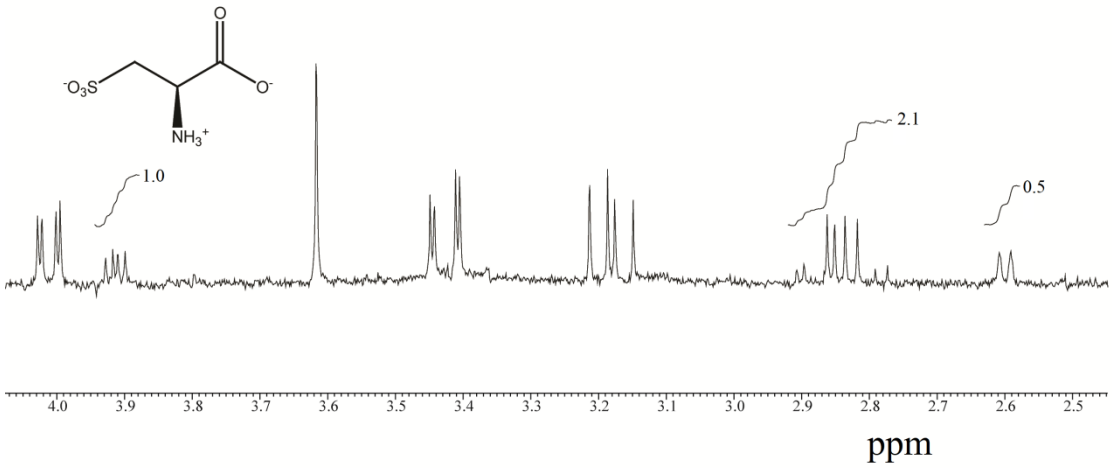

Figure 3.19. NMR spectrum in presence of L-cysteic acid (*K4*). NMR spectrum of the reaction, L-cysteic acid, 1mM initial concentration of substrate (aspartate) and 2.8 μM ADC after 30 min of the reaction. The peaks corresponding to aspartate and the product (β-alanine) were integrated.

In the presence of **succinate** (***K5***), percentage of conversion was 32% with k_{rel} 0.64 after 30 min of reaction (Fig.3.20B). Succinate alone in D_2O showed corresponding peaks at ~ 2.02, ~2.42 and ~3.68 ppm (Fig.3.20A).

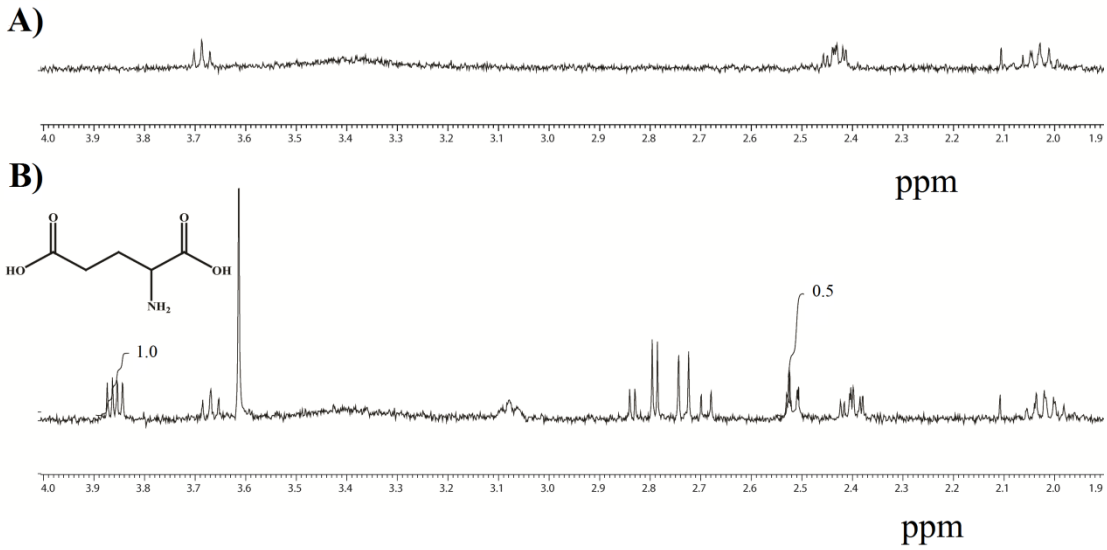

Figure 3.20. NMR spectra in presence of succinate(*K5*). (A) NMR spectrum in presence of only succinate in D_2O. **(B)** NMR spectrum of the reaction, with succinate, with 1mM initial concentration of substrate (aspartate) and 2.8 μM ADC after 30 min of the reaction. The peaks corresponding to aspartate and the product (β-alanine) were integrated.

In the presence of **L-serine** (***K6***) (Fig. 3.21) and **D-serine** (***K7***) (Fig. 3.22), percentage of conversion was 45% and 48% with k_{rel} 0.90 and 0.96, respectively after 30 min of reaction. Both isoforms of serine showed weak/insignificant inhibitory property.

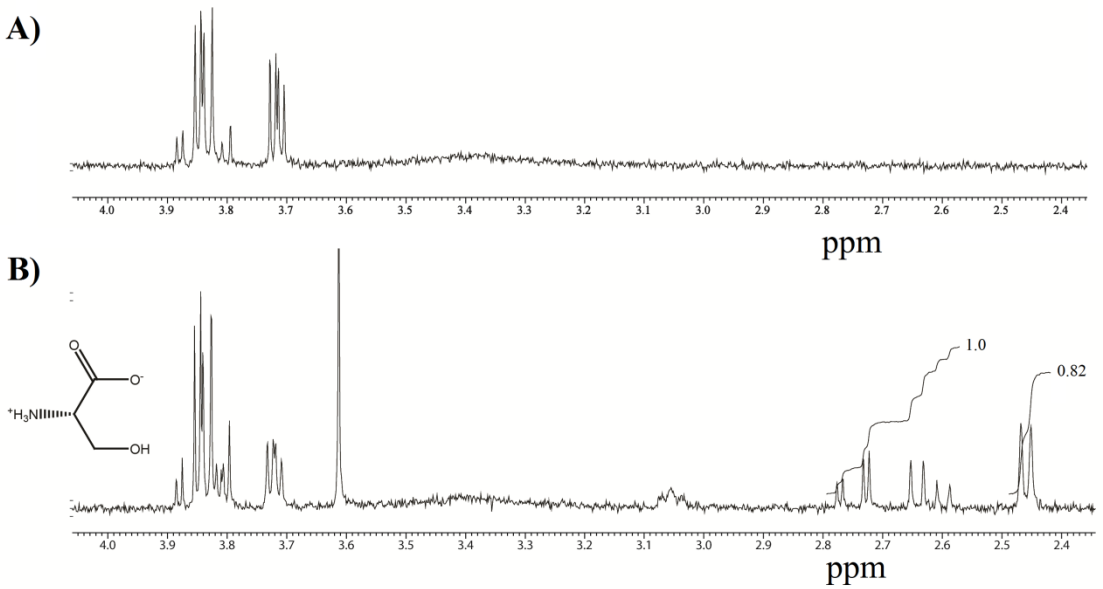

Figure 3.21. NMR spectra in presence of L-serine (*K6*). (A) NMR spectrum in presence of only L-serine in D_2O.. **(B)** NMR spectrum of the reaction, with L-serine, with 1mM initial concentration of substrate (aspartate) and 2.8 μM ADC after 30 min of the reaction. The peaks corresponding to aspartate and the product (β-alanine) were integrated.

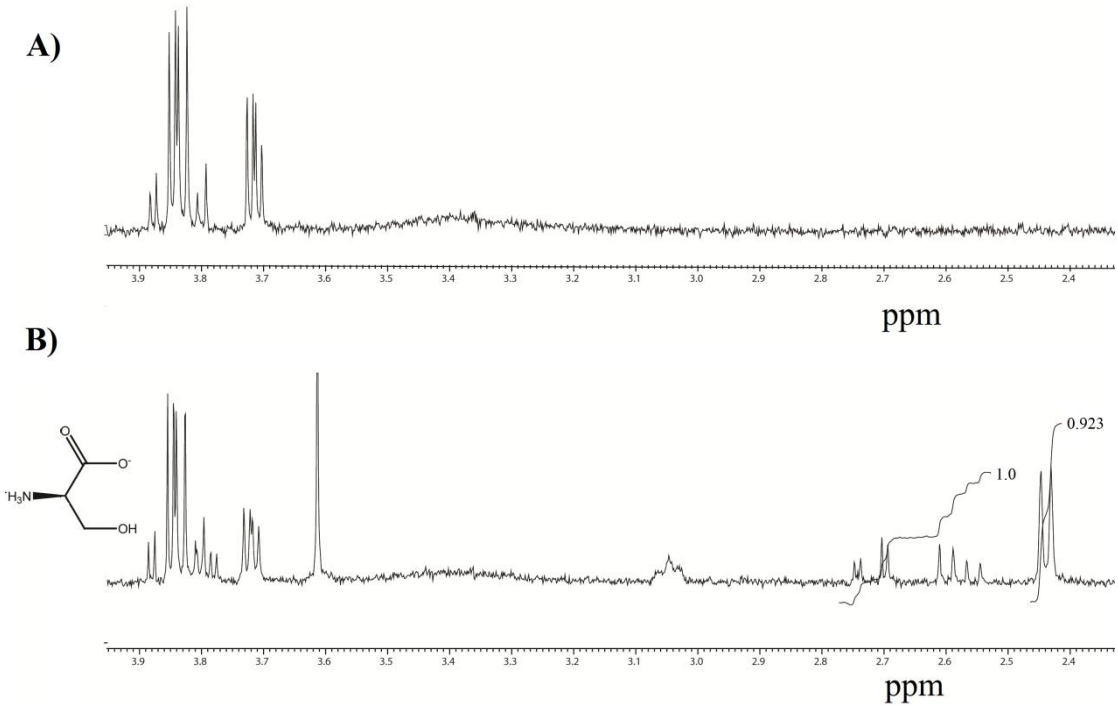

Figure 3.22. NMR spectra in presence of D-serine (*K7*). (A) NMR spectra in presence of only D-serine in D_2O. **(B)** NMR spectra of the

reaction, with D-serine, with 1mM initial concentration of substrate (aspartate) and 2.8 μM ADC after 30 min of the reaction. The peaks corresponding to aspartate and the product (β-alanine) were integrated.

Table 3.4. The inhibition properties of selected known **(coded with 'K')** inhibitors against *Mycobacterium tuberculosis* L-aspartate α-decarboxylase (MtbADC) (Fig. 3.15).

Entry	Compound	Conversion %[b]	k_{rel}[c]	Classification
	none	50	1.00	reference
	Reported compounds(Williamson and Brown, 1979b)			
K1	oxaloacetate[d]	0	0	very strong
K2	β-hydroxyaspartate	18	0.36	strong
K3	L-glutamate	20	0.40	strong
K4	L-cysteate	20	0.40	strong
K5	succinate	32	0.64	moderate
K6	L-serine	45	0.90	weak
K7	D-serine	48	0.96	insignificant

[a] The measurements were performed using 1 mM L-aspartate, 2.8 μM ADC, and 1 mM compound (potential inhibitor) in D_2O at 25 ^oC.

[b] The conversion percentage corresponds to the product formed by integration of the ^1H NMR signals corresponding to substrate and product of the enzymatic reaction after ca. 30 min upon addition of the enzyme. The time was adjusted to correspond to 50% conversion in the *absence* of inhibitor (reference). The absolute values were averaged from at least two independent assays.

[c] The relative inhibitory effect, k_{rel}, was calculated as the ratio of the conversion percentages in the presence and absence of compound.

[d] While full inhibition was also observed when using double the enzyme concentration, i.e., 6 µM, only a small nhibitory effect could be detected (k_{rel} = 0.9) when the assay was performed with 100 µM oxaloacetate, i.e., at a 10-fold lower inhibitor concentration.

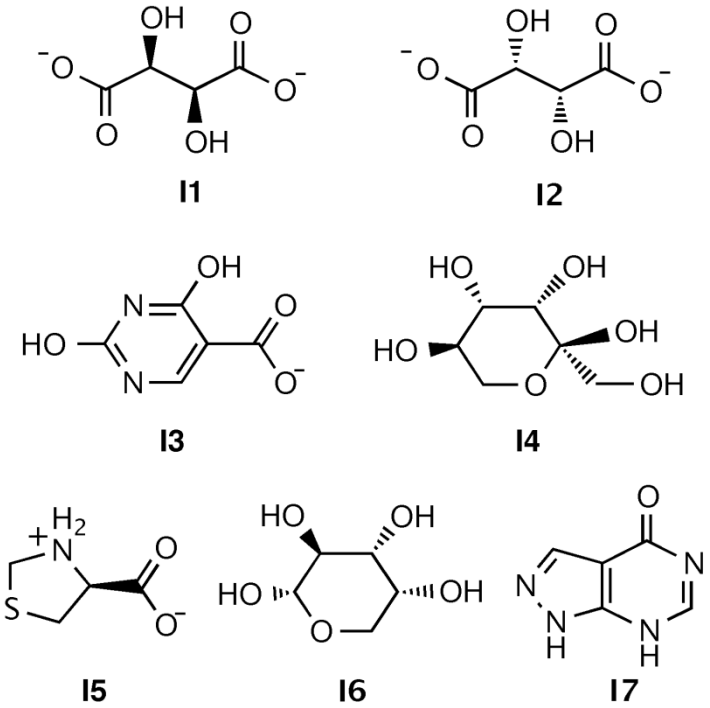

Figure 3.23. Structure of novel potential inhibitors identified by *in silico* studies to be validated using proton NMR. D -tartrate (***I1***, ZINC00895296), L-tartrate (***I2***, ZINC00895301), 2,4-dihydroxypyrimidine-5-carboxylate (***I3***, ZINC00901606), D-tagatose (***I4***, ZINC03830878), (4S)-1,3-thiazolidin-3-ium-4-carboxylate (***I5***, ZINC00967474), a-D-arabinopyranose (***I6***, ZINC03606295), and 1,2-dihydropyrazolo[3,4-d]pyrimidin-4-one (***I7***, ZINC05177572) were tested for inhibitory activity.

In the presence of **D-tartrate** (***I1***), percentage of conversion was 18% with k_{rel} 0.36 after 30 min of reaction (Fig. 3.24A). D-tartrate alone in D_2O showed

corresponding peaks at ~ 4.5 ppm (Fig. 3.24B). Percentage of substrate and product after 30 min of reaction in presence of D-tartrate has been depicted in Fig. 3.25.

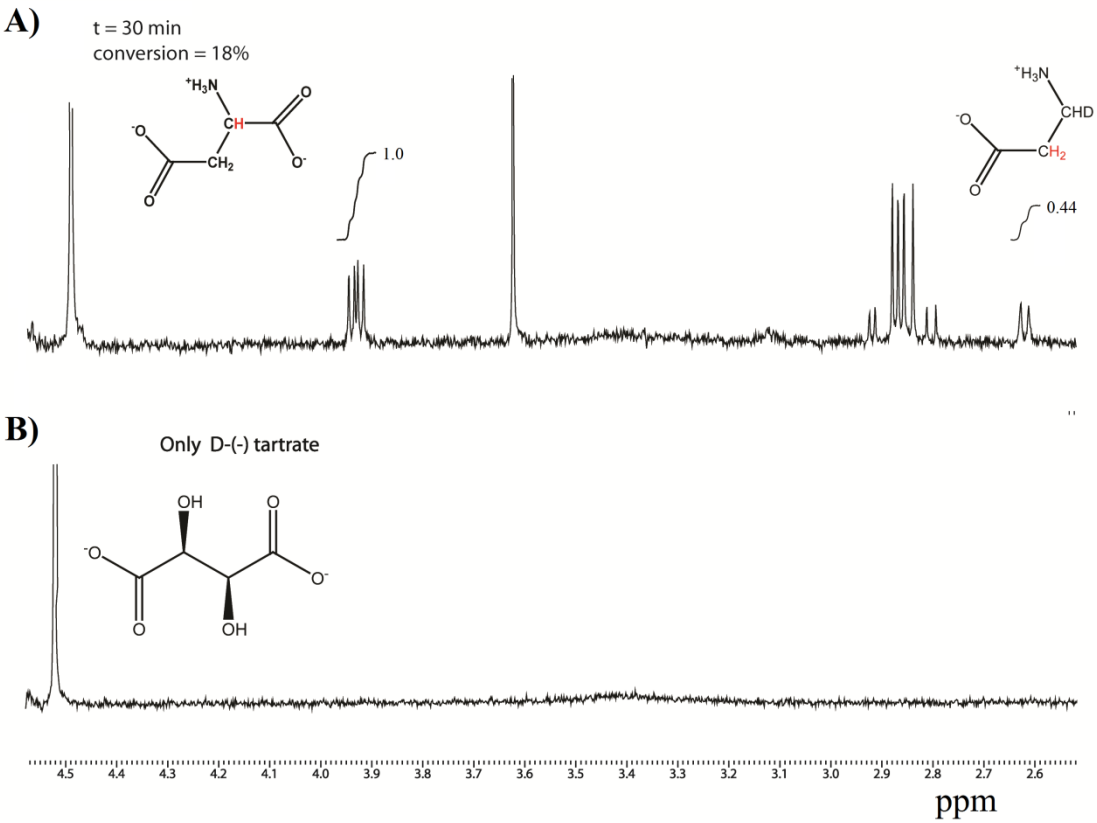

Figure 3.24. NMR spectra in presence of D-tartrate (*I1*, ZINC00895296). (A) NMR spectra of the reaction, with D-tartrate, with 1mM initial concentration of substrate (aspartate) and 2.8 μM ADC after 30 min of the reaction. The peak corresponding to aspartate and β-alanine are integrated. **(B)** NMR spectra in presence of only D-tartrate in D_2O.

In an attempt to identify novel inhibitors against MtbADC, D -tartrate (***I1***, ZINC00895296), L-tartrate (***I2***, ZINC00895301), 2,4-dihydroxypyrimidine-5-carboxylate (***I3***, ZINC00901606), D-tagatose (***I4***, ZINC03830878), (4S)-1,3-thiazolidin-3-ium-4-carboxylate (***I5***, ZINC00967474), a-D-arabinopyranose (***I6***, ZINC03606295), and 1,2-dihydropyrazolo[3,4-d]pyrimidin-4-one (***I7***,

ZINC05177572) (Fig. 3.23) were tested for their inhibitory property using proton NMR based assay.

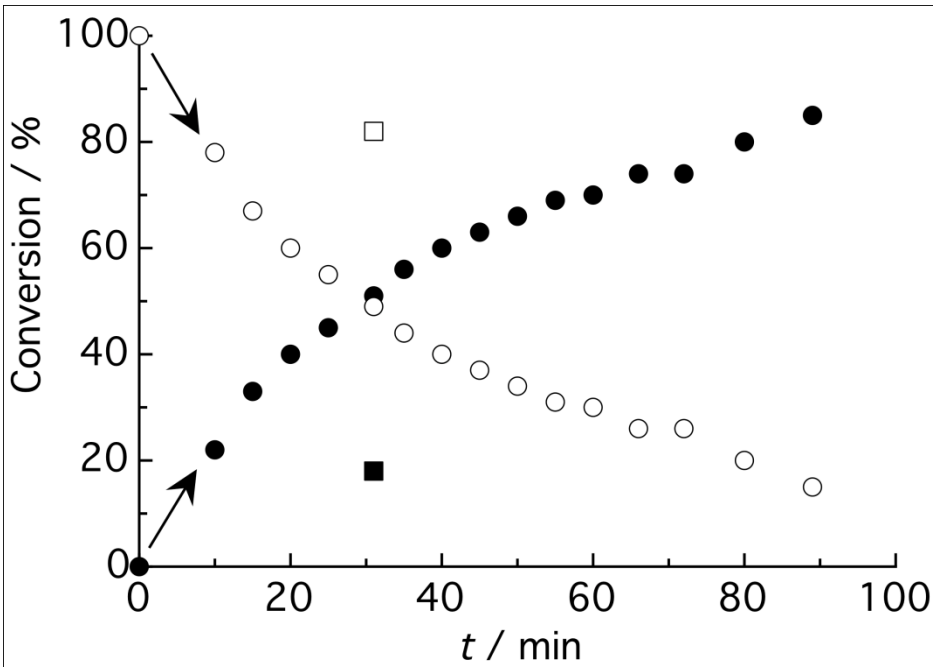

Figure 3.25. Enzyme kinetics of the decarboxylation reaction in presence of D-tartrate after 30 min of reaction. Kinetic monitoring of ADC activity carried out using 1 mM L-aspartate and 2.8 µM enzyme. The different points correspond to conversion percentages of the individual 1H NMR spectra taken at increasing reaction times after initiation of the reaction in D_2O at 25°C. Percentage of product formation and substrate depletion is represented by filled and empty circles, respectively. The percentage of product and substrate after 30 min of the reaction in the presence of D-tartrate is represented by filled and empty squares

In the presence of **L-tartrate (*I2),*** percentage of conversion was 19% with k_{rel} 0.38 after 30 min of reaction (Fig. 3.26B). Similar to D-tartrate, L-tartrate alone in D_2O showed corresponding peaks at ~ 4.5 ppm (Fig. 3.26A). L- tartrate and D tartrate showed similar inhibitory property with k_{rel} 0.38 and 0.36, respectively.

In the presence of **2,4-dihydroxypyrimidine-5-carboxylate** (***I3),*** percentage of conversion was 27% with k_{rel} 0.54 after 30 min of reaction. 2,4-dihydroxypyrimidine-5-carboxylate alone in D_2O showed no overlapping peaks with aspartate and β-alanine (Fig.3.27).

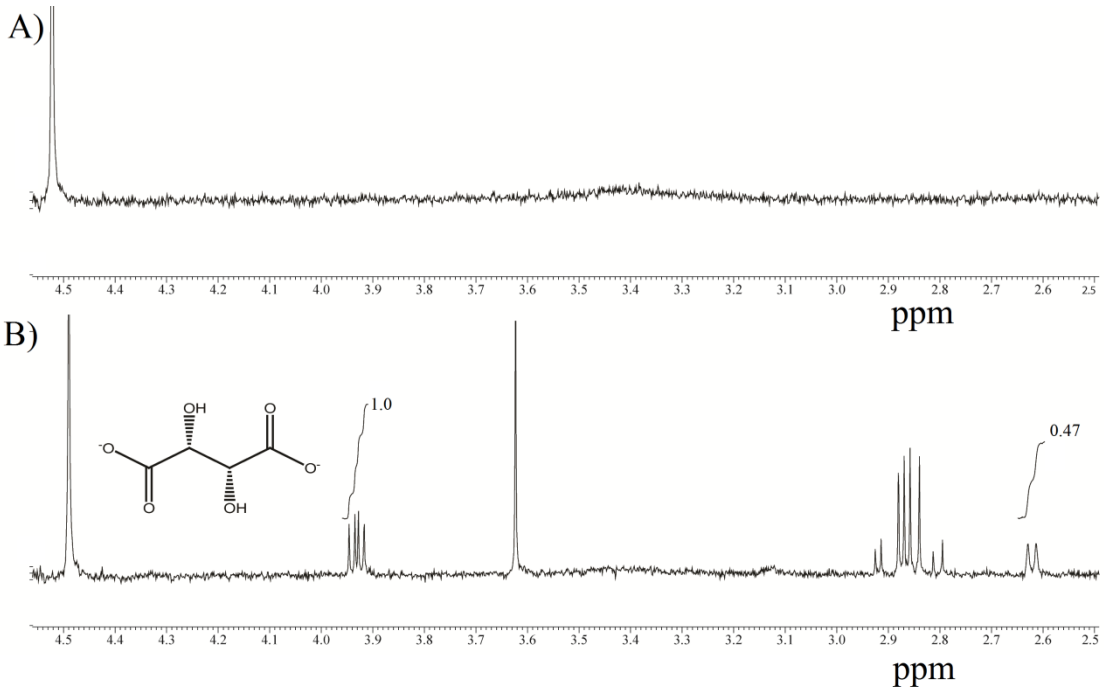

Figure 3.26. NMR spectra in presence of L-tartrate (*I2*, ZINC00895301). (A) NMR spectra in presence of only L-tartrate in D_2O. **(B)** NMR spectra of the reaction, with L-tartrate, with 1mM initial concentration of substrate (aspartate) and 2.8 μM ADC after 30 min of the reaction. The peaks corresponding to aspartate and the product (β-alanine) were integrated.

In the presence of **D-tagatose** (***I4*),** percentage of conversion was 45% with k_{rel} 0.90 after 30 min of reaction (Fig. 3.28), classified as weak inhibitor.

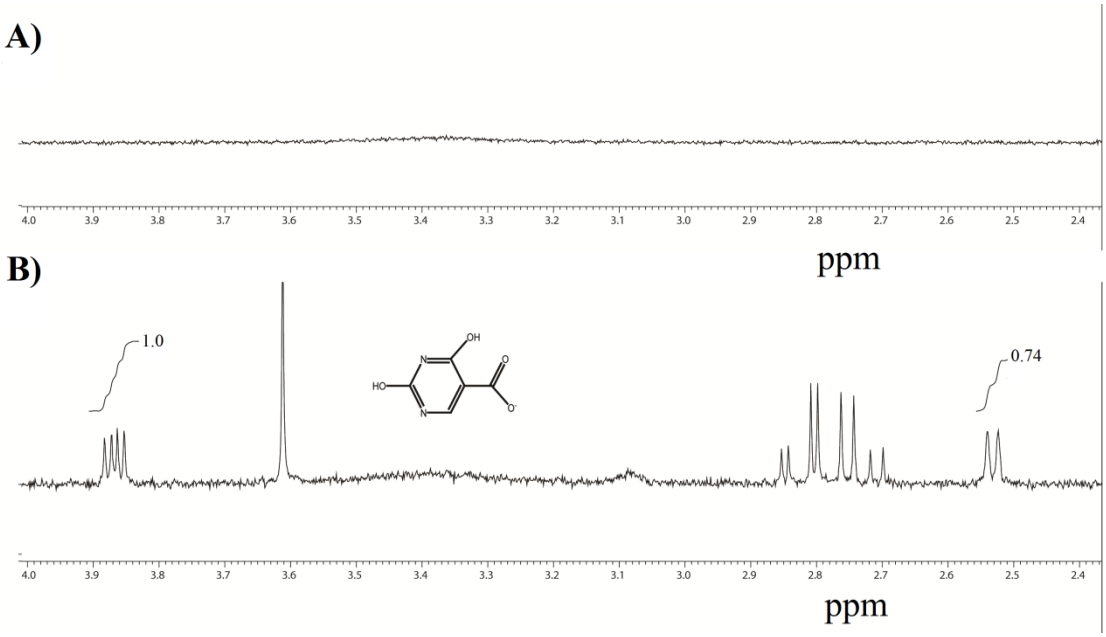

Figure 3.27. NMR spectra in presence of 2,4-dihydroxypyrimidine-5-carboxylate (*I3*, ZINC00901606). (A) NMR spectra in presence of only 2,4-dihydroxypyrimidine-5-carboxylate in D_2O. **(B)** NMR spectra of the reaction, with 2,4-dihydroxypyrimidine-5-carboxylate, with 1mM initial concentration of substrate (aspartate) and 2.8 μM ADC after 30 min of the reaction. The peaks corresponding to aspartate and the product (β-alanine) were integrated.

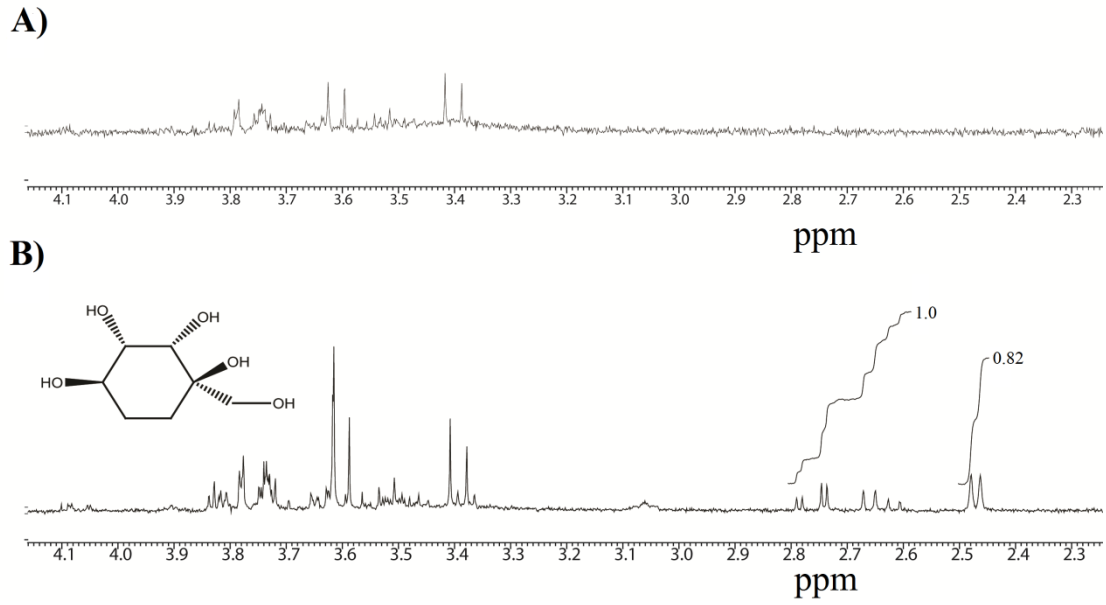

Figure 3.28. NMR spectra in presence of D-tagatose (*I4*, ZINC03830878). **(A)** NMR spectra in presence of only D-tagatose in

D_2O. **(B)** NMR spectra of the reaction, with D-tagatose, with 1mM initial concentration of substrate (aspartate) and 2.8 μM ADC after 30 min of the reaction. The peaks corresponding to aspartate and the product (β-alanine) were integrated.

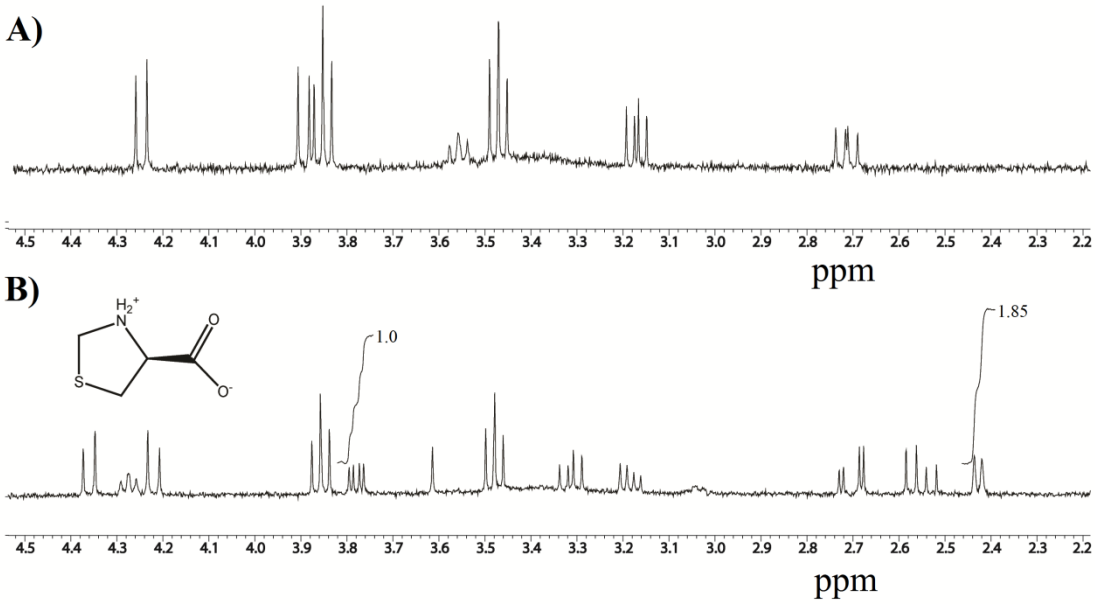

Figure 3.29. NMR spectra in presence of (4S)-1,3-thiazolidin-3-ium-4-carboxylate (*I5*, ZINC00967474). (A) NMR spectra in presence of only (4S)-1,3-thiazolidin-3-ium-4-carboxylate in D_2O. **(B)** NMR spectra of the reaction, with (4S)-1,3-thiazolidin-3-ium-4-carboxylate, with 1mM initial concentration of substrate (aspartate) and 2.8 μM ADC after 30 min of the reaction. The peaks corresponding to aspartate and the product (β-alanine) were integrated.

(4S)-1,3-thiazolidin-3-ium-4-carboxylate (*I5*, ZINC00967474) (Fig. 3.29)**, α-D-arabinopyranose (*I6*, ZINC03606295)** (Fig. 3.30) and **1,2-dihydropyrazolo[3,4-d]pyrimidin-4-one (*I7*, ZINC05177572)** (Fig. 3.31) in the reaction showed insignificant inhibitory property with percentage of conversion 48% and k_{rel} 0.96.

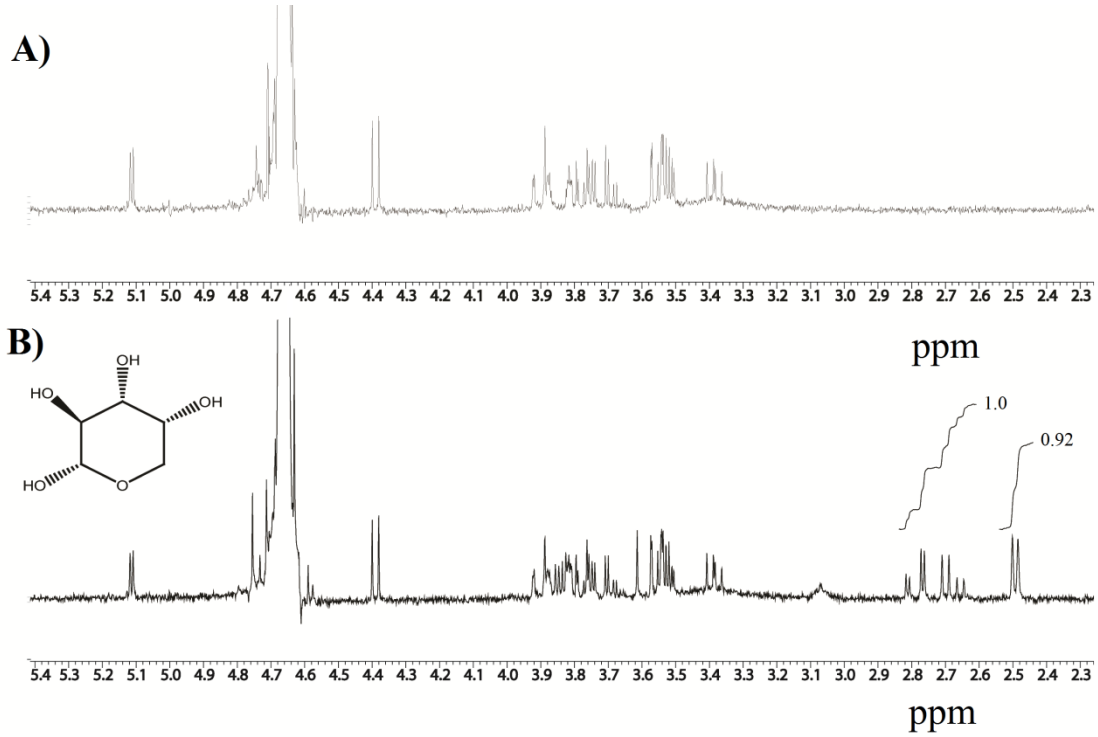

Figure 3.30. NMR spectra in presence of á-D-arabinopyranose (*I6*, ZINC03606295). (A) NMR spectra in presence of only á-D-arabinopyranose in D_2O. **(B)** NMR spectra of the reaction, with á-D-arabinopyranose, with 1mM initial concentration of substrate (aspartate) and 2.8 µM ADC after 30 min of the reaction. The peaks corresponding to aspartate and the product (β-alanine) were integrated.

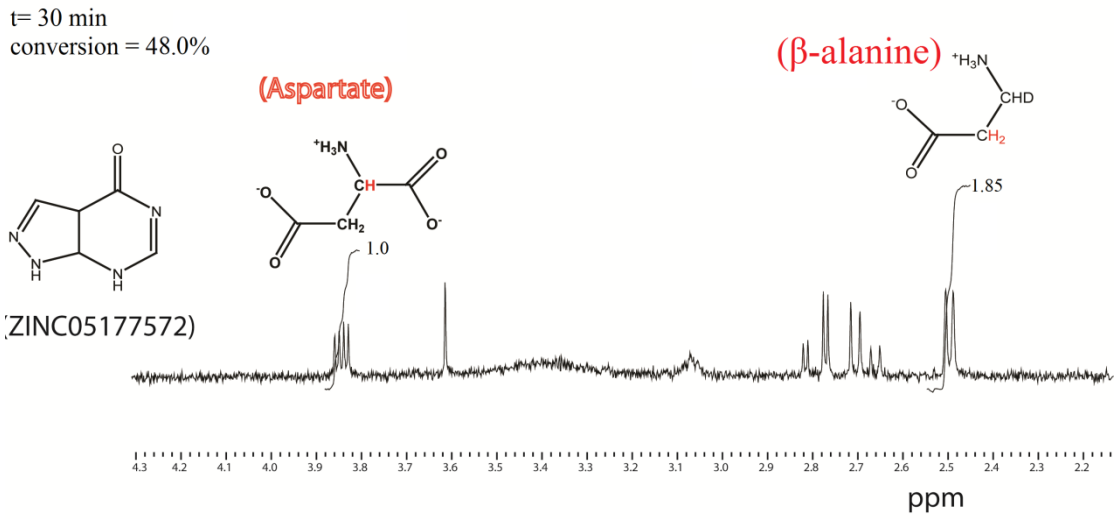

Figure 3.31. NMR spectra in presence of 1,2-dihydropyrazolo[3,4-d]pyrimidin-4-one (*I7*, ZINC05177572). NMR spectra of the reaction, with 1,2-dihydropyrazolo[3,4-d]pyrimidin-4-one, with 1mM initial concentration of substrate (aspartate) and 2.8 μM ADC after 30 min of the reaction. The peaks corresponding to aspartate and the product (β-alanine) were integrated

Table 3.5. The inhibition properties of newly identified **(coded with 'I')** lead molecules against MtbADC (Fig.3.23)

Entry	Compound	Conversion %[b]	k_{rel}[c]	Classification
	none	50	1.00	reference
Newly tested compounds				
I1	D-tartrate	18	0.36	strong
I2	L-tartrate	19	0.38	strong
I3	2,4-dihydroxypyrimidine-5-carboxylate	27	0.54	moderate
I4	D-tagatose	45	0.90	weak
I5	(4S)-1,3-thiazolidin-3-ium-4-carboxylate	48	0.96	insignificant
I6	á-D-arabinopyranose	48	0.96	insignificant
I7	1,2-dihydropyrazolo[3,4-d]pyrimidin-4-one	48	0.96	insignificant

[a] The measurements were performed using 1 mM L-aspartate, 2.8 µM ADC, and 1 mM compound (potential inhibitor) in D_2O at 25 ^oC.

[b] The conversion percentage corresponds to the product formed by integration of the ^1H NMR signals corresponding to substrate and product of the enzymatic reaction after ca. 30 min upon addition of the enzyme. The time was adjusted to correspond to 50% conversion in the *absence* of inhibitor (reference). The absolute values were averaged from at least two independent assays.

[c] The relative inhibitory effect, k_{rel}, was calculated as the ratio of the conversion percentages in the presence and absence of compound.

Of the previously known inhibitors, oxaloacetate was the strongest, followed by β-hydroxyaspartate, L-glutamate, L-cysteate and succinate (Table 3.4). L-cysteic acid also showed complete inhibition if it was incubated with the enzyme for an hour before the reaction while other molecules had no profound effect upon incubation. D-tartaric acid and L-tartaric acid are the strongest newly identified inhibitors of ADC using bioinformatics (Sharma et al., 2012a) with k_{rel} of 0.36 and 0.38, respectively, followed by 2,4-dihydroxy pyrimidine-5-carboxylic acid with a k_{rel} value of 0.54 (Table 3.5).

3.5. *IN VITRO* ACTIVITY AGAINST *MYCOBACTERIUM TUBERCULOSIS*

The inhibitors, validated by the NMR based assay, were further checked for their ability to inhibit the growth of Mtb in culture. Three newly identified inhibitors with low k_{rel} and DL-threo-β-Hydroxyaspartic acid, a previously reported inhibitor, were used. DL-threo-β-Hydroxyaspartic acid showed 42.5% inhibition at 100 µg/ml concentration. However, none of the newly identified inhibitor has shown significant inhibition (Table 3.6).

Table 3.6. *In vitro* activity against *Mycobacterium tuberculosis*

S.No	Compound	Solvent	Stock Conc. (mg/ml)	Inhibition at 100 µg/ml
1	D- (-) Tartaric acid	Water	10	Nil
2	L-(+)-Tartaric acid	Water	10	Nil
3	Fmoc-Asp-NH_2	DMSO	10	Nil
4	2,4-Dihydroxypyrimidine-5-carboxylic acid	DMSO	5	Nil
5	DL-threo-β-Hydroxyaspartic acid	DMSO	5	42.5%

CHAPTER 4

DISCUSSION

CHAPTER 4. DISCUSSION

4.1 DISCUSSION

We have identified eight drug-like lead molecules, from three available public ligand databases, that interact with the known functionally conserved residues of L-aspartate α-decarboxylase. These residues have experimentally been shown to interact with substrate analogs fumarate and isoasparagine.

Four of the eight lead molecules, (D-tagatose (***I4***, ZINC03830878), (4S)-1,3-thiazolidin-3-ium-4-carboxylate (***I5***, ZINC00967474), a-D-arabinopyranose (***I6***, ZINC03606295), and 1,2-dihydropyrazolo[3,4-d]pyrimidin-4-one (***I7***, ZINC05177572)), identified after considering pharmacokinetic properties (Sharma et al., 2012a) and three new lead molecules, (D -tartrate (***I1***, ZINC00895296), L-tartrate (***I2***, ZINC00895301), 2,4-dihydroxypyrimidine-5-carboxylate (***I3***, ZINC00901606)), identified after ignoring their pharmacokinetic kinetics were tested for their inhibitory property by the use of a novel NMR based assay. D-tartrate (ZINC00895296) and 2,4-dihydroxypyrimidine-5-carboxylate (***I3***, ZINC00901606) showed strong and moderate, respectively inhibitory property with high glide scores of -6.8 kcal/mol and-5.8 kcal/mol, respectively (Table 3.1). L-tartrate (ZINC00895301) being an isomer of D-tartrate was checked for its inhibitory property using NMR based assay(Sharma et al., 2012b) and was found to inhibit nearly as strong as D-tartrate with k_{rel} 0.38. L-tartrate (ZINC00895301) proved to be a strong inhibitor in spite of having glide score lower than fumarate, suggests that we may have missed other possible leading inhibitors having glide score lower than that of fumarate.

D-tartrate and L-tartrate are strong novel inhibitors of the protein even though they failed ADMET properties criteria suggests that may be too stringent criteria in

drug designing protocol ignored the potential strong candidates from our bioinformatics study even though they had better glide score and pose. *In silico* study suggested **QPPCaco**, a parameter for cell permeability (acceptable range: 25 is poor and 500 is great) for D-tartrate (ZINC00895296), L-tartrate (ZINC00895301) and 2,4-dihydroxypyrimidine-5-carboxylate (ZINC00901606) is 1.57, 1.55 (not shown), 6.46 (Table 3.2). These ligands failed to inhibit Mtb culture at maximum concentration of 100 µg/ml justifies the same.

In our study, we used drug-like properties (e.g. Lipinski's rule) as one of the selection criterion in the procedure as last step. If it could have applied before docking, computational burden may had reduced. However, if we had applied it in the beginning itself then our novel inhibitors D-tartrate (ZINC00895296), L-tartrate (ZINC00895301) and 2,4-dihydroxypyrimidine-5-carboxylate (ZINC00901606) would had filtered and we were not able to understand the stringent thresholds in ADMET criterion. Ghose et al. have suggested several variations of Lipinski's rule and stringent thresholds for drug discovery (Ghose et al., 1998).

Although the novel strong and moderate inhibitors are not part of human metabolic databases, yet it would have been strategic to exclude all human metabolic ligands to eliminate any potential lead compounds found in humans.

As both SAM and ADC shares pyruvoyl group as cofactor in active site, we checked the *in silico* binding of the ligands with other human pyruvoyl dependent enzyme, SAM. Richardson et al suggests that active site resides plays an important role in binding where aspartate decarboxylase and glutamate decarboxylase in spite of sharing high sequence identity with each other are highly specific to their respective substrates. Aspartate decarboxylase shows no activity with glutamate. Similarly, glutamate decarboxylase shows no activity with aspartate suggests that high sequence

similarity may not be necessary for the activity(Richardson et al., 2009). SAM and ADC do not share high sequence similarity but has pyruvoyl group, essential for catalysis of reaction is in active site. Mtb ADC dimer can accommodate small ligands whereas active site of SAM is bigger and can accommodate larger ligands as well. It is possible that ligands may bind to multiple targets that may not be specific to the reaction, could lead to side effects in *in vivo* conditions. For example, DL-threohydroxyaspartic acid, a known inhibitor of MtbADC, also inhibits Na(+) dependent Glu transporter in mammalian cells(Frank et al., 2002).

From our bioinformatics study, we aimed to identify potential lead molecules that interact with functionally important conserved residues, as current literature supports the functionally important residues present at active site of the protein (see the introduction). However, if any residue is known to be essential for ADCs structure or function should be targeted irrespective of its presence at active site.

The exact role of the conserved residue Tyr22 in catalysis is not clear as its flexible side chain is not oriented towards the substrate analog in the HpyADC:isoasparagine (Lee and Suh, 2004) complex. However, it binds to fumarate in the TthADC:fumarate complex structure. To understand its role, an alternate rotamer was chosen in our chemoinformatics approach by placing it towards the active site, mimicking the TthADC:fumarate complex structure. To our surprise, the glide score was better with -5.27 kcal/ mol (instead of -4.2 kcal/mol), representing a favorable binding mode. The analysis of this binding pose suggests the interaction of ligands with Tyr22 may follow the TthADC:fumarate complex structure. However, this is in contrast to the HpyADC:isoasparagine complex structure, where Tyr22 does not interact with the substrate analog. Hence, the role of Tyr22 needs to be further verified with additional mutational, structural and biochemical experiments.

The central dogma for the identification of new anti-TB drugs is that the inhibitors should be active against both latent (or dormant) and non-dormant bacilli. Mtb, as a pathogen, has evolved to exploit dormancy or latency to its advantage. Since most of the current drugs target the rapidly growing organism, the current drug regimens in the treatment of this infection tend to be of extraordinarily long durations, which lead to tremendous problems, like patient noncompliance and development of multi drug resistant (MDR) strains. This is where the uniqueness of targeting ADC as a drug target may be of considerable importance. An inhibitor or drug that is developed against ADC could be used in conjunction with conventional antibiotics. This combined attack can shorten the time frame of the current therapy and help for an effective clearance of the bacterium from patients.

Identification and quantification of molecules using NMR is simple, effective, accurate and less time consuming (Carlomagno, 2005; Fielding, 2007; Heighton et al., 2011; Salem et al., 2006; Vandenberg et al., 1986; Yung-Chi and Prusoff, 1973). NMR can also be used to study the kinetics of a reaction (Heighton et al., 2011; Vandenberg et al., 1986) and protein-ligand complex formation (Carlomagno, 2005; Fielding, 2007) . It requires comparatively a very small volume (700 µl) of reaction mixture. The assay is not destructive and hence can be used for further analysis. The low sensitivity of the NMR technique is compensated by its several advantages over other known methods. The statistical Student's F-test (Salem et al., 2006) has revealed no significant differences in precision between the NMR and HPLC methods. Compared to the levels of difficulty in the traditional methods, like tagging substrate and product with fluorescamine, followed by quantitation by High Performance Liquid Chromatography (HPLC) (Chopra et al., 2002; Ramjee et al., 1997), trapping radioactive carbon dioxide released from aspartate (Cronan, 1980;

Williamson and Brown, 1979a), or measuring the released carbon dioxide manometrically in a stopped assay (Abell and O'Leary, 1988), the NMR based approach does not require any tagging and hence once a reaction is setup, it can be easily monitored at specific time interval. The assay does not require any radioactive molecule and no cumbersome separation or purification steps.

Furthermore, we checked if the lead molecules that were identified by our bioinformatics study could inhibit Mtb *in vitro*. Coincidentally, the inhibitors oxaloacetate, fumarate, L-serine and succinate are present in abundant quantity in human as well as bacterium in the form of metabolites. The chance of growth arrest by these inhibitors will not be very favorable and we did not test these inhibitors It is not very shocking that none of the newly identified inhibitors showed appreciable inhibition *in vitro* against Mtb. Additional studies should be undertaken to assess the ability of these inhibitors to penetrate the thick cell wall of the bacterium and arrest growth.

For activity of inhibitors against MtbADC, tartaric acid and β-hydroxyaspartate were dissolved in water and DMSO,respectively, which may not have any effect in penetration and activity as their respective controls also had the same solvent.

Protein –ligand docking is about determination of pose(s) with minimizing total energy of the protein. It is generally defined by how well the proposed conformation(s) match with the measured ones (experimental data). In our study, as one of the *in silico* validation docked pose of fumarate-MtbADC was superimposed to experimental measure with minimum RMSD (< 1 Å). Our drug designing protocol used Glide program to identify novel inhibitors. Several docking programs are available either free or commercial. Autodock (Morris et al., 1996), Glide (Halgren et

al., 2004), FlexX (Rarey et al., 1996) and Gold(Jones et al., 1995; Jones et al., 1997) are a few among them. Glide being a fast and accurate docking program, can undergo high throughput ligand-receptor docking for fast screening of library. It identifies best binding mode through Monte Carlo sampling, it can predict binding affinity rapidly with a reasonable level of accuracy, that's why it greatly enhance the success of drug discovery program (Halgren et al., 2004). Autodock undergoes automated docking of flexible ligands to macromolecules. A freely available software, designed to predict how small molecules bind to 3D structure(Morris et al., 1996). FlexX is a fast computer program for predicting interactions of protein-ligand. Two main applications of FlexX includes protein-ligand complex prediction, it creates and ran a series of possible protein-ligand complexes and virtual screening. Gold is another commercial program used for virtual library screening, calculates docking modes of small molecules into protein binding sites. It uses genetic algorithm for protein-ligand docking(Jones et al., 1995; Jones et al., 1997).

For searching poses and conformations, some common searching algorithms include Molecular dynamics, Monte Carlo methods, Genetic algorithms, Fragment-based methods, Simulated annealing methods and Rotamer libraries Systematic searches and Scoring functions include molecular mechanics, empirical functions and knowledge based.

Systematic search involves uniform sampling of each space. It represents the brute force solution to the docking problem. It systematically go through all possible conformations. It is exhaustive and deterministic in nature, possible only for low dimensional problems.

Molecular dynamics is another algorithm for searching pose and conformation. After starting from a random or specific state, moves in direction

indicated by derivatives of energy function and stops when local minimum is achieved.

In Simulated annealing (Monte Carlo search) for searching pose and conformation, after starting from a random or specific state, changes to random states by reducing temperature after each move and stop after temperature gets very small.

Genetic Algorithm is another algorithm for searching pose and conformation. It involves starting with a random population of states and then performs mutations and cross overs to generate children. High scored children are selected to populate next generation. It is repeated for a number of iterations. Some docking programs like Gold and Autodock use genetic algorithm.

Fragment based methods involves division of a ligand into fragments, fragments are docked and at last fragments are linked together. These methods require subjective decisions on the importance of the various functional groups in the ligand. The base fragment must contain the predominant interactions with the receptor. FlexX is a well known program which uses fragment based method for searching pose and conformation.

Rotamer libraries describe rigid docking of many conformations. All low energy conformations of ligands are precomputed and each precomputed conformations (treated as rigid bodies) are docked. Glide, a virtual screening program uses rotamer libraries for searching poses and conformation.

Bursulaya et al. compared the performance of FlexX 1.8, Autodock 3.0, Gold 1.2, ICM 2.8 and Dock 1.4 for flexible molecular docking. Their results suggested that ICM has highest accuracy, followed by Gold, Autodock, FlexX and Dock. In terms of speed, FlexX is the fastest and AutoDock is the slowest among them (Bursulaya et al., 2003)

CHAPTER 5

FUTURE DIRECTIONS

CHAPTER 5. FUTURE DIRECTIONS

5.1 FUTURE DIRECTIONS

In order to counter multi drug resistance (MDR), attenuate *Mycobacterium tuberculosis*'s virulence and expedite the recovery and prolong the survival of patients, additional drugs, in combination with conventional antibiotics, are continuously needed. This warrants faster and easier enzymatic assays and drug validation.

The identified inhibitors in this study and already known inhibitor backbones can be used to design new lead molecules and testing their activity against MtbADC. The interaction between the MtbADC protein and lead molecules can be identified from co-crystallization of the enzyme-inhibitor complex. Thermodynamic parameters of the interaction in solution can be obtained by isothermal titration calorimetry.

Table 3.1 highlights the potential interacting residues of the 28 ligands hits after *in silico* study. Asn72 prominently appears in the table as binding the lead molecules but its functionally essential role is not evident from experimental method. Sequence alignment of 16 ADCs have shown Asn72 (MtbADC numbering) as highly conserved residue (Lee and Suh, 2004). To understand the structural and functional role of it and other strictly and highly conserved residues (see the introduction), site directed mutation studies could be performed to check the affect on activity of the protein. However, it is possible that more than one residue are responsible for structural, binding or catalysis significance.

The assay of amino acid decarboxylase activity has until recently involved laborious manometric, radiometric or multistep colorimetric methods. This elaborate and expensive assay is clearly unsuitable for medium to high throughput applications.

The principle behind label-free continuous fluorimetric assay method, reported by our collaborator Prof. Werner Nau of Jacobs University, Germany, for the amino acid decarboxylases that are specific for lysine, arginine, histidine and ornithine (Hennig et al., 2007) was used initially to develop an assay to monitor enzyme activity. This 'supramolecular tandem assay' is based on the displacement by reaction products (cadaverine, agmatine, histamine or putrascine) of a fluorophore from its complex with a macrocycle (Fig. 4.1). The macrocycle, in this case cucurbit-7-uril, has lower affinity for amino acid substrates relative to amine product. As the amine (a di-cation) is produced by enzymatic decarboxylation, it competes with a fluorescent dye (dapoxyl) for binding to the macrocycle. Monitoring of the change in fluorescence intensity gives a sensitive real time read-out of the enzyme activity. However, in our brief attempt of developing an assay was of little success where we identified a host (macrocycle)-guest (dye) complex but this binding was not efficiently replaced by substrate or by product. Our collaborators are continuing to identify suitable host-guest complexes, which could be used to develop the fluorescence based study.

In our bioinformatics study, 803 molecules were subjected to glide extra-precision mode, glide score (correlating to binding affinity) and pose of ligand was obtained. As limited candidates were selected for inhibitory property, other candidates could be experimentally validated as inhibitors using high throughput study.

Various docking programs could be compared to identify potential inhibitors. Validity of the method and algorithm can be compared with respect to other successes and failures of other algorithm.

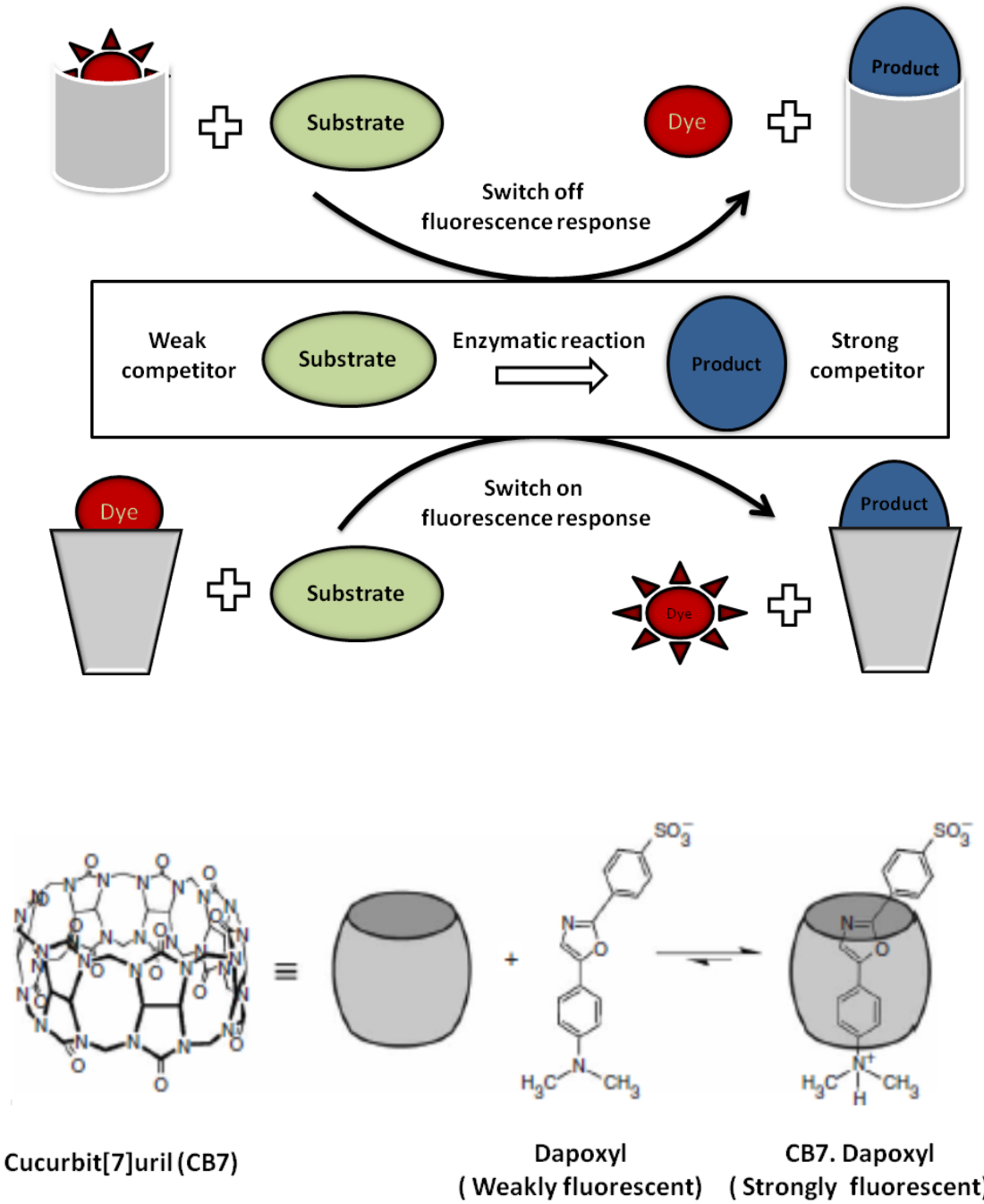

Figure 5.1. Fluorescence based assay. The principle of the supramolecular tandem assay in which the product of the enzyme-catalysed reaction (middle) displaces, from its complex with the macrocycle (grey), a dye leading to either a quenching (upper) or an enhancement (lower) of fluorescence (Hennig et al., 2007).

Role of functional groups of ligands can be correlated with the mode of binding and its ability to penetrate cell wall of the micro-organism, Hence, based on the structure of identified molecules, novel drug-like inhibitors able to enter the microbe can be designed and experimentally validated. Breakdown of binding energy into contributions from different functional groups of ligand or of protein residue can help to provide evolutionary significance and can help in designing better drug-like inhibitors.

Ligands which do not appear to interact with pyruvoyl moiety or other residues of active site could interact with the protein through structurally important water molecules present at active site. Hence, role of water molecules in computational drug design need to be considered. It is possible that some molecules may not directly interact with the residues of the enzyme and yet be stabilized by intervening water molecules. Beer et al. has suggested role of water molecules in computational drug design (Beer et al., 2010)

As proteins are flexible in solution hence protein flexibility need to be considered in *in silico* studies. New conformations of the protein could be generated using freely available software concord (Groot et al., 1997) and docked the hits into them to see the variability.

Further, Inhibitors were checked for their ability to inhibit Mtb *in vitro.* However, animal models study need to be conducted as the molecules inhibiting Mtb *in vitro* may not be able to do the same in *in vivo* conditions.

We are confident that backbone scaffolds of the identified inhibitors can provide suitable platforms for the development of potential therapeutics, after adequate experimental follow up, in the treatment of tuberculosis.

REFERENCES

REFERENCES

2009. Protein Preparation Wizard, Maestro, LigPrep, Schrödinger LLC, New York.

Abell, L.M., M.H. O'Leary, 1988. Isotope effect studies of the pyruvate-dependent histidine decarboxylase from Lactobacillus 30a. Biochemistry 27, 5933-5939.

Albert, A., V. Dhanaraj, U. Genschel, G. Khan, M.K. Ramjee, R. Pulido, B.L. Sibanda, F.v. Delft, M. Witty, T.L. Blundell, A.G. Smith, C. Abell, 1998. Crystal structure of aspartate decarboxylase at 2.2 A resolution provides evidence for an ester in protein self-processing. Nat Struct Mol Biol 5, 289-293.

Andrews, N.C., 2000. IRON METABOLISM: Iron Deficiency and Iron Overload. Annual Review of Genomics and Human Genetics 1, 75-98.

Armstrong, J.A., P.D. Hart, 1975. Phagosome-lysosome interactions in cultured macrophages infected with virulent tubercle bacilli. Reversal of the usual nonfusion pattern and observations on bacterial survival. The Journal of Experimental Medicine 142, 1-16.

Bale, S., W. Brooks, J.W. Hanes, A.M. Mahesan, W.C. Guida, S.E. Ealick, 2009. Role of the sulfonium center in determining the ligand specificity of human S-adenosylmethionine decarboxylase. Biochemistry 48, 6423-6430.

Banerjee, A., E. Dubnau, A. Quemard, V. Balasubramanian, K.S. Um, T. Wilson, D. Collins, G. De Lisle, W.R. Jacobs Jr, 1994. inhA, a gene encoding a target for isoniazid and ethionamide in Mycobacterium tuberculosis. Science 263, 227-230.

Beer, S.B.A.d., N.P.E. Vermeulen, C. Oostenbrink, 2010. The Role of Water Molecules in Computational Drug Design. Current Topics in Medicinal Chemistry 10, 55-66.

Belanger, A.E., G.S. Besra, M.E. Ford, K. Mikusová, J.T. Belisle, P.J. Brennan, J.M. Inamine, 1996. The embAB genes of Mycobacterium avium encode an arabinosyl transferase involved in cell wall arabinan biosynthesis that is the target for the antimycobacterial drug ethambutol. Proceedings of the National Academy of Sciences 93, 11919-11924.

Belliveau, K.A., L.B. Romero-Zerón, 2009. Monitoring the enzymatic degradation of sinigrin from B. juncea meal using 1H NMR spectroscopy. Natural Product Research 24, 24-33.

Bernstein, J., W.A. Lott, B.A. Steinberg, H.L. Yale, 1952. Chemotherapy of experimental tuberculosis. V. Isonicotinic acid hydrazide (nydrazid) and related compounds. Am. Rev. Tuberc. 65, 357-364.

Brightbill, H.D., 1999. Host Defense Mechanisms Triggered by Microbial Lipoproteins Through Toll-Like Receptors. Science 285, 732-736.

Bursulaya, B.D., M. Totrov, R. Abagyan, C.L.B. III, 2003. Comparative study of several algorithms for flexible ligand docking. Journal of Computer-Aided Molecular Design 17, 755–763.

Cáceres, N.E., N.B. Harris, J.F. Wellehan, Z. Feng, V. Kapur, R.G. Barletta, 1997. Overexpression of the D-alanine racemase gene confers resistance to D-cycloserine in Mycobacterium smegmatis. Journal of Bacteriology 179, 5046-5055.

Carlomagno, T., 2005. LIGAND-TARGET INTERACTIONS: What Can We Learn from NMR? Annual Review of Biophysics and Biomolecular Structure 34, 245-266.

Carter, A.P., W.M. Clemons, D.E. Brodersen, R.J. Morgan-Warren, B.T. Wimberly, V. Ramakrishnan, 2000. Functional insights from the structure of the 30S ribosomal subunit and its interactions with antibiotics. Nature 407, 340-348.

CDC, 2003. Update: adverse event data and revised American Thoracic Society/CDC recommendations against the use of rifampin and pyrazinamide for treatment of latent tuberculosis infection--United States. Morbidity and Mortality Weekly Report 735.

Chopra, S., H. Pai, A. Ranganathan, 2002. Expression, purification, and biochemical characterization of Mycobacterium tuberculosis aspartate decarboxylase, PanD. Protein Expression and Purification 25, 533-540.

Cox, J.S., B. Chen, M. McNeil, W.R. Jacobs, 1999. Complex lipid determines tissue-specific replication of Mycobacterium tuberculosis in mice. Nature 402, 79-83.

Cronan, J.E., 1980. Beta-alanine synthesis in Escherichia coli. J. Bacteriol. 141, 1291-1297.

Daffé, M., P. Draper, 1997. The envelope layers of mycobacteria with reference to their pathogenicity, p. 131-203, in: Poole, R K, (Ed.), Academic Press, Vol. Volume 39, pp. 131-203.

David, H.L., K. Takayama, D.S. Goldman, 1969. Susceptibility of mycobacterial D-alanyl-D-alanine synthetase to D-cycloserine. American Review of Respiratory Disease 100, 579-581.

de Villiers, J., L. Koekemoer, E. Strauss, 2010. 3-Fluoroaspartate and Pyruvoyl-Dependant Aspartate Decarboxylase: Exploiting the Unique Characteristics of Fluorine To Probe Reactivity and Binding. Chemistry - A European Journal 16, 10030-10041.

DeLano, W.L., 2002. The Pymol molecular graphics system. The Pymol molecular graphics system.

Dye, C., B.G. Williams, 2010. The Population Dynamics and Control of Tuberculosis. Science 328, 856-861.

Eswar, N., B. Webb, M.A. Marti-Renom, M.S. Madhusudhan, D. Eramian, M.-y. Shen, U. Pieper, A. Sali, 2001. Comparative Protein Structure Modeling Using MODELLER, Current Protocols in Protein Science, John Wiley & Sons, Inc.

Feng, Z., R.G. Barletta, 2003. Roles of Mycobacterium smegmatisD-Alanine:D-Alanine Ligase and D-Alanine Racemase in the Mechanisms of Action of and Resistance to the Peptidoglycan Inhibitor D-Cycloserine. Antimicrobial Agents and Chemotherapy 47, 283-291.

Fielding, L., 2007. NMR methods for the determination of protein–ligand dissociation constants. Progress in Nuclear Magnetic Resonance Spectroscopy 51, 219-242.

Frank, C., A.M. Giammarioli, L. Falzano, C. Fiorentini, S. Rufini, 2002. Glutamate-induced calcium increase in myotubes depends on up-regulation of a sodium-dependent transporter. FEBS Letters 527, 269-273.

Garvin, R.T., D.K. Biswas, L. Gorini, 1974. The Effects of Streptomycin or Dihydrostreptomycin Binding to 16S RNA or to 30S Ribosomal Subunits. Proceedings of the National Academy of Sciences 71, 3814-3818.

Ghose, A.K., V.N. Viswanadhan, J.J. Wendoloski, 1998. A Knowledge-Based Approach in Designing Combinatorial or Medicinal Chemistry Libraries for Drug Discovery. 1. A Qualitative and Quantitative Characterization of Known Drug Databases. Journal of Combinatorial Chemistry 1, 55-68.

Glickman, M.S., J.S. Cox, W.R. Jacobs, 2000. A novel mycolic acid cyclopropane synthetase is required for cording, persistence, and virulence of Mycobacterium tuberculosis. Molecular cell 5, 717-727.

Glynn, J.R., J. Whiteley, P.J. Bifani, K. Kremer, D.v. Soolingen, 2002. Worldwide Occurrence of Beijing/W Strains of Mycobacterium tuberculosis: A Systematic Review Emerging Infectious Diseases 8, 843–849.

Gopalan, G., S. Chopra, A. Ranganathan, K. Swaminathan, 2006. Crystal structure of uncleaved L-aspartate-alpha-decarboxylase from Mycobacterium tuberculosis. Proteins 65, 796-802.

Groot, B.L.d., D.M.F.v. Aalten, R.M. Scheek, Amadei, G. Vriend, H.J.C. Berendsen, 1997. Prediction of Protein Conformational Freedom From Distance Constraints. PROTEINS: Structure, Function, and Genetics 29, 240–251.

Halgren, T.A., R.B. Murphy, R.A. Friesner, H.S. Beard, L.L. Frye, W.T. Pollard, J.L. Banks, 2004. Glide: A New Approach for Rapid, Accurate Docking and Scoring. 2. Enrichment Factors in Database Screening. Journal of Medicinal Chemistry 47, 1750-1759.

Heighton, L., W.F. Schmidt, R.L. Siefert, 2011. Kinetic and Equilibrium Constants of Phytic Acid and Ferric and Ferrous Phytate Derived from Nuclear Magnetic Resonance Spectroscopy. J. Agric. Food Chem. 56, 9543-9547.

Heilman, R.D., 1995. Drug development history, " overview", what are GCPs? . the quality assurance journal 4.

Hennig, A., H. Bakirci, W.M. Nau, 2007. Label-free continuous enzyme assays with macrocycle-fluorescent dye complexes. Nat Meth 4, 629-632.

Irwin, J.J., B.K. Shoichet, 2005. ZINC − a free database of commercially available compounds for virtual screening. Journal of Chemical Information and Modeling 45, 177-182.

Jackowski, S., 1996. Escherichia coli and Salmonella: cellular and molecular biology. American Society for Microbiology Press, Washington DC.

Jones, G., P. Willett, R.C. Glen, 1995. Molecular recognition of receptor sites using a genetic algorithm with a description of desolvation. Journal of Molecular Biology 245, 43-53.

Jones, G., P. Willett, R.C. Glen, A.R. Leach, R. Taylor, 1997. Development and validation of a genetic algorithm for flexible docking. Journal of Molecular Biology 267, 727-748.

Jorgensen, W.L., 2006. Qikprop, Schrödinger LLC, New York.

Jorgensen, W.L., D.S. Maxwell, J. Tirado-Rives, 1996. Development and testing of the OPLS all-atom force field on conformational energetics and properties of organic liquids. Journal of the American Chemical Society 118, 11225-11236.

Karakousis, P.C., 2009. Mechanisms of action and resistance of antimycobacterial agents, p. 271-291, in: Mayers, D L, (Ed.), Humana Press, pp. 271-291.

Kaufmann, S.H.E., 2000. Is the development of a new tuberculosis vaccine possible? Nat Med 6, 955-960.

Kaufmann, S.H.E., 2001. How can immunology contribute to the control of tuberculosis? Nat Rev Immunol 1, 20-30.

Kaufmann, S.H.E., 2004. New issues in tuberculosis. Annals of the Rheumatic Diseases 63, ii50-ii56.

Kaufmann, S.H.E., A.J. McMichael, 2005. Annulling a dangerous liaison: vaccination strategies against AIDS and tuberculosis. Nature Medicine 11, S33-S44.

Kennedy, J., 2004. Tools for metabolic engineering in Escherichia coli: inactivation of panD by a point mutation. Analytical Biochemistry 327, 91-96.

Kiss, R., B. Kiss, Á. K

, 2008. Discovery of Novel Human Histamine H4 Receptor Ligands by Large-Scale Structure-Based Virtual Screening. Journal of Medicinal Chemistry 51, 3145-3153.

Klees, J.E., R. Joines, 1997. Occupational health issues in the pharmaceutical research and development process. Occupational Medicine 12.

Kolb, P., C.B. Kipouros, D. Huang, A. Caflisch, 2008. Structure-based tailoring of compound libraries for high-throughput screening: Discovery of novel EphB4 kinase inhibitors. Proteins: Structure, Function, and Bioinformatics 73, 11-18.

Kolb, P., R.S. Ferreira, J.J. Irwin, B.K. Shoichet, 2009. Docking and chemoinformatic screens for new ligands and targets. Current Opinion in Biotechnology 20, 429-436.

Kraulis, P., 1991. MOLSCRIPT: a program to produce both detailed and schematic plots of protein structures. Journal of Applied Crystallography 24, 946-950.

Lee, B.I., S.W. Suh, 2004. Crystal structure of the schiff base intermediate prior to decarboxylation in the catalytic cycle of aspartate alpha-decarboxylase. J Mol Biol 340, 1-7.

Libermann, D., M. Moyeux, N. Rist, F. Grumbach, 1956. Preparation of new pyridinic thioamides active in experimental tuberculosis. C. R. Hebd. Seances Acad. Sci. 242, 2409-2412.

Lipinski, C.A., F. Lombardo, B.W. Dominy, P.J. Feeney, 1997. Experimental and computational approaches to estimate solubility and permeability in drug

discovery and development settings. Advanced Drug Delivery Reviews 23, 3-25.

Lounis, N., C. Truffot-Pernot, J. Grosset, V.R. Gordeuk, J.R. Boelaert, 2001. Iron and Mycobacterium tuberculosis infection. Journal of Clinical Virology 20, 123-126.

Maas, W.K., B.D. Davis, 1950. Pantothenate studies I.: Interference by d-Serine and l-Aspartic Acid with pantothenate synthesis in Escherichia coli. J. Bacteriol. 60, 733-745.

Malone, L., A. Schurr, L. H., D. McKenzie, J.S. Kiser, J.H. Williams, 1952. The effect of pyrazinamide (aldinamide) on experimental tuberculosis in mice. Am. Rev. Tuberc. 65.

Manabe, Y.C., W.R. Bishai, 2000. Latent Mycobacterium tuberculosis-persistence, patience, and winning by waiting. Nat Med 6, 1327-1329.

McKinney, J.D., K.H. zu Bentrup, E.J. Munoz-Elias, A. Miczak, B. Chen, W.-T. Chan, D. Swenson, J.C. Sacchettini, W.R. Jacobs, D.G. Russell, 2000. Persistence of Mycobacterium tuberculosis in macrophages and mice requires the glyoxylate shunt enzyme isocitrate lyase. Nature 406, 735-738.

Merritt, E.A., D.J. Bacon, 1997. Raster3D Photorealistic Molecular Graphics. Methods Enzymol 277, 19.

Montes, M., E. Braud, M.A. Miteva, M.-L. Goddard, O. Mondesert, S. Kolb, M.-P. Brun, B. Ducommun, C. Garbay, B.O. Villoutreix, 2007. Receptor-Based Virtual Ligand Screening for the Identification of Novel CDC25 Phosphatase Inhibitors. Journal of Chemical Information and Modeling 48, 157-165.

Morris, G., D. Goodsell, R. Huey, A. Olson, 1996. Distributed automated docking of flexible ligands to proteins: Parallel applications of AutoDock 2.4. Journal of Computer-Aided Molecular Design 10, 293-304.

Nathan, C., M.U. Shiloh, 2000. Reactive oxygen and nitrogen intermediates in the relationship between mammalian hosts and microbial pathogens. Proceedings of the National Academy of Sciences 97, 8841-8848.

Ostrov, D.A., J.A. Hernandez Prada, P.E. Corsino, K.A. Finton, N. Le, T.C. Rowe, 2007. Discovery of Novel DNA Gyrase Inhibitors by High-Throughput Virtual Screening. Antimicrobial Agents and Chemotherapy 51, 3688-3698.

Pereira, H.M., V. Berdini, A. Cleasby, R.C. Garratt, 2007. Crystal structure of calf spleen purine nucleoside phosphorylase complexed to a novel purine analogue. FEBS Letters 581, 5082-5086.

Pierce, A.C., M. Jacobs, C. Stuver-Moody, 2008. Docking Study Yields Four Novel Inhibitors of the Protooncogene Pim-1 Kinase†. Journal of Medicinal Chemistry 51, 1972-1975.

Ramjee, M.K., U. Genschel, C. Abell, A.G. Smith, 1997. Escherichia coli L-aspartate-alpha-decarboxylase: preprotein processing and observation of reaction intermediates by electrospray mass spectrometry. Biochem J 323 (Pt 3), 661-9.

Rarey, M., B. Kramer, T. Lengauer, G. Klebe, 1996. A Fast Flexible Docking Method using an Incremental Construction Algorithm. J. Mol. Biol 261, 261, 470–489.

Ravel, J.M., W. Shive, 1946. Biochemical transformations as determined by competitive analogue-metabolite growth inhibitors. Journal of Biological Chemistry 166, 407-415.

Raviglione, M.C., R.J. Brien, 2004. Harrison's principles of internal medicine. McGraw-Hill Professional, New York.

Recsei, P.A., E.E. Snell, 1984. Pyruvoyl enzymes. Annual Review of Biochemistry 53, 357-387.

Reece, S.T., S.H.E. Kaufmann, 2008. Rational design of vaccines against tuberculosis directed by basic immunology. International Journal of Medical Microbiology 298, 143-150.

Richardson, G., H. Ding, T. Rocheleau, G. Mayhew, E. Reddy, Q. Han, B.M. Christensen, J. Li, 2009. An examination of aspartate decarboxylase and glutamate decarboxylase activity in mosquitoes. Molecular Biology Reports 37, 3199-3205.

Saldanha, S.A., L.M. Birch, M.E. Webb, B.K. Nabbs, F. von Delft, A.G. Smith, C. Abell, 2001. Identification of Tyr58 as the proton donor in the aspartate-alpha-decarboxylase reaction. Chem Commun (Camb), 1760-1.

Salem, A.A., H.A. Mossa, B.N. Barsoum, 2006. Application of nuclear magnetic resonance spectroscopy for quantitative analysis of miconazole, metronidazole and sulfamethoxazole in pharmaceutical and urine samples. Journal of Pharmaceutical and Biomedical Analysis 41, 654-661.

Sambandamurthy, V.K., X. Wang, B. Chen, R.G. Russell, S. Derrick, F.M. Collins, S.L. Morris, W.R. Jacobs, 2002. A pantothenate auxotroph of Mycobacterium tuberculosis is highly attenuated and protects mice against tuberculosis. Nat Med 8, 1171-1174.

Sassetti, C.M., D.H. Boyd, E.J. Rubin, 2003. Genes required for mycobacterial growth defined by high density mutagenesis. Molecular Microbiology 48, 77-84.

Schaible, U.E., H.L. Collins, S.H. Kaufmann, 1999. Confrontation between intracellular bacteria and the immune system. Advances in Immunology 71, 267-377.

Schatz, A., S.A. Waksman, 1944. Effect of streptomycin and other antibiotic substances upon Mycobacterium tuberculosis and related organisms. Proceedings of the Society for Experimental Biology and Medicine, 244-248.

Schmitzberger, F., M.L. Kilkenny, C.M. Lobley, M.E. Webb, M. Vinkovic, D. Matak-Vinkovic, M. Witty, D.Y. Chirgadze, A.G. Smith, C. Abell, T.L. Blundell, 2003. Structural constraints on protein self-processing in L-aspartate-alpha-decarboxylase. EMBO J 22, 6193-204.

Schorey, J.S., 1997. A Macrophage Invasion Mechanism of Pathogenic Mycobacteria. Science 277, 1091-1093.

Shao, Y., M.Q. Xu, H. Paulus, 1996. Protein splicing: evidence for an N-O acyl rearrangement as the initial step in the splicing process. Biochemistry 26.

Sharma, R., R. Kothapalli, A.M.J. Van Dongen, K. Swaminathan, 2012a. Chemoinformatic Identification of Novel Inhibitors against <italic>Mycobacterium tuberculosis</italic> L-aspartate α-decarboxylase. PLoS ONE 7, e33521.

Sharma, R., M. Florea, W.M. Nau, K. Swaminathan, 2012b. Validation of Drug-Like Inhibitors against <italic>Mycobacterium Tuberculosis</italic> L-Aspartate α-Decarboxylase Using Nuclear Magnetic Resonance (¹H NMR). PLoS ONE 7, e45947.

Shatsky, M., R. Nussinov, H.J. Wolfson, 2002. MultiProt - a multiple protein structural alignment algorithm, p. 235-250, Springer-Verlag, pp. 235-250.

Shi, W., X. Zhang, X. Jiang, H. Yuan, J.S. Lee, C.E. Barry, H. Wang, W. Zhang, Y. Zhang, 2011. Pyrazinamide Inhibits Trans-Translation in Mycobacterium tuberculosis. Science 333, 1630-1632.

Shive, W., J. Macow, 1946. Biochemical transformations as determined by competitive analogue-metabolite growth inhibitors. Journal of Biological Chemistry 162, 451-462.

Spry, C., K. Kirk, K.J. Saliba, 2008. Coenzyme A biosynthesis: an antimicrobial drug target. FEMS Microbiology Reviews 32, 56-106.

Steuber, H., A. Heine, G. Klebe, 2007. Structural and Thermodynamic Study on Aldose Reductase: Nitro-substituted Inhibitors with Strong Enthalpic Binding Contribution. Journal of Molecular Biology 368, 618-638.

Thomas, J.P., C.O. Baughn, R.G. Wilkinson, R.G. Shepherd, 1961. A new synthetic compound with antituberculous activity in mice: ethambutol (dextro-2,2'-(ethylenediimino)-di-l-butanol). The American review of respiratory disease 83, 891-893.

Tikhonova, I.G., C.S. Sum, S. Neumann, S. Engel, B.M. Raaka, S. Costanzi, M.C. Gershengorn, 2008. Discovery of Novel Agonists and Antagonists of the Free Fatty Acid Receptor 1 (FFAR1) Using Virtual Screening. Journal of Medicinal Chemistry 51, 625-633.

Timmins, G.S., V. Deretic, 2006. Mechanisms of action of isoniazid. Molecular Microbiology 62, 1220-1227.

van Poelje, P.D., E.E. Snell, 1990. Pyruvoyl-dependent enzymes. Annual Review of Biochemistry 59, 29-59.

Vandenberg, J.I., P.W. Kuchel, G.K. King, 1986. Application of progress curve analysis to in situ enzyme kinetics using 1H NMR spectroscopy. Analytical Biochemistry 155, 38-44.

Wang, J.-G., Y.-J. Xiao, Y.-H. Li, Y. Ma, Z.-M. Li, 2007. Identification of some novel AHAS inhibitors via molecular docking and virtual screening approach. Bioorganic & Medicinal Chemistry 15, 374-380.

Webb, M.E., A.G. Smith, C. Abell, 2004. Biosynthesis of pantothenate. Nat. Prod. Rep. 21, 695-721.

Webb, M.E., E. Stephens, A.G. Smith, C. Abell, 2003. Rapid screening by MALDI-TOF mass spectrometry to probe binding specificity at enzyme active sites. Chem. Commun., 2416-2417.

WHO, 2011. Global Tuberculosis Control, ISBN 978 924 156438 0.

WHO, W.H.O., 2008. Global tuberculosis control- surveillance, planning, financing.

Williamson, J.M., G.M. Brown, 1979a. Purification and properties of L-aspartate-alpha-decarboxylase, an enzyme that catalyzes the formation of beta-alanine in Escherichia coli. J Biol Chem 254, 8074-82.

Williamson, J.M., G.M. Brown, 1979b. J. Biol. Chem. 254, 8074-8082.

Winder, F.G., P.B. Collins, 1970. Inhibition by Isoniazid of Synthesis of Mycolic Acids in Mycobacterium tuberculosis. Journal of General Microbiology 63, 41-48.

Yung-Chi, C., W.H. Prusoff, 1973. Relationship between the inhibition constant (KI) and the concentration of inhibitor which causes 50 per cent inhibition (I50) of an enzymatic reaction. Biochemical Pharmacology 22, 3099-3108.

Zhang, Y., D. Mitchison, 2003. The curious characteristics of pyrazinamide: a review. The International Journal of Tuberculosis and Lung Disease 7, 6-21.

Zhang, Y., M.M. Wade, A. Scorpio, H. Zhang, Z. Sun, 2003. Mode of action of pyrazinamide: disruption of Mycobacterium tuberculosis membrane transport and energetics by pyrazinoic acid. Journal of Antimicrobial Chemotherapy 52, 790-795.